An experimental investigation of fuel assisted electrolysis as a function of fuel and reactant utilization

G. Cinti [a,*], G. Bidini [a], K. Hemmes [b]

[a] Università degli Studi di Perugia, Dipartimento di Ingegneria, Via Duranti 67, 06125, Perugia, Italy
[b] Delft University of Technology, Jaffalaan 5, 2628 BX Delft, The Netherlands

ARTICLE INFO

ABSTRACT

In this paper we describe and analyze the results of experiments on a Solid Oxide Electrolyzer Cell with and without the supply of a fuel to the oxygen producing electrode. In the experiments a 5×5 cm^2 Solid Oxide Fuel Cell is used operating in electrolyzer mode. We have tested the influence of varying reactant utilization (i.e. steam utilization) and fuel utilization in fuel assisted electrolysis. In particular the effect of insufficient fuel supply was studied experimentally as well as theoretically. In doing so we defined a turning point at which all the fuel is utilized. It was shown that by supplying not enough fuel all the fuel is oxidized and as in conventional electrolysis, oxygen production will start and oxygen is leaving the cell. Moreover the cell performance approaches conventional electrolysis and the effect of adding fuel on reducing the necessary amount of electric power almost vanishes. As in conventional high temperature steam electrolysis conversion efficiencies of more than hundred percent can be achieved also with fuel assisted electrolysis, under the condition that sufficient fuel is supplied i.e. fuel utilization must be lower than hundred percent.

We have put the concept of fuel assisted electrolysis in the framework of multisource multiproduct energy systems (MSMP's) and emphasized for example the benefits of using bio(syn)gas as the fuel in fuel assisted electrolysis. When using bio(syn)gas, the gas is de facto upgraded to pure hydrogen. This is an additional benefit next to the lowering of the electric power consumption for producing the same amount of hydrogen in the fuel assisted electrolysis process. Furthermore the suitability of these flexible MSMP systems in a market with volatile electricity prices due to increasing penetration of intermittent renewable energy sources is highlighted.

© 2016 Hydrogen Energy Publications LLC. Published by Elsevier Ltd. All rights reserved.

Introduction

With a growing contribution of renewable energy for electricity production mainly from solar and wind we are facing more and more problems with the integration of these fluctuating electricity sources into our electric grid, in which always an exact balance between supply and demand must be maintained. Often the standard solution of storage is

* Corresponding author.
  E-mail address: giovanni.cinti@unipg.it (G. Cinti).

proposed for this problem. However, there are more solution directions such as demand side management and flexible production from more conventional sources. A recent development is the so-called multisource multiproduct energy system that can also contribute to the solution of the above problem, often in a much more efficient way (economic efficiency as well as technical efficiency) than the standard solution of storage. In one solution direction we can coproduce multiple products next to electricity and when we need less electricity because of low demand or high production from renewable energy we can decrease the production of electricity from our device, while increasing the production of one of the co-products, for example hydrogen. An example of such a multisource multiproduct energy system (MSMP) is what has been named the 'superwind' concept [1,2]. Contrary to just reducing electricity production from a conventional source or stopping the power plant completely, in the superwind concept always valuable goods (be it electricity or hydrogen) are produced using a high temperature internal reforming fuel cell, keeping the economic efficiency at a high level. As an additional bonus also the total technical efficiency is increased instead of reduced [in the coproduction of hydrogen and electricity less waste heat is produced]. This concept is very suitable as long as penetration of wind and solar is relatively modest. It is found that in those situations, from the wind turbine owner's economic perspective, it is more important to 'fill in the gaps,' than to apply peak shaving. Wind turbine owners operating on the electricity market have to offer in advance a certain amount of electricity to the market for certain price. Whenever the wind falls short of predictions wind turbine owners can be faced with heavy financial penalties downgrading overall economic performance significantly. Therefore having the ability to produce additional power by alternative means (adjusting the settings of the superwind multisource multiproduct energy system to more electricity production and less hydrogen production) is much more beneficial to them than peak shaving. We call this 'filling in the gaps.' However if the penetration of wind energy and solar keeps increasing, situations might occur that there really is a surplus of electricity for which no other purpose is available (assuming the limits for demand side management are also reached). Under these conditions, -- which today are still very rare even in areas with large wind penetration such as Denmark and the North of Germany-, conversion of electricity into for example hydrogen might be meaningful (the Power to Gas or P2G concept). In the strict definition of storage we would later on convert this hydrogen back into electricity. Of course there is also the possibility to use this hydrogen produced by power to gas as hydrogen in industrial applications such as in the glass industry, or for example in fuel cell vehicles. Although the power to gas concept in principle refers to any process in which electricity can be converted into a gaseous fuel, almost always one refers to the electrolysis of water (or steam) into hydrogen and oxygen. However also electrolysis of CO_2 into CO or even into carbon is possible as shown by Shi et al. [3]. Also in these processes oxygen is formed. Since oxygen is freely available in the air, often it is not economic to store the produced oxygen for later use and it is just vented into the air. From a thermodynamic point of view it does however cost energy (electricity). It would save a

lot of electricity if we could prevent the formation of oxygen by supplying a fuel to the oxygen producing electrode. This is an old idea that has been applied already for many years in aluminum production, where carbon electrodes are used to prevent oxygen formation. The aluminum production process is in fact the electrolysis of aluminum oxide in which in principle pure aluminum and pure oxygen would be formed [4]. However, by the use of carbon electrodes the formation of oxygen is prevented and instead CO_2 is released. The use of a sacrificing carbon electrode can be seen as the integration of a Direct Carbon Fuel Cell [5] in series with the electrolysis process and thereby the amount of electric power needed externally to produce a fixed amount of aluminum is reduced significantly, compared to the case in which we would have an inert electrode with oxygen formation. Applying the same principle to electrolysis of water we can also use a carbon electrode as is done by Ewan et al. [6] and Gopalan et al. [7]. Alternatively a gaseous fuel can be supplied to the oxygen producing electrode [8,9]. The latter is more convenient, because we can simply choose a standard design of a fuel cell, which is now operated in reverse with the modification that in addition to the energy in the form of electric power also fuel gas is supplied to one electrode. Note that thereby the concept has become a Multi-Source Multi-Product energy system [1]. This electrolyzer concept, while proposing natural gas as the fuel, has been patented by Pham et al., in 2000 [10]. If we take the solid oxide fuel cell (SOFC) as an example, putting it in reverse creates a high temperature electrolyzer called Solid Oxide Electrolyzer Cell or SOEC. When supplying fuel to the electrode that normally would produce oxygen, we get what has been called 'fuel assisted electrolysis' in a Solid Oxide Fuel-assisted Electrolyzer cell or SOFEC [8,9,11-15].

So fuel cells in principle can also be operated in reverse and we can apply electrolysis with which real peak shaving can be obtained when needed. An innovative step forwards relative to electrolysis in which steam is converted into hydrogen and oxygen is so called 'fuel assisted electrolysis', in which as explained above, we can prevent the formation of oxygen by supplying a fuel gas to the oxygen electrode. Thereby we create a so-called Multi-Source Multi-Product energy system (MSMP) in which electricity and the added fuel are converted into hydrogen (and heat). Moreover we can choose the additional fuel to be bio(syn)gas, by which we mean any fuel gas mixture derived from biomass in whatever way. Thereby in effect we have created a bio(syn)gas purification/conversion device, through which the value of the bio(syn)gas is significantly increased. This latter option would be a significant improvement in the conversion of bio(syn)gas which presently suffers from low conversion efficiencies to electricity even when using fuel cells, or a cumbersome conversion into pure hydrogen or the conversion into methane for injection into the natural gas grid. Fuel assisted electrolysis using bio(syn)gas has not been discussed in literature as far as we know, but it is an illuminating example that shows that multisource multiproduct energy systems are often also multipurpose energy systems. In effect it gives us a system that, if operated as a fuel cell (SOFC) on natural gas, offers the possibility for flexible coproduction of hydrogen and electric power in almost any desired ratio; secondly the switch to hydrogen production under the consumption of a surplus of

electricity in SOEC mode and thirdly the highly efficient production of pure hydrogen from bio(syn)gas and a surplus of electricity in bio(syn)gas assisted electrolysis in SOFEC mode. This multifunctional system can adapt to the fluctuating conditions caused by an increasing amount of renewable electricity supply from wind and solar sources fed into the electricity grid. To a large extent the system also overcomes the chicken and egg problem encountered in the development of a hydrogen infrastructure for fuel cell vehicles. In practice we have to determine what operation conditions are most optimal given our optimization criteria; be it cost minimization, profit optimization, overall technical efficiency or lowest CO_2 emissions or other criteria or a combination thereof. This however falls outside the scope of this paper. Here we will focus on the SOFEC and present experimental data on its performance under various conditions. Contrary to previous work we include the parameter of fuel utilization in the experiments, since we use SOFC bench cells of 5 × 5 cm operated in SOFEC mode. To our knowledge this has not been done before. Only Martinez-Frias et al. [12] applied different methane utilization in their tubular SOFEC, however they used just one I–V curve for the electrolyzer, independent of utilization. Therefore they have not taken Nernst loss due to fuel utilization into account.

We did not address material issues but merely used the standard solid oxide fuel cell/solid oxide electrolyzer cell components. Notably: It is not trivial that the traditional materials can withstand the new oxidizing/reducing environments. For practical applications, endurance of the existing and newly designed materials must be tested under practical operating conditions. This however falls outside the scope of this paper. In order to be able to understand the experimental results it is necessary to give some theoretical background behind fuel assisted electrolysis, including Nernst loss caused by the fuel utilization. We will do so in the next section.

Theory of fuel assisted electrolysis

In conventional electrolysis the overall electrolysis reaction is the well-known splitting of water:

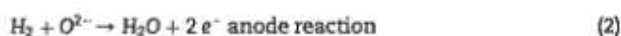$$H_2O \rightarrow \tfrac{1}{2}O_2 + H_2 \tag{1}$$

In this process pure hydrogen is obtained from electricity as the energy source and water as the reactant.
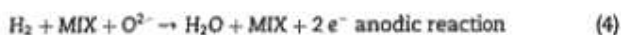
An application of the SOFEC concept is considering as a fuel at the anode, a mixture of hydrogen and other gasses, for example bio(syn)gas = $H_2 + CO + CH_4$ (+$CO_2 + H_2O$) as the product of anaerobic digestion, pyrolysis or any form of gasification. We note however that any other fuel or compound that can be oxidized can be envisaged, including no hydrogen-containing gases such as CO or NH_3. Therefore many other applications of the SOFEC concept can be developed. In our experiments for simplicity we will use a mixture of nitrogen and hydrogen to mimic the bio(syn)gas, while avoiding its complexity.

In Fig. 1 the schematic's are given of the concept of fuel assisted electrolysis using hydrogen with or without other gasses (MIX).

The electrochemical reactions at the anode and cathode are following:

$$H_2 + O^{2-} \rightarrow H_2O + 2e^- \quad \text{anode reaction} \tag{2}$$

$$H_2O + 2e^- \rightarrow H_2 + O^{2-} \quad \text{cathode reaction} \tag{3}$$

The overall reaction that results is a perfect equilibrium with the only effect that hydrogen and steam flows are inverted in the anode and cathode off gasses. It also shows that it would be quite meaningless to use pure hydrogen in fuel assisted electrolysis in practice. This situation changes if the hydrogen is not pure but mixed with other gasses:

$$H_2 + MIX + O^{2-} \rightarrow H_2O + MIX + 2e^- \quad \text{anodic reaction} \tag{4}$$

$$H_2O + 2e^- \rightarrow H_2 + O^{2-} \quad \text{cathodic reaction} \tag{5}$$

In these reactions it appears that the hydrogen is extracted from the fuel gas mixture (bio(syn)gas) and finds its way to the cathode outlet side. We say it appears because it is not the same hydrogen atoms that we supplied on the anode side that we find back in the cathode outlet. The hydrogen atoms in the hydrogen molecules that we produce at the cathode originate from the steam that we supplied to the inlet of the cathode side of course. So in that strict sense we do not separate hydrogen from the bio(syn)gas mixture but from a practical point of view, just looking at inputs and outputs it does appear that way and we can still use that effect beneficially in practice to upgrade the biogas to pure hydrogen (after condensing out the water).

Some scholars suggest that at the anode still oxygen is formed, which in a chemical reaction will be reduced by the fuel supplied. Of course this is a possibility and this parallel reaction, with oxygen formation as in conventional electrolysis, could still occur. Depending on the kinetics of the subsequent pathways nature will divide the electrochemical current between the possible pathways. In terms of thermodynamics it does not matter which anodic reaction to consider for determining the Nernst potential of the electrode since at OCV we assume equilibrium. That means equilibrium of all possible reactions, so also all possible chemical reactions between the species available -in this case at the anode-will all be in equilibrium yielding equilibrium concentrations of all the species in those reactions. So considering first oxygen formation and then the subsequent chemical reaction with the fuel (combustion) the Nernst potential is determined by the electrochemical reaction of oxygen formation from oxide ions:
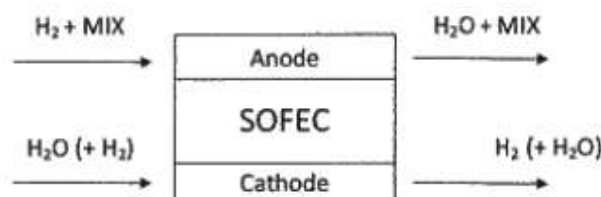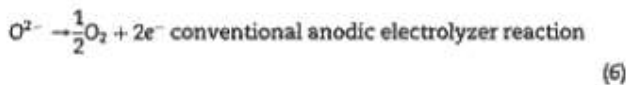

Fig. 1 – Experimental conditions for fuel assisted electrolysis in an SOFEC.

$$O^{2-} \to \tfrac{1}{2}O_2 + 2e^- \text{ conventional anodic electrolyzer reaction}$$

(6)

The presence of the fuel will eliminate the oxygen up to a very small equilibrium partial pressure. Filling in this small oxygen partial pressure in the Nernst equation belonging to reaction (6) will yield the same potential as reaction (2) (or (4) in case of a fuel gas mixture). If this would not be the case, then one of the two reactions would not be in equilibrium since the electrode can only assume one potential. This then would contradict our assumption of equilibrium. Also see Coleman and White [16] and Peelen and Hemmes [17] for a further explanation and determination of chemical and electrochemical equilibrium reactions in a system with many species and possible (electro-) chemical reactions.

To obtain pure hydrogen from the cathode off gas, only water still must and can simply be condensed out of the gas blend with hydrogen. We can also consider the cell as a concentration cell in which the concentration of hydrogen at the anode and cathode may differ, yielding a small potential difference. When a higher partial pressure of hydrogen is available at the fuel-assisted side than at the hydrogen production electrode, the reaction in principle will proceed spontaneously when the electrodes are short circuited (negative Gibbs free energy change). However, in practical applications we want significant hydrogen production and will therefore apply an electric potential next to the chemical energy in the form of a fuel. In electrolysis of water also an amount of heat equal to $T\Delta S$ has to be supplied to the process. This is completely analogous to a hydrogen fuel cell in which always a minimum amount of heat equal to $T\Delta S$ must be produced. Next to this negative thermodynamic heat term $T\Delta S$ (uptake of heat) both processes suffer from losses that will generate heat. In fuel cell operation this heat adds on to the thermodynamically produced amount of heat $T\Delta S$, whereas in electrolysis heat losses in general are sufficient to provide the heat $T\Delta S$ needed for the electrolysis reaction. Obviously the higher the temperature the higher the amount of heat taken up by the electrolysis process and the lower the overall heat losses. The latter is a great advantage of high temperature electrolysis, as is well known. This process of heat uptake by an electrochemical process is also encountered in a Direct Carbon Fuel Cell producing CO from carbon. Readers are further referred to a chapter on fuel cells written by one of the authors for further information on the thermodynamics of fuel cells and electrolysis cells [18].

Process losses are due to electrochemical- and ohmic polarization losses occurring in the electrolyzer cell. Such losses in the form of heat can be recovered directly in the chemicals with an appropriate selection of operating point called thermoneutral operation by adjusting the operating temperature such that the endothermic term $T\Delta S$ equals the amount of heat produced due to the reversible process losses [19].

We will explain more about local driving forces as a function of local conditions such as gas composition when discussing Nernst loss in the next section. Here it is emphasized that by using bio(syn)gas as the fuel in fuel assisted electrolysis, the bio(syn)gas mixture is upgraded to pure hydrogen as a beneficial coproduct of the electrolysis process next to the benefit of reduced electric power needed for the electrolysis of steam (See Fig. 1 and Equations (4) and (5)).

Nernst loss-gain

Nernst loss appears in electrolyzer units just as in fuel cells. The losses are caused by changes in local gas composition due to reactant utilization and production of reaction products that lead to a lower, respectively higher partial pressure of reactants and products, while going from inlet to outlet side of the cell [18,20].

In fuel cells the utilization of the fuel (U_f) is defined as follows:

$$U_f = \frac{H_{2r}}{H_{2in}} = \frac{I}{2FH_{2in}} = \frac{j}{2Fh_{2in}}$$

(7)

where H_{2r} and H_{2in} are the amount of reacting hydrogen and the amount of hydrogen supplied to the inlet respectively (both in mole/sec), F is Faraday's constant and j and h_{2in} are current density and specific inlet hydrogen flow (in mole/sec cm²) respectively. Notably; the area (unit = cm2) refers to the reactive cell area. Similarly in electrolyzers the reactant utilization (RU) is defined as:

$$RU = \frac{R_r}{R_{in}} = \frac{I}{2FR_{in}} = \frac{j}{2Fr_{in}}$$

(8)

where R_r and R_{in} are the amount of H_2O that has reacted and the amount of H_2O supplied to the inlet respectively (both in mole/sec), while r_{in} is specific H_2O inlet flow (in mole/sec cm²).

Therefore the local driving force for the desired reaction [either fuel cell or electrolyzer overall reaction] decreases when going from inlet to outlet. The local driving force is the difference between the local Nernst potential given by the local gas composition and the actual electrode potential. For convenience we can measure both versus the opposite electrode, while assuming constant conditions at that electrode.

For fuel cells F. Standaert [20,21] has derived the following formula for the Nernst loss:

$$V_{Nernst\ losses} = \left| V_{eq}(0) - \frac{1}{Uf}\int_0^{uf} V_{eq}(u)du \right|$$

(9)

With:

$$V_{eq}(u) = E_0 + \frac{RT}{nF}\ln\left(\frac{pH_2(u) \cdot pO_2(u)^{1/2}}{pH_2O(u)}\right)$$

(10)

In which the symbols have their usual meaning and the partial pressures are a function of local fuel utilization.

In these equations u is the local utilization of fuel for fuel cells or reactant (steam) utilization in electrolyzer mode, $V_{eq}(0)$ is the open cell voltage and $V_{eq}(u)$ is the local Nernst potential difference between anode and cathode determined by the local gas compositions at the anode and cathode. Variable u varies from zero at the inlet to Uf at the outlet of the fuel cell anode. The Nernst loss can then simply be calculated as the difference between OCV and the averaged Nernst potential of the anode. This is illustrated in Fig. 2. We note that

the Nernst loss is equal to the surface area between the line $V_{eq}(0)$ and the function $V_{eq}(u)$ up to u = Uf both for SOFC and SOEC operation.

As for fuel cells, in electrolysis we define the local reactant utilization (ru) as the fraction of steam that has been utilized up to a certain point in the cell. The overall total reactant utilization (RU) is the utilization at the outlet side of the electrolyzer. In fuel cell operation one has to subtract this surface area from OCV whereas in electrolyzer mode the surface area representing Nernst loss, in this case called Nernst gain, has to be subtracted from the Nernst local potential at RU calculated as the Nernst potential difference between anode and cathode at the outlet of the cell Veq(RU), where the total reactant utilization (RU) has been achieved.

$$V_{Nernst\ gain} = \left| V_{eq}(RU) - \frac{1}{Uf} \int_0^{RU} V_{eq}(u)du \right| \qquad (11)$$

In Fig. 2 potentials were calculated assuming inlet anode composition H_2:H_2O 50:50, and 100% oxygen at the cathode.

When the oxygen concentration at the cathode is not fixed at hundred percent also the change in gas composition at the cathode as a function of gas utilization going from inlet to outlet has to be taken into account in determining the Nernst loss. This can be done using Equation (10) and calculating the local oxygen partial pressure as a function of utilization, or one can rewrite the Equation (10) and use the local partial pressure of hydrogen in the added fuel in 'fuel assisted electrolysis'.

Nernst gain in fuel assisted electrolysis

In fuel assisted electrolysis the average potential difference between the local Nernst potential at the anode versus the local Nernst potential at the cathode at the same position in the cell measured from inlet to outlet is much lower than in conventional electrolysis without the fuel. In fact, throughout the cell it is a concentration cell if the fuel supplied is hydrogen. Nevertheless, similar to fuel cell and electrolyzer operation it does vary going from inlet to outlet and it can even
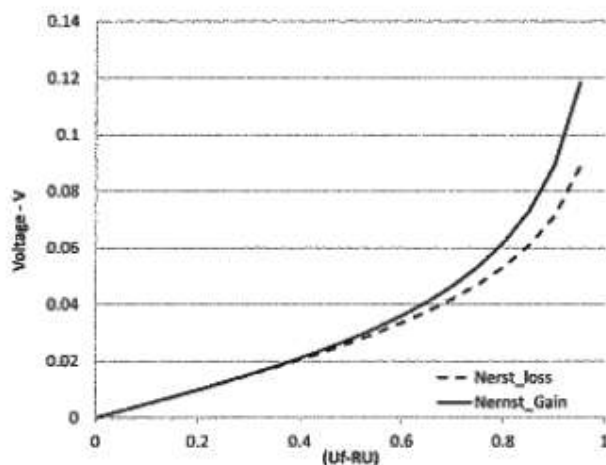

Fig. 2 – Nernst losses and Nernst gain as a function of Uf respectively.

change sign along the way. However, the driving force being the difference between the applied potential and the difference in local Nernst potentials at the anode versus cathode will always be positive. It cannot be that one side (say the inlet side) of the cell is functioning as a fuel cell whereas the other (outlet) side is acting as an electrolyzer of course. For those who need a proof we can use a proof by contradiction. If the cell would switch from fuel cell to electrolyzer mode the sign of the current density would reverse somewhere in the cell. At that point the local current density would be zero. However if the local current density is zero, no net reactions would take place anymore and the composition of the gases would remain the same. Therefore the local conditions would remain the same including the current density which is zero. This would hold up to the end of the cell. This contradicts the assumption that the last part of the cell has a current density with opposite sign to the beginning of the cell Q.E.D. Note however that the local Nernst potential difference can switch signs depending on the gas composition. This local Nernst potential difference is compensated or overruled by the applied external voltage.

A peculiar situation appears when we do not supply sufficient fuel in the fuel assisted electrolyzer mode to keep fuel utilization below hundred percent. In other words; there is (virtually) no fuel leaving the electrolyzer from the anode side. Somewhere between inlet and outlet the electrolyzer changes from fuel assisted electrolysis to conventional electrolysis in which oxygen is produced. This point is defined as SOFEC turning point and corresponds to a specific operating condition of the cell in which a stoichiometric reaction occurs between the amount of fuel supplied in the process and the amount of oxygen that would have been produced without the fuel. We can thus identify for the cell a turning point current density (J_{tp}), and reactant utilization (RU_{tp}). Note that reaction stoichiometry is the same at both sides of the cells, this means that at the turning point we are producing at the cathode the same amount of hydrogen that we are consuming at the anode and it appears as if the cell operates as a membrane that separates H_2 moving it from one side to the other of the membrane. But again we emphasized that it just appears that way, but there is no physical separation.

In fuel cell operation we always want to avoid situations in which (in some cells) hundred percent fuel utilization occurs because in that case the cell potential collapses and can even become negative. In fuel assisted electrolysis one can have hundred percent fuel utilization because, as stated, the electrolyzer just switches to conventional mode for the last part of the electrolyzer cell near the outlet side. We can wonder what this does to the overall performance of the electrolyzer cell. One would expect an average performance of the 2 parts of the cell, however we have to acknowledge, as stated above that it cannot switch from electrolyzer to fuel cell mode in the same cell. Therefore the overall cell potential is always higher than the highest local equilibrium potential difference between anode and cathode. In other words also the last part of the cell should still function as an electrolyzer, meaning overall cell potential will approach the cell potential as for conventional operation of the electrolyzer. This is indeed what we found in the experiments. Therefore the addition of fuel is not very helpful if we do not supply sufficient fuel to prevent oxygen

formation. What will happen, just as in a fuel cell with a shortage of fuel supply, is that in the beginning of the cell a large overpotential will develop causing a large driving force and hence a large current density. Therefore all the fuel will react at the beginning of the cell. The large current density and large overpotential cause large losses in the form of heat production and hence overall efficiency loss.

So if we do not supply sufficient fuel to reduce all the oxygen that would have been produced in conventional electrolysis, there will be a point in the cell between inlet and outlet, where the fuel has fully reacted and oxygen production starts. How sharp this transition will be depends among others on diffusion in the gas phase and reaction rates of hydrogen and oxygen combustion. In the transition region the partial pressure of the fuel will decrease and the partial pressure of the oxygen will increase when going from inlet to outlet side. Due to these concentration differences net forward diffusion of hydrogen and net backward diffusion of oxygen will occur, next to the overall flow from inlet to outlet. This might explain part of the missing hydrogen we found in our experiments. We will come back to this further on in the paper.

In our experiments three cases were studied. The first one (case A) has an anodic flow of pure air, second one (Case B) has pure nitrogen, while in the last one (Case C) a mix of nitrogen and hydrogen is supplied to the anode (oxygen producing electrode) with an amount of hydrogen calculated so as to just have complete reduction of all the oxygen (hypothetically) produced at an overall reactant utilization of $RU_{tp} = 33\%$ (ratio between anodic hydrogen and cathodic steam concentration: $15/45 = 0.33$). At the cathode side steam is mixed with nitrogen and hydrogen. Nitrogen, in same concentration to steam, was used having in mind the experimental conditions where nitrogen is used as sweep gas, while hydrogen is added at a concentration of 10% of the inlet flow to guarantee a reducing atmosphere and avoid oxidation of the electrode. Such a requirement is necessary considering the utilization of a commercial cell like the one used in our experiments.

Similarly, to what happens for water in an SOFC and for hydrogen in an SOEC in a SOFEC Nernst calculation a minimum amount of steam (in this case we used 10^{-20}) is assumed for the calculations at the anode side for case B and the same concentration is also assumed for the anode steam concentration for case C in order to prevent the logarithm in the Nernst equation to become infinite.

Fig. 3 reports the results of the theoretical study of the local Nernst potentials as a function of local reactant utilization ru, calculated using Equation (10). For case C the Nernst gain was calculated as for a concentration cell until RU = 0,33 was obtained. After that value only conventional electrolyzer contribution was considered. This approach produced a small

Table 1 — Inlet gas compositions for cases A, B and C.

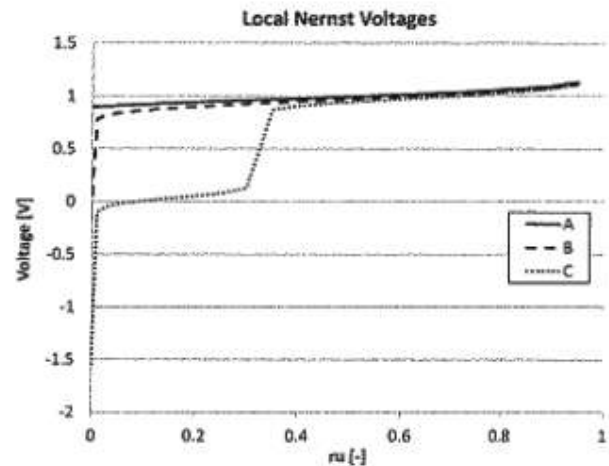| Case	Cathode (%)			Anode (%)			
	H_2O	N_2	H_2	$O2$	N_2	H_2	H_2O
A	45	45	10	21	79	0	0
B	45	45	10	0	100	0	0
C	45	45	10	0	85	15	0

Fig. 3 — Local Nernst potential difference between anode and cathode corresponding to the three gas compositions A,B and C depicted in Table 1.

discontinuity in the graph. To correctly evaluate the advantages obtained with the selected compositions it is possible to calculate the Nernst differential gain (NDG) between the curves as defined below. Such a value permits to evaluate the advantage, in terms of potential, of compositions B and C compared to composition A. The Nernst differential gain (NDG) parameters are a function of RU and defined as follows:

$$NDG_B = \frac{1}{RU} \int_0^{RU} [V_{eq}(ru)_B - V_{eq}(ru)_A] dru \qquad (12a)$$

$$NDG_C = \frac{1}{RU} \int_0^{RU} [V_{eq}(ru)_C - V_{eq}(ru)_A] dru \qquad (12b)$$

Results are plotted in Fig. 4.

Fig. 4 shows how there is a reduction of voltage and consequently a reduction of electrical power input moving from case A to B to C as expected.

Experimental

The experimental study was performed on a commercial electrolyte supported Solid Oxide Fuel Cell supplied by the company NexTech Materials. The cell is based on a 150 μm (±20 μm) zirconia-based electrolyte with a 50 μm Ni-GDC/Ni-YSZ multi-layer anode (SOFEC cathode) and a 50 μm LSM/LSM-GDC multi-layer cathode (SOFEC anode). The cell was tested inside a furnace operating at 850 °C. Two manifolds made of Crofer material, one for each electrode, were used as current collectors and gas distributors while a silver mesh was used at the anode side and a nickel mesh at the cathode to conduct current from the electrodes. Gas flow meters permitted pure gas flow control while a liquid flow meter was used to measure water evaporated in the cathode inlet tube. A power supply was used to set the desired current, while temperatures and voltage were sampled at 1 Hz frequency with a data acquisition unit. A 5 cm side square cell was used
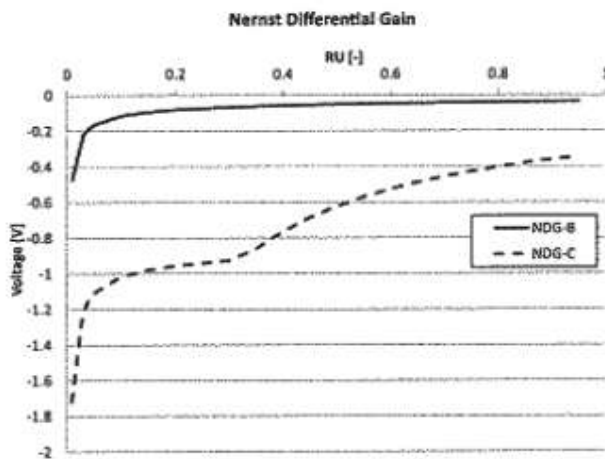
Fig. 4 – Nernst differential gain (NDG) as a function of RU calculated using Equation (12a,B).

with an active area of 12.87 cm^2 calculated from measurements of the mesh active area. Regarding the effect of heat absorption for example due to the term TΔS, we do not comment upon this in this experimental part of the study. It is impossible to perform any heat evaluation when making tests on our single cell, because system effects such as heat losses, impact of the furnace and heat transport by gas flows usually cover up heat flows related to the cell's internal reactions and heat produced by electrochemical reactions.

The experimental campaign was realized to evaluate real cell performance under the studied conditions. The normalized condition was extrapolated from European harmonized procedure FCTesQA indication. In such protocol, developed for SOFC cell testing, a specific flow of 10.7 ml/min cm^2 is considered. This value was also used as a reference to calculate reactant flow, in this case resulting in 6.43 g/h of steam. Gas mixtures were calculated based on Table 2. In addition to composition C, two additional compositions were tested: C2 and C3. Table 3 details the approach used to define the three C compositions. The current density turning point is defined as the current density in fuel assisted electrolysis mode at which just enough oxygen would have been produced to fully oxidize the amount of supplied fuel. In other words all the fuel supplied in fuel assisted electrolysis is fully oxidized at this current density. Test C was designed so to have a current density turning point J$_{tp}$ at 500 mA/cm^2. In tests C2 and C3 the J$_{tp}$ was set at 250 and 125 mA/cm^2 respectively by decreasing the input fuel flow as indicated in Table 3. Corresponding reactant

(steam) utilization is reported in Table 3, using the fact that we kept the steam flow constant at 6.43 g/h.

In Fig. 5 we report a typical example of the experimental voltage and current variation over time during test C. In the experiments the current is changed stepwise and the voltage response including experimental noise is also recorded. The small negative voltage value at zero current density means in this case fuel cell operation i.e. when short-circuiting the cell a spontaneous fuel cell reaction would take place. The figure shows how the cell moves from fuel cell to electrolysis operation with an OCV close to zero. Fig. 6 summarizes the results of all experimental tests. Polarization curves are plotted in Fig. 6a, while, to get a better understanding of the graphs, the differences between each case and the reference case (case A) was calculated and plotted in Fig. 6-b. As expected composition B performs better than A (smaller values) while for cases C the presence of hydrogen causes the cell voltage values to be very low, even negative, for small current density as previously commented. Also for case C2 we first see a small dip in Fig. 6a, i.e. a relative improvement compared to case A as shown as a peak at small current density in Fig. 6b. The absolute value of the voltage however stays almost constant in the first current step from zero as shown in Fig. 6a case C2. When the electrochemical reaction is enhanced by hydrogen oxidation electrolyzer cell voltage reaches acceptable values below cases A and B with hence an increase of performance as expected.

When moving from case C3 to case C, i.e. increasing the amount of fuel, the cell voltage becomes even lower thus further reducing the electric power needed. Note that the alienation of the curves with case A and B occurs, as expected, for higher current densities when moving from C3 to C, yet far before the expected current density and RU (see Table 3). It is as if less fuel (H$_2$) is supplied than we actually did supply. There seems to be hydrogen missing. This could be explained by a possible leakage of hydrogen along the cell so that the amount of H$_2$ in the electrode was actually smaller than planned, consequently reducing RU$_{tp}$. A second explanation might be that, analogous to fuel cells, supplying insufficient fuel will lead to a complete utilization of the fuel and in the case of a fuel cell to the collapse of the cell voltage. In fuel assisted electrolysis it will lead to an increase in the cell voltage needed to maintain the current. In a transition region the partial pressure of the fuel will decrease and the partial pressure of oxygen will increase, when going from inlet to outlet side. How sharp this transition will be depends among others on diffusion in the gas phase and reaction rate of hydrogen and oxygen combustion. This could also be part of the explanation for the shift of the curves in Fig. 6 to the left, compared to what is expected and depicted in Table 3. Gas diffusion is normally very fast, as well as the reaction between

Table 2 – Test campaign for the experiments.

Case		Cathode			Anode		
		H$_2$O [g/h]	N$_2$ [Nl/h]	H$_2$ [Nl/h]	Air [Nl/h]	N$_2$ [Nl/h]	H$_2$ [Nl/h]
A	Air	6.43	8.01	1.78	17.8	0	0
B	N2	6.43	8.01	1.78	0.0	17.8	0
C	N2 + H2	6.43	8.01	1.78	0.0	15.20	2.61
C2	N2 + H2	6.43	8.01	1.78	0.0	16.50	1.30
C3	N2 + H2	6.43	8.01	1.78	0.0	17.15	0.65

Table 3 – Turning point current density and RU$_{tp}$ for cases C, C2 and C3.

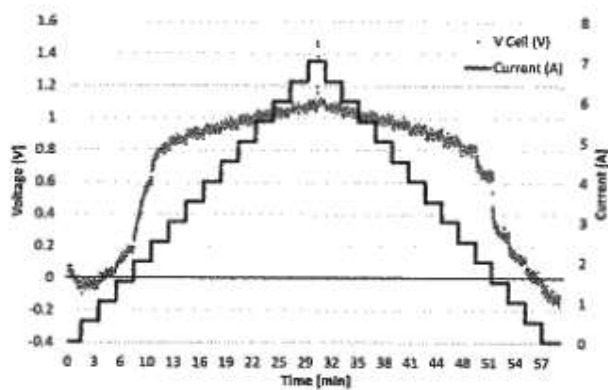|	J$_{tp}$ [mA/cm^2]	RU$_{tp}$
C	500	33%
C2	250	16.5%
C3	125	8.25%

Fig. 5 — Voltage and Current as function of time for test C.

hydrogen and oxygen, so part of the fuel (hydrogen) that we supply in fuel assisted electrolysis could chemically react with the oxygen that we produce at the same electrode at the end of the cell, in case we supply insufficient fuel, thereby explaining the 'missing hydrogen'.

Fig. 6-b shows how the trend of the curves collapses to zero at high reactant utilization RU. Specifically for cases C is important to notice that before the turning point, the cell operates as a fuel upgrader, with the overall result of obtaining a hydrogen production at the cathode equivalent to the amount consumed at the anode. In that operation condition no more hydrogen is produced on the cathode side as consumed on the anode. After the turning point real electrolysis occurs with the production of a larger quantity of hydrogen compared to the amount of hydrogen consumed. The figure shows how in these operating conditions there still is a difference, in terms of voltage going from case A to C, yet there is only a minor change in the voltage and hence also a minor change in the required electric power at higher current density and thus higher reactant utilization RU.

Efficiency

It is well known that in high temperature steam electrolysis efficiencies larger than hundred percent can be achieved because of the entropy term in the relation between the Gibbs
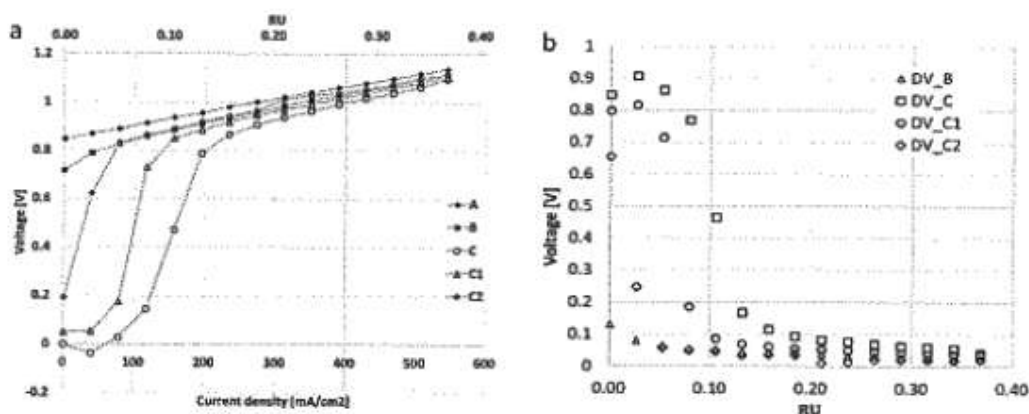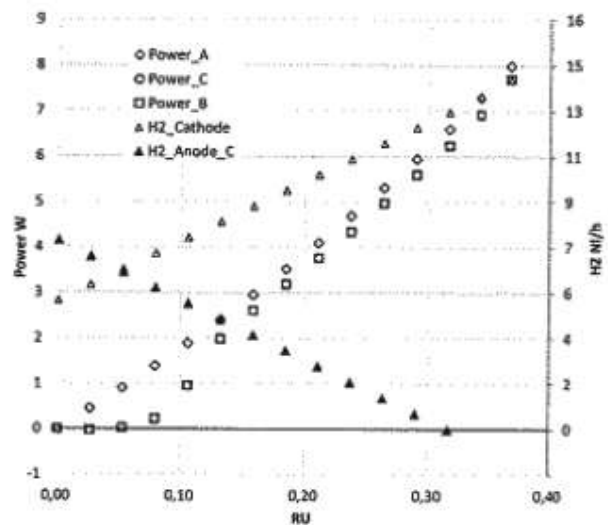

Fig. 7 — Input and output power streams for cases A, B and C as a function of reactant (steam) utilization RU.

free energy change and the enthalpy change of the reaction. We may wonder if this still holds for fuel assisted electrolysis. Therefore we calculated the power (energy per unit time) in every input and output energy flow excluding heat flows. Energy flows in terms of chemical energy were calculated based on Low Heating Value (LHV). In Fig. 7 we have depicted the electric power input as a function of reactant utilization (RU) for the 3 cases A, B and C as well as the amount of hydrogen produced at the cathode and the amount of hydrogen consumed at the anode in the fuel assisted electrolysis mode of case C.

The amount of hydrogen produced at the cathode is offset by the amount of hydrogen that we added to the inlet flow of the cathode of the electrolyzer cell in our experiments (5.29 Watt). The linear decrease in the amount of hydrogen leaving the anode in fuel assisted electrolysis (case C) reflects the linear relations between current density, reactant utilization, hydrogen production and fuel utilization. It shows the experimentally set condition that the amount of hydrogen supplied in fuel assisted mode is fully oxidized at the reactant utilization of 0.33. That is, we adjusted the amount of supplied

Fig. 6 — Experimental results of tested compositions: polarization curves (a) and voltage differences with case A (b).
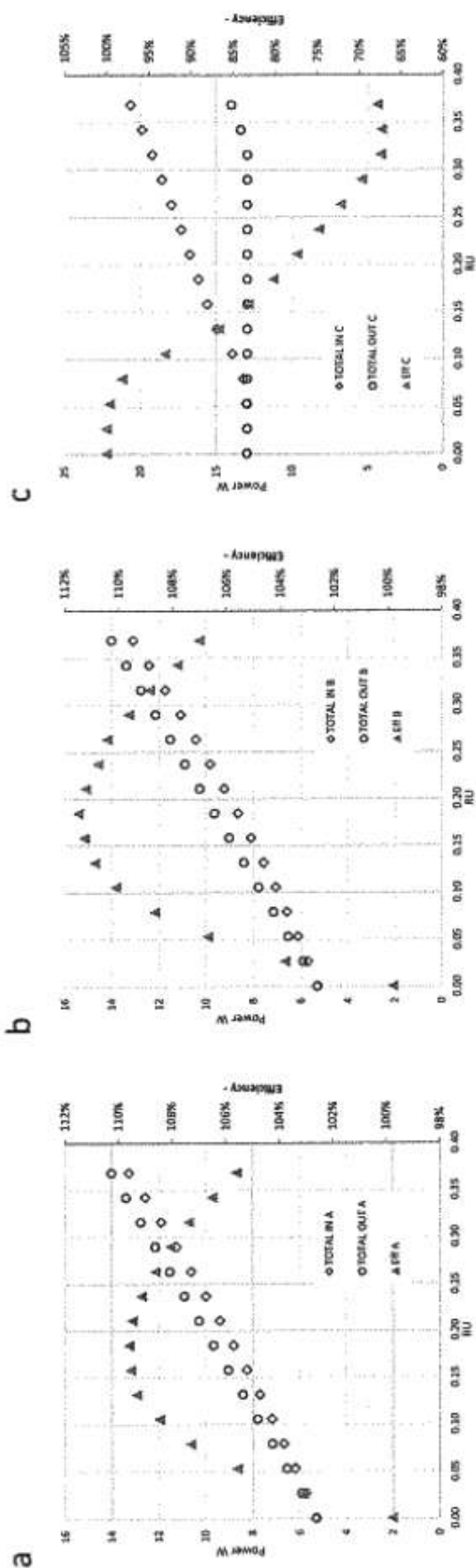
Fig. 8 – Total power input and total power output (excluding heat) and their ratio; the efficiency, as a function of reactant (steam) utilization RU for case A(a), B (b) and C (c).

hydrogen to the amount of steam that we supplied to the cell. For all 3 cases the amount of hydrogen produced at the cathode is the same because of the mentioned linear relation between reactant utilization and current density and that we have kept the supply of steam constant. The amount of electric power needed in case A reflects the polarization curve of conventional electrolysis which deviates a little bit from a linear relation because of increasing losses at higher current density (and thus higher reactant utilization). At low reactant utilization (and low current density) the electric power needed in fuel assisted electrolysis is very low up to a reactant utilization of about 0.08. As discussed above we would expect this 'turning point' to happen much closer to a reactant utilization of 0.3 because there the fuel is nearly fully utilized/oxidized.

In Fig. 8 we have plotted the input and output power flows and the efficiency being defined as their ratio for the cases A (a), B (b) and C (c). Note that we have excluded heat flows from the input and output streams as is usually done in defining the efficiency. In Fig. 8-a we see that total output is a little bit higher than total input over a wide range of reactant utilization leading to an efficiency higher than hundred percent. This is common in high temperature electrolysis in which heat is converted into chemical energy due to the sign of the entropy term $T\Delta S$ as explained in the theory section. Additional heat evaluation related to furnace were not performed because system effects such as heat losses or gas flows cover up heat flows related to cell internal reaction and heat produced by electrochemical reactions. For case A experimentally we found an optimum in the efficiency of 109% at a reactant utilization (RU) between 0.15 and 0.20.

By flushing with nitrogen instead of air (case B) we can increase the efficiency to 112% at a reactant utilization of 0.18 as shown in Fig. 8-b. The flow of nitrogen keeps the oxygen partial pressure (especially in the beginning of the cell) quite low, therefore at low reactant utilization little external electric power is needed to drive the process.

When we supply fuel in fuel assisted electrolysis we keep the oxygen partial pressure very low and thereby obtain significant Nernst gain. As long as the fuel is not fully oxidized, i.e. fuel utilization is kept below hundred percent, we maintain this low oxygen partial pressure at the anode at all times and places inside the cell and therefore can maintain this Nernst gain, leading to low electric power demand. Since we do add energy in another form, namely the fuel, total efficiency is somewhat reduced to around one hundred percent decreasing after the turning point which appears at a reactant utilization of about 0.08 (See Fig. 8-c). Contrary to cases A and B we note that in case C the total power output remains more or less constant. This is because as reactant utilization increases more fuel is utilized (hence less fuel is leaving the cell at the anode, as clearly shown in Fig. 7). This decrease in fuel output compensates the increase in hydrogen output at the cathode side.

Conclusions

In this paper we report on experimental studies on the performance of fuel assisted electrolysis in a 5×5 cm^2 solid oxide electrolyzer cell (SOEC). As is known from literature by adding a fuel to the oxygen producing electrode the amount of electricity needed for producing a certain amount of hydrogen by electrolysis is reduced. The effect of reactant (steam) utilization and fuel utilization in fuel assisted electrolysis, was taken into account in this study. In particular the effect of too little fuel was studied experimentally as well as theoretically. In doing so we defined a turning point at which all the fuel is utilized. It was shown that by supplying too little fuel i.e. all the fuel is oxidized and as in conventional electrolysis oxygen production is started and oxygen is leaving the cell; the cell performance approaches conventional electrolysis and the effect of adding fuel on reducing the necessary amount of electric power almost vanishes. Therefore when applying fuel assisted electrolysis one should take care to always supply sufficient fuel and keep fuel utilization below hundred percent.

In our experimental study in the laboratory, we use pure hydrogen as a fuel for the SOFEC. Any other fuel including methane or compound that can be oxidized at the anode can however be considered in SOFEC applications, opening up this concept to many additional fields other than energy, including the chemical industry.

We have put the concept of fuel assisted electrolysis in the framework of multisource multiproduct energy systems (MSMP's) and emphasized for example the benefits of using bio(syn)gas as the fuel in fuel assisted electrolysis. In that case bio(syn)gas is, as it were, upgraded to pure hydrogen. The described multisource multiproduct energy systems offers flexibility in input and output, which is very suitable in (future) energy system with a growing amount of (fluctuating) renewable energy from solar, wind and biomass.

REFERENCES

[1] Hemmes K. (Towards) multi-source multi-product and other integrated energy systems. Int J Integr Energy Syst 2009;1(1):1–15.
[2] Hemmes K, Kamp LM, Vernay ABH, de Werk G. A multi-source multi-product internal reforming fuel cell energy system as a stepping stone in the transition towards a more sustainable energy and transport sector. Int J Hydrogen Energy 2011;36(16):10221–7.
[3] Shi YX, Luo Y, Cai NS, Qian JQ, Wang SR, Li WY, et al. Experimental characterization and modeling of the electrochemical reduction of CO2 in solid oxide electrolysis cells. Electrochim Acta 2013;88:644–53.
[4] Welch BJ, Hyland MM, James BJ. Future materials requirements for the high-energy-intensity production of aluminum. JOM J Miner Met Mater Soc 2001;53(2):13–8.
[5] Hemmes K, Cooper JF, Selman JR. Recent insights concerning DCFC development: 1998-2012. Int J Hydrogen Energy 2013;38(20):8503–13.

[6] Ewan BCR, Adeniyi OD. A demonstration of carbon-assisted water electrolysis. Energies 2013;6(3).1657–68.

[7] Gopalan S, Ye GS, Pal UB. Regenerative, coal-based solid oxide fuel cell-electrolyzers. J Power Sources 2006;162(1):74–80.

[8] Tao G, Butler B, Virkar AV. Hydrogen and power by fuel-assisted electrolysis using solid oxide fuel cells. ECS Transactions (SOFC Xii) 2011;35(1):2929–39.

[9] Luo Y, Shi YX, Li WY, Ni M, Cai NS. Elementary reaction modeling and experimental characterization of solid oxide fuel-assisted steam electrolysis cells. Int J Hydrogen Energy 2014;39(20):10359–73.

[10] **Pham A, Wallman PH, Glass RS, Wallman H, Glass S. Production of hydrogen by steam electrolysis using a steam electrolyzer involves supplying natural gas to the anode side of the electrolyzer to reduce the electrical energy consumption. In. Univ California, Univ California Los Angeles (editors).**

[11] Jiang HQ, Wang HH, Werth S, Schiestel T, Caro J. Simultaneous production of hydrogen and synthesis gas by combining water splitting with partial oxidation of methane in a hollow-fiber membrane reactor. Angew Chem Int Ed 2008;47(48):9341–4.

[12] Martinez-Frias J, Pham AQ, Aceves SM. A natural gas-assisted steam electrolyzer for high-efficiency production of hydrogen. Int J Hydrogen Energy 2003;28(5):483–90.

[13] Wang W, Gorte RJ, Vohs JM. Analysis of the performance of the electrodes in a natural gas assisted steam electrolysis cell. Chem Eng Sci 2008;63(3):765–9.

[14] Wang WS, Vohs JM, Gorte RJ. Hydrogen production via CH4 and CO assisted steam electrolysis. Top Catal 2007;46(3–4):380–5.

[15] Wang Y, Liu T, Fang SM, Xiao GL, Wang HT, Chen FL. A novel clean and effective syngas production system based on partial oxidation of methane assisted solid oxide co-electrolysis process. J Power Sources 2015;277:261–7.

[16] Coleman DH, White RE. Linear algebra used to determine independent half-cell equations. J Electrochem Soc 1996;143(6):1781–3.

[17] Hemmes K, Peelen WHA, De Wit JHW. Study of the (electro) chemical equilibria in molten carbonate under the MCFC cathode gas atmosphere. Part I: selection of independent sets of equilibria to describe the (electro)chemical equilibrium in molten carbonate under the MCFC cathode gas atmosphere. Electrochim Acta 1998;43(14–15):2025–31.

[18] Hemmes K. Fuel cells. In: White RE, Conway BE, Vayenas CG, editors. Modern aspects of electrochemistry, vol. 37. New York: Kluwer Academic/Plenum Publishers; 2004. p. 131–251.

[19] Penchini D, Cinti G, Discepoli G, Desideri U. Theoretical study and performance evaluation of hydrogen production by 200 W solid oxide electrolyzer stack. Int J Hydrogen Energy 2014;39(17):9457–66.

[20] Standaert FRAM, Hemmes K, Woudstra N. Analytical fuel cell modeling. J Power Sources 1996;63(2):221–34.

[21] Standaert FRAM, Hemmes K, Woudstra N. Analytical fuel cell modeling: non-isothermal fuel cells. J Power Sources 1998;70(2):181–99.
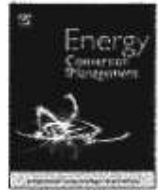
Biomass integrated gasifier-fuel cells: Experimental investigation on wood syngas tars impact on NiYSZ-anode Solid Oxide Fuel Cells

CrossMark

Arianna Baldinelli [a], Giovanni Cinti [a,*], Umberto Desideri [b], Francesco Fantozzi [a]

[a] Dipartimento di Ingegneria, Università degli Studi di Perugia, Italy
[b] DESTEC, Università degli Studi di Pisa, Italy

ARTICLE INFO

ABSTRACT

The aim of this work is to assess the feasibility of a Biomass Integrated Gasifier Fuel Cell (B-IGFC) plant. High temperature Solid Oxide Fuel Cells (SOFC) are the most efficient energy systems currently being developed and they show good fuel flexibility thanks to their high operational temperature. For the application here discussed, the fuel major active species are H_2, CO and CH_4; yet, in wood-derived syngas small amounts of higher hydrocarbons are produced too. Among them, tars are claimed to be biomass Achille's heel, causing severe issues in internal combustion engines and turbines. Conversely, SOFCs might be able to decompose tars with a gain on cell performance. However, in order to avoid fast degradation, tars concentrations have to be below a critical threshold. In this work, SOFC operation with real wood syngas from a pilot batch gasifier is firstly demonstrated. Then, longer tests are repeated under controlled conditions, artificially reproducing wood syngas with and without tars. Tests demonstrated that commercial NiYSZ-anode cells are able to work on syngas with a model tar (toluene) concentration up to 10 g/N m^3, exhibiting a voltage gain with regard to performances on syngas without model tar. No material degradation was observed after the experiments. As a final result, this paper aims at providing a proof of concept of a simplified B-IGFC system design, in order to reach its cost-effectiveness on small-scale installations.

© 2016 Elsevier Ltd. All rights reserved.

1. Introduction

Climate change and resources exploitation have become one of the hardest challenges humanity is facing. COP21 recently stressed the importance of energy saving, clean and efficient energy generation and fuel supply diversification. In this scenario, renewable energy resources (RES) are a promising alternative to traditional fuels and, among them, a key-role is played by biomass [1], which are spread all over the world. In addition to that, biomass allows an easier energy storage, so that power production can be scheduled according to power demand thus overcoming the issue of availability which is the main drawback of other RES, such as solar and wind.

Solid Oxide Fuel Cells (SOFCs) are one of the most efficient energy systems and they are able to work with a wide variety of fuels. As reported in [2–4], SOFCs are good candidates for the realization of efficient integrated systems. In particular, SOFCs can run on wood-derived synthetic gas, a mixture containing hydrogen, carbon monoxide, carbon dioxide, methane, nitrogen and other minor species [5,6]. Feedstock heterogeneity and gasification process parameters (e.g. gasification agents [7]) variability might influence SOFCs performances. However, modelling studies on the utilization of bio-derived fuels in SOFC devices predicted an efficiency up to 50% based on biomass lower heating value [8–11]. Such interesting figures call for an experimental validation.

System modelling studies usually do not take into account syngas minor components influence on SOFC performance. In a real system operation, despite very low concentration, they can have a heavy impact. In particular, regarding biomass gasification syngas minor components, tars are of primary concern. They include many organic compounds (phenols, 1-ring aromatics, PAHs) with a high boiling temperature. In conventional systems, they are claimed to be responsible of equipment failure: in [12,13], it is reported that ICEs and GTs tolerance limits are 50–100 mg/N m^3 and 5 mg/N m^3 respectively. Conversely, SOFC tolerance is

Nomenclature

A	SOFC active area, [cm^2]	n_{ij}	Partial flow rate of species i in stream j
F	Faraday constant, 96485 C/mol	p_{oi}	Saturation pressure of species i, [kPa]
j	Current density, [mA/cm^2]	p_{otot}	Total pressure, [kPa]
i	Current, [A]	T	Temperature, [°C],[K]
LHV	Low heating value, [kJ/Nl],[kJ/mol]	V	Voltage, [V]
n_{eq}	Equivalent fuel flow rate, [mol/s],[ml/min]	x_{ij}	Molar fraction of species i, in stream j [%]

expected to be higher, thanks to high operational temperature and catalysts (e.g. Nickel) enabling tar decomposition. Therefore, it is challenging to investigate whether SOFC tolerance to tars is within typical wood syngas tar loads, in order to achieve SOFCs bio-syngas feeding without meeting with quick degradation issues [14–16]. As a consequence, wood syngas featuring a small tar concentration might not require a dedicated cleaning unit interposed between the gasifier and the end-user device (SOFC). This is a key-point, especially in the outlook of small-scale distributed applications that call for complexity and capital expenditure reduction to achieve techno-economic feasibility [17].

In the literature, just few experimental works deal with the coupling of gasification and SOFCs. In particular, [18–20] evaluated SOFC operation with commercial gasifiers equipped with robust cleaning units. In those works, the most used gasification technology is the fluidized bed, which is typically suitable for application in the power range of 100 kW. Conversely, Biomass Integrated Gasifier Fuel Cell (B-IGFC) low-capacity applications are far more affordable in the outlook of distributed power generation systems. In this frame, fixed bed gasifiers seem to be the most promising choice.

According to the specific fixed bed inner design and process conditions, syngas components percentages and tars content are variable. Among fixed bed configurations, downdraft fixed bed gasifiers syngas output features good properties for the utilization in a SOFC [21], such as a low tar content: literature reports that the expected tar concentration for downdraft syngas is less than 1 g/N m^3 [22,23]. More recent experimental works confirmed that, after condensing low boiling-point components, tar residue was measured to be in the neighbourhood of 1 g/N m^3. Other authors [16] measured a larger tar concentration on wood syngas, albeit smaller than 10 g/N m^3. Low tar load is due to the temperature profile inside the reactor: temperature higher than 800 °C enables primary and secondary pyrolysis products decomposition into tertiary tars (alkyl-aromatics, PAHs) [22]. Because of that, downdraft tars are mainly aromatic hydrocarbons, such as those shown in Table 1. Table 2 displays typical wood syngas bulk compositions achieved when air is used as oxidizing medium.

SOFC tolerance to tars was investigated in a few studies, usually reproducing fuel mixtures with technical gases. Most scientific works assess SOFC behaviour with a simulated syngas enriched with a single tar compound (or at most a blend of few compounds),

referred as model tar. The authors of [29] investigated tar impact on NiYSZ-anode SOFC performances using both 1-ring aromatics (toluene and benzene) and a mixture of several compounds. They found out that 1-ring aromatic model tar caused a higher polarization resistance, because of their propensity towards catalytic breakdown into carbon. With similar results, in [30] a comparison between real tar and 1-ring model tar (toluene) impact on different SOFC anode materials was accomplished. Furthermore, in [31,33], other tests with benzene model tar were carried out, exposing a NiGDC-anode cell to hydrogen plus 15 g/N m^3 benzene. Although they did not observe overpotential changes, post-experimental SEM showed large carbon deposits on the anode surface. For these reasons, they claim that a longer exposure to such benzene concentrations, in a hydrogen matrix, could lower cell performance. Then, using a simulated syngas as fuel with 5 g/N m^3 benzene concentration, they measured higher overpotential but no carbon deposition. Despite coking issues, model tar addition results in increasing cell open circuit voltage as a consequence of model tar decomposition, as demonstrated by [33,34] (model tar naphthalene) and by [35,36] (model tar toluene, NiGDC-anode cells). SOFC stable operation under toluene-laden syngas was demonstrated in [37], up to 20 g/N m^3 toluene concentration in a syngas matrix made of 16% H$_2$, 16% CO$_2$ and 7.6% CH$_4$. On the contrary, when tar content exceeds SOFC tolerance threshold, it causes cell performances loss and material degradation, mainly because of carbon deposition and catalyst deterioration [38–40].

Hence, with regard to the state of the art, this paper aims at producing advances in the integration of SOFCs with a gasification facility. In particular, the application of small-scale downdraft gasifiers equipped with a simplified cleaning unit is discussed and experimentally tested. In this outlook, it is important to define a good management of the gasification process so that wood syngas bulk composition is compatible with a long-lasting SOFC operation. In this framework, current literature reports experiments performed on simulated fuel mixture which are not consistent with a real gasification process. Thus, the main target is to provide an experimental proof of concept that makes modelling projections easily available in the scientific literature more interesting. For what concerns SOFC technology, to provide results that are relevant for a pilot or demonstration installation, commercial NiYSZ-anode SOFCs are employed. NiYSZ is the material which is more mature from a manufacturing point of view, although it is not optimized for the operation under tar-laden fuels.

2. Experimental activity

Experimental results presented in this work are meant to demonstrate the feasibility of the B-IGFC concept, with a specific focus on SOFC tar tolerance. To accomplish this, at first SOFC is fed directly with clean real wood syngas; then, wood syngas is artificially reproduced with technical gases, both neglecting and considering tars, so that a longer test is performed with SOFC. Tests with simulated wood syngas are useful to verify SOFC material

Table 1
Average composition of the tar fraction in wood syngas produced by downdraft gasifiers, as reported into other researches [24].

Tar compound	Percentage (%)
Toluene	28
Naphthalene	18
Styrene	9
Indene	9
Phenol	7
Others	29

Table 2
Air-downdraft gasifier wood-syngas compositions.

Reference	Source	H_2 [%]	CO [%]	CO_2 [%]	CH_4 [%]	N_2 [%]
Ref. [25]	Average literature data	15.0	23.5	12.0	2.5	47.0
Ref. [26]	Experimental	15.5	19.0	11.5	1.0	53.0
Ref. [27]	Experimental	14.0	17.0	12.0	2.0	55.0
Ref. [16]	Experimental	15.0	14.5	15.0	3.0	52.5
Ref. [28]	Experimental	17.0	20.1	12.5	2.5	47.0

compatibility with wood syngas bulk composition. Then, tar effect is evaluated, by adding a model tar to simulated syngas. Since, according to the scientific literature, toluene is the most abundant compound in such kind of fuel [41,42], it is chosen as model compound. This aims at simulating SOFC feeding after a simplified cleaning unit, which offers a lean and cheaper solution in the outlook of small-scale systems [43].

Hence, this section describes the experimental setup and the test plan. Moreover, a paragraph is devoted to explain how fundamental parameters of the test plan are calculated.

2.1. Set-up: materials and hardware

In order to evaluate the feasibility of a B-IGFC system, an experimental set-up was developed, connecting two sections: a pilot air downdraft gasifier fed with biomass and a SOFC. There is a syngas cleaning unit between gasifier and the SOFC to achieve a better fuel quality. In particular, the cleaning unit is made of three components: a cyclone, an oil scrubber and an impinger bottle-train (bottles are kept at 0 °C and filled with isopropanol). Fig. 1 shows the pictures of these components. A detailed description of both gasifier and SOFC is given hereinafter.
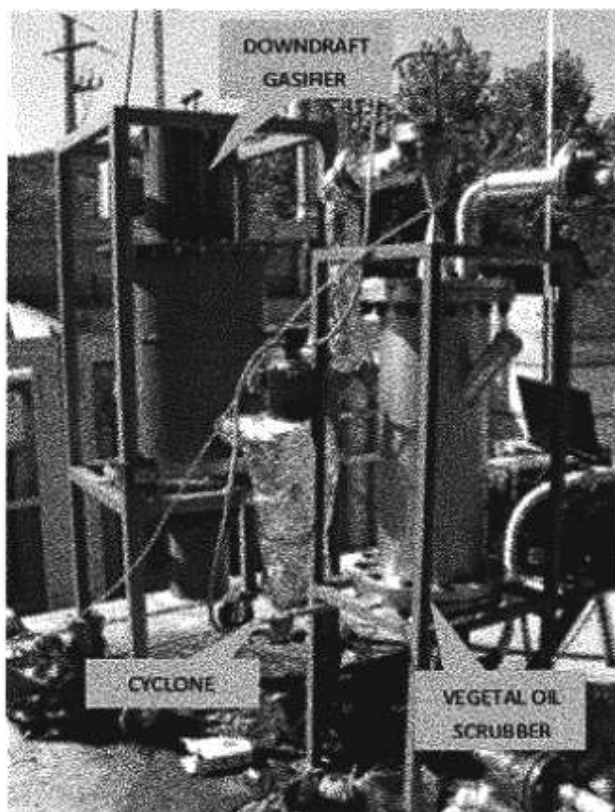

Fig. 1. Pilot air-downdraft gasifier equipped with a cyclone and a scrubber.

2.1.1. Gasifier section

The gasifier used for this work is a 30 kW$_{th}$ pilot facility that was built in the University of Perugia. It is a batch downdraft reactor using atmospheric air as oxidizing medium.

According to the downdraft configuration, biomass and syngas streams are co-current: this means that fresh feedstock is introduced from the top of the reactor and then it moves down through drying, pyrolysis and gasification zones. Syngas is finally spilled out from the reactor bottom. Air is forced in the reactor core by means of a blower and its flow rate is controlled in order to achieve an equivalence ratio of 3.3 in the reaction zone. Biomass feedstock used for this work is chestnut chips, whose features are reported in Table 3. In particular, wood chips were characterized through proximate analysis (Thermogravimetric method), ultimate analysis (providing the elemental composition of the sample) and calorimetric analysis (for the heating value).

2.1.2. Syngas cleaning

Wood syngas is firstly cleaned by a cyclone, then by a vegetal oil scrubber. A fraction of the gasifier outflow is sent to either an internal combustion engine or a flare by a blower (Fig. 2). After the oil scrubber, wood syngas is sent to a six impinger bottles train for TARs removal. Impinger bottles are filled with isopropanol, which acts as solvent for the mentioned compounds. Then, according to the Tar Protocol [44], bottles are kept at 0 °C, in order to trap into the solvent also lighter tar fractions that exhibits higher volatility. Hence, clean syngas is splitted into two streams: the first going to a Thermoscientific C2V fast micro gas-chromatograph for continuous sampling, the second feeding the SOFC rig.

2.1.3. SOFC section

SOFC rig configuration is depicted in the right part of Fig. 2, according to the experimental setup that allows direct feeding from the gasifier. In this case, syngas flow rate is controlled by means of a rotameter equipped with a needle valve. Conversely, for tests with simulated syngas mixtures, SOFC anode inlet is connected to a rail fed by several digital flow meter controllers (FMCs). Cathode is fed with air by means of a dedicated flow meter controller.

For all tests, anode feeding is enriched with moisture with a temperature-controlled water evaporator; then, pipe heating avoids water condensation and guarantees fuel preheating. Cell under test is housed into a thermoregulated furnace: anode and cathode compartments are separated using a ceramic sealing for

Table 3
Wood chips composition: ultimate analysis of a dry biomass sample; wet biomass sample proximate characterization via thermogravimetric analysis; dry biomass low heating value.

Ultimate analysis [%$_{db}$]		Proximate analysis [%$_{wb}$]	
C	44.5	Char	12.8
H	5.89	Ashes	1.72
N	0.31	Volatiles	76.37
O	49.3	Moisture	9.11

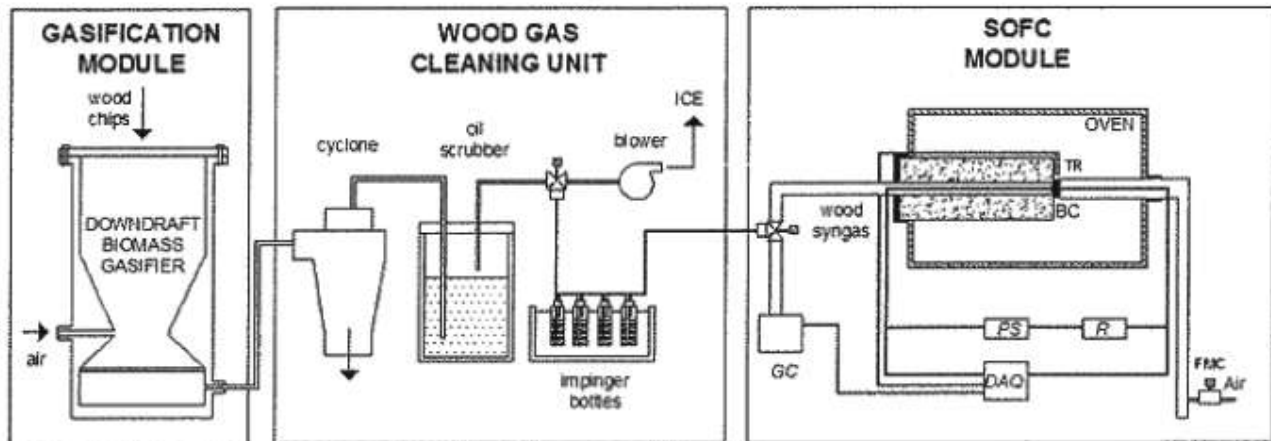Heating value 15.65 $\frac{kJ}{kg_{db}}$.

Fig. 2. Experimental setup for part 1 experiment (reproducing the B-IGFC concept). System consists of three units: a gasifier, a SOFC and a syngas cleaning section in between.

high temperature operation. Anode and cathode gases are conveyed to the active electrode sites via alumina pipes equipped with a porous flat end performing gas distribution. Furthermore, the contact between the porous ends and the electrodes is achieved by means of metal meshes (Nickel for the anode, Gold for the cathode) that are connected to a voltage sensor and to a DC electrical circuit. Furnace and cell temperatures are measured by two K-type thermocouples.

For the tests with model tar toluene, anode feeding line is equipped with an additional temperature-controlled evaporator. Liquid toluene is stored at atmospheric pressure inside an impinger bottle which is kept into a water bath. Nitrogen is chosen as carrier gas to collect toluene vapours, since its solubility into liquid toluene is negligible. Hence, toluene-rich nitrogen is collected at the gas end of the impinger bottles and it is mixed with the rest of the anode feeding. Toluene vapours concentration in carrier nitrogen only depends on temperature and pressure, as it is explained by Antoine's Law (see Eq. (3)). However, toluene concentration in SOFC anode feeding is determined by the ratio between carrier nitrogen flow rate and overall anode feeding flow rate. Accordingly, in order to set the proper toluene concentration, it is necessary to control accurately carrier nitrogen flow rate with a dedicated FMC. When model tar toluene is added to anode feeding stream, also the temperature of the water evaporator is changed in order to get the same moisture percentage in the final mixture.

Regarding cell materials, tests are run on SolidPower commercial planar Anode Supported Cell with Ni-YSZ anode, YSZ electrolyte and GDC/LSCF cathode. All the details about electrodes and electrolyte thickness and composition are disclosed in Table 4. SOFC operation is monitored continuously, acquiring temperature, voltage, current and gas flow rates signals with a digital system with a sampling frequency of 1 Hz.

Table 4
SOFC button cell data sheet.

Technology	SOFC	
Manufacturer	SolidPower	
Design	Anode Supported Planar Cell	
Cell type	BC	
Active area	2 cm^2	
Cell layers	Composition	Thickness
Anode	Ni/8YSZ	240 ± 20 μm
Electrolyte	8YSZ	8 ± 2 μm
Cathode	GDC + LSCF	50 ± 10 μm

2.2. Parameters definition

Before introducing the test campaign, it is worth to define some parameters to characterize the fuel.

- Equivalent fuel flow rate:
  In order to compare SOFC performances while changing anode feeding composition, single gas components flow rates are calculated to get a given equivalent fuel flow rate. Thus, equivalent fuel flow rate is determined according to the following expression (Eq. (1)):

$$n_{eq} = n_{H_2} + n_{CO} + 4n_{CH_4} \tag{1}$$

This definition derives from the fact that H_2 and CO yield the same electrons amount (2 electrons moles per mole of H_2 or CO) and CH_4 potentially yields 4 times the electrons amount given by H_2. The equivalent fuel flow rate will be used in our test in order to calculate, for each feeding condition, the total gas flow that potentially achieves the same electrons current.

- Model tar concentration:
  Under the assumption that nitrogen (carrier gas) is not soluble into toluene liquid phase, toluene vapours partial pressure in the gas phase is approximated with toluene saturation pressure. From this identity, toluene vapours concentration is calculated using Eq. (2). Toluene saturation pressure is defined by Antoine's Law, at Eq. (3): $p_{0,tol}$ is toluene saturation pressure, expressed in kPa, T is temperature expressed in °C and numeric constants are referred to phase balance in the temperature range of 13–136 °C [45].

$$x_{tol_{N2,carrier}} \approx p_{0,tol}/p_{tot,gas} \tag{2}$$

$$\ln(p_{0,tol}) = 13.93 - \frac{3056.96}{217.63 + T} \tag{3}$$

Finally, to calculate carrier nitrogen flow rate, mass balance is performed considering toluene concentration in carrier nitrogen and toluene concentration in SOFC feed, which is a design specification for the experiment (Eq. (4)). Overall nitrogen flow rate must satisfy superimposed syngas composition ($x_{N2,SOFCfeed}$ –in detail, reference SOFC feed composition are disclosed in next paragraph). Hence, also nitrogen flow rate in the main syngas stream is determined (Eq. (5)).

$$x_{tol_{N2,carrier}} * n_{N2,carrier} = x_{tol_{SOFCfeed}} * (n_{N2} + n_{syngas}) \tag{4}$$

$$x_{N2_{SOFCfeed}} = \frac{n_{N2,carrier} + n_{N2,syngas}}{n_{N2,carrier} + n_{syngas}} \tag{5}$$

2.3. Test campaign: planning and methods

Experimental campaign consists of two parts: firstly, direct SOFC operation on clean real wood syngas coming from the pilot gasifier and, secondly, SOFC operation on simulated wood syngas. Simulated wood syngas recalls the average composition obtained by analysing a slipstream of clean real syngas with the gas chromatograph. Thus, four experiments are presented: test 1 for the first part, the others concerning the second part. In particular, SOFC is run on simulated syngas without model tar in test 2.1 and on toluene-laden simulated syngas in tests 2.2a and 2.2b (the difference stands in toluene concentration: 5 and 10 g/N m^3 respectively). Toluene is a proper model tar for the application here debated for the following reasons [41,42]: (1) it is the most abundant tar species in downdraft gasifier syngas (Table 1), (2) since it is a 1-ring aromatic, it is more volatile than PAHs; thus it could bypass cleaning devices even if gas cleaning is provided, (3) according to the literature, 1-ring aromatics kinetics in coking is much quicker with regard to PAHs, resulting in an accelerated degradation test. Toluene addition is gradual (0–5–10 g/N m^3), up to a maximum concentration that overestimates typical downdraft wood syngas tar loads. Beside tar concentration, part 2 simulated syngas bulk composition (2.1, 2.2a, 2.2b) is retrieved from real wood-gas characterization performed within part 1. Details are discussed in next section.

Tests were carried out keeping constant the equivalent fuel flow rate, anode feeding steam content (2.8%), cell temperature (800 °C), and current density (250 mA/cm^2). Cathode feeding is air (300 ml/min) in each case. All the parameters concerning anode feeding and tests duration are reported in Table 5.

3. Results

In this section, experimental results are presented, while discussion follows later on. Two cells were used for the campaign. Both cells were started up with a conventional procedure, until operational temperature was reached. A preliminary performance characterization under hydrogen feeding assessed that both cells passed acceptance test. Here below in Fig. 3, the characteristic curves of the SOFC button cells used in this experimental campaign.

3.1. SOFC operation on real wood syngas: direct feeding from the downdraft gasifier

After being loaded with wood chips, the pilot gasifier worked successfully for more than one hour. Temperature was measured in several spots of the reactor, giving the following results: pyrolysis zone was in the range 660–700 °C, gasification zone in the range 720–770 °C and oxidation zone in the range 800–840 °C.

Once produced syngas had reached flow stabilization, SOFC test rig anode feeding was switched from hydrogen to wood syngas, connecting SOFC anode inlet to the impinger bottles train outflow, as it is shown in Fig. 2. After completing the fuel transition, SOFC was run successfully on real wood syngas. SOFC performances
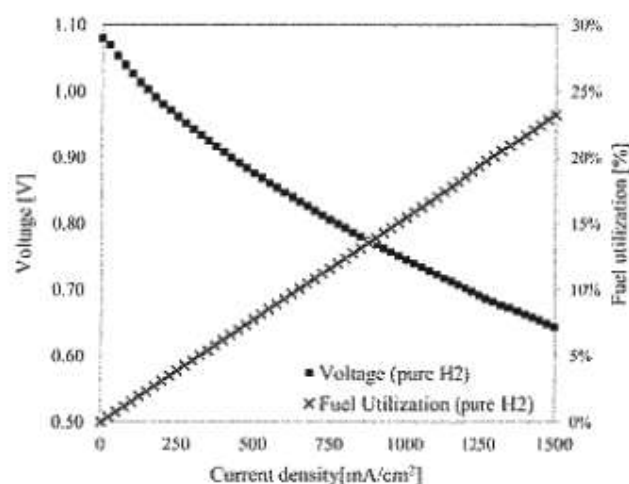

Fig. 3. SOFC button cells characteristic curves: voltage and fuel utilization vs. current density. Curves are referred to pure hydrogen feeding at the anode.

are reported in Fig. 5, in terms of voltage measured for a current density of 250 mA/cm^2. In the same figure, also wood syngas low heating value (LHV) is depicted. Online gas chromatographic analysis allowed to estimate instantaneous syngas LHV. Wood syngas composition fluctuations registered during the test with the gasifier are reported in Fig. 4, where major syngas components molar fractions are plotted against time. With regard to Fig. 5, Fig. 4 reports a wider time range. Fig. 4 horizontal axis begins at $t = 30$ min, cutting out SOFC information relative to hydrogen-to-syngas transient.

Then, real syngas supply was stopped, coping with the need to stop the gasifier operation. Consequently, the SOFC was supplied with pure hydrogen.

From Fig. 5 it is clear that during SOFC operation syngas composition had slight variations: this fact influenced cell voltage, which fluctuated between 0.804 V and 0.848 V throughout the test duration. The correlation between gas composition and cell voltage is evident, because voltage and LHV curves in Fig. 5 have almost the same shape. Imperfect overlapping is due to gas chromatograph sample injection lag, with regard to cell voltage measurement. Thus, during this short test on wood syngas, in view of an average LHV of 3.23 kJ/Nl, the average cell voltage measured was 0.826 V.

Then, from the analysis of wood syngas produced during test 1 (Fig. 4), a reference gas mixture is defined to carry out part 2 tests. Hence, basing on gas chromatographic analysis, the average wood syngas composition is determined and it is set as reference for simulated syngas. Specifically, it is H$_2$ 8%, CO 11.5%, CH$_4$ 2.5%, CO$_2$ 19% and N$_2$ 59%.

Temperature distribution in the gasifier volume was sampled with three thermocouples, placed at different levels (pyrolysis zone, gasification zone and oxidation zone). Measured values are in their expected ranges; in particular, core temperature was about 800 °C. According to the tar maturation model put forth by [22],

Table 5
Test plan: fuel compositions and test parameters. Fuel compositions are referred to dry gas prior toluene addition.

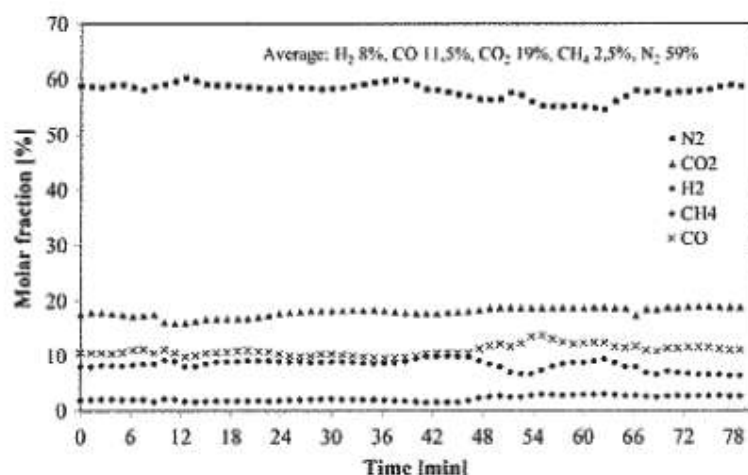| Test num.	Anode total flow rate [ml/min]	H$_2$ [%]	CO [%]	CH$_4$ [%]	N$_2$ [%]	CO$_2$ [%]	H$_{2eq}$ [ml/min]	Model tar [g/N m^3]	Duration [h]
1	300				Wood syngas from pilot gasifier				⩽1
2.1	300	8	11.5	2.5	59	19	90	0	48
2.2a	300	8	11.5	2.5	59	19	90	5	1
2.2b	300	8	11.5	2.5	59	19	90	10	1

Fig. 4. Wood syngas gas chromatographic characterization: wood syngas major components molar fraction over the time.
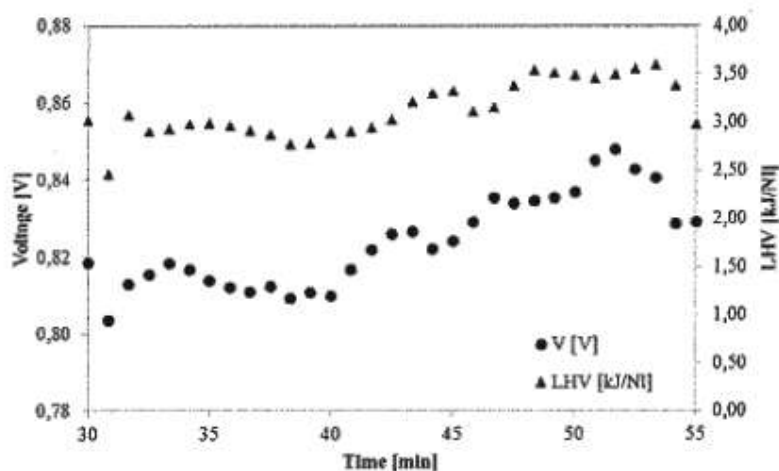

Fig. 5. SOFC operation on wood syngas (test 1): SOFC voltage for a current density of 250 mA/cm² and wood-syngas LHV over the time of the trial.

this implies the conversion of primary and secondary tars into tertiary compounds (tertiary tars are mainly aromatic compounds), thus supporting the choice of model tar toluene for tests 2.2a/2.2b.

3.2. SOFC operation on simulated clean wood syngas and simulated tar-laden wood syngas

The second part of the experimental activity was performed under simulated gas feeding; before starting the trials, anode feeding compositions (Table 5) were examined in order to predict carbon deposition occurrence at equilibrium. Thus, in Fig. 6 all compositions used alongside part 2 are plotted in a CHO diagram: all of them fall in the central part of the diagram, meaning that neither carbon deposition nor Nickel re-oxidation is expected to occur. Indeed, dots corresponding to fuel mixtures are between two boundary lines, limiting gas composition domain for SOFC safe operation at 800 °C (that is the temperature superimposed for the tests).

Before fuelling the cell with simulated syngas, anode feeding was 100% hydrogen (90 ml/min); afterwards, the other gas components were gradually added. Firstly, H_2 was diluted with N_2, which is an inert species in the electrochemical conversion;
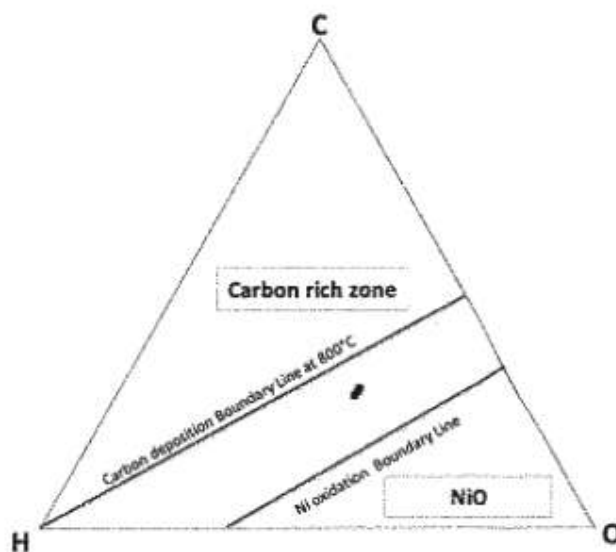

Fig. 6. CHO diagram for tests 2.1 and 2.2a/2.2b simulated syngas compositions.
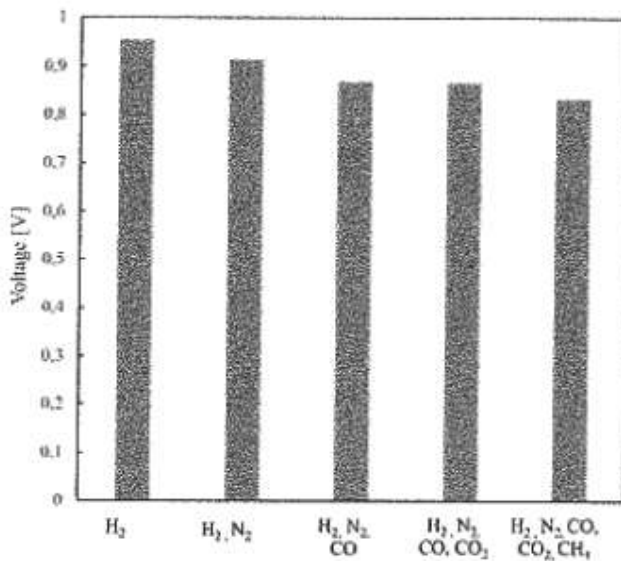
Fig. 7. Voltage measurements on different cell feeding, showing the effect of progressive gas dilution and substitution of hydrogen with carbon monoxide and methane. For all compositions, cell voltage is measured at 250 mA/cm².

Table 6
LHV and voltage during part 2 tests: 2.1, 2.2a and 2.2b.

Test no.	Syngas heating value			Cell voltage		
	LHV (kJ/Nl)	ΔLHV (kJ/Nl)	ΔLHV% (%)	Vcell (V)	ΔVcell (mV)	ΔVcell% (V)
2.1	3.19	–	–	0.828	–	–
2.2a	3.39	0.20	+6.26%	0.834	5.6	+0.67%
2.2b	3.59	0.40	+12.54%	0.842	14.0	+3.81%

Table 7
Results summary.

Specimen no.	Average voltage measured @ 250 mA/cm² (V)	Post-analysis comments
1	0.826	No degradation observed
2	0.842	No degradation observed

then, CO₂ was added, reaching a total flow of 300 ml/min at the anode inlet. While adding inert gases, H₂ flow rate was kept constant. Conversely, when CO was added to the mixture, H₂ flow rate was reduced accordingly, to keep constant the equivalent fuel flow rate. Finally, CH₄ was added to the mixture reaching the syngas composition displayed on the top of Fig. 4 (again, H₂ flow rate is reduced so as to introduce an equivalent amount of CH₄). Voltage measurements for every step are shown in Fig. 7: in particular, voltage reported in this plot is calculated as the average value measured after 30 min stabilization on any given fuel mixture. As clear from Fig. 7, experimental findings are in good agreement with theoretical calculations. After reaching the final composition for simulated syngas-fed SOFC experiments, test 2.1 began: SOFC performances resulted almost stable for 48 h and measured voltage kept around the value shown in Fig. 7.

In the final experimental tests (2.2a and 2.2b), model tar toluene was added to the simulated syngas, keeping the same syngas bulk composition used for test 2.1. At first, toluene concentration was 5 g/N m³ (2.2a), then it was set at 10 g/N m³ (2.2b) by changing the ratio between carrier nitrogen flow rate and nitrogen flow rate in the main SOFC feeding. Cell electric load was constant

and resulting voltage is depicted in Fig. 8: after stabilization of feeding line, cell voltage was 0.834 V and 0.842 V for tests 2.2a and 2.2b respectively. Cell temperature history is illustrated on the same picture.

To get a concise overview of part 2 tests outcomes, cell performance measures and anode feeding parameters are summarized in Table 6.

Before starting the 48-h test on simulated syngas (test 2.1), simulated syngas components were added gradually. With reference to Fig. 7 data, electric measurements on the cell running at 250 mA/cm² on the complete simulated syngas mixture gave a lower voltage with regard to the intermediate run without methane, albeit equivalent fuel flow rate had not changed. Since CH₄ must undergo complete reforming to supply the corresponding equivalent H₂ and CO moles, partial reforming is supposed to occur because of voltage loss registered during the last step of hydrogen-to-syngas transition. Nevertheless, voltage loss is limited if comparing the performances obtained with the complete simulated syngas mixture to the performances achieved on the simulated syngas mixture without methane (−4%). Conversely, the overall loss from hydrogen to syngas is higher (−12%) (see Table 7).

However, the simulated syngas mixture (Table 5-test 2.1) is claimed to be good for the SOFC, since performance is rather stable over the time and no quick decrease is observed. This is in agreement with thermodynamic forecast of carbon deposition (Fig. 6). After observing single component impact on cell performance, test 2.1 was successfully carried out for 48 h. The average voltage
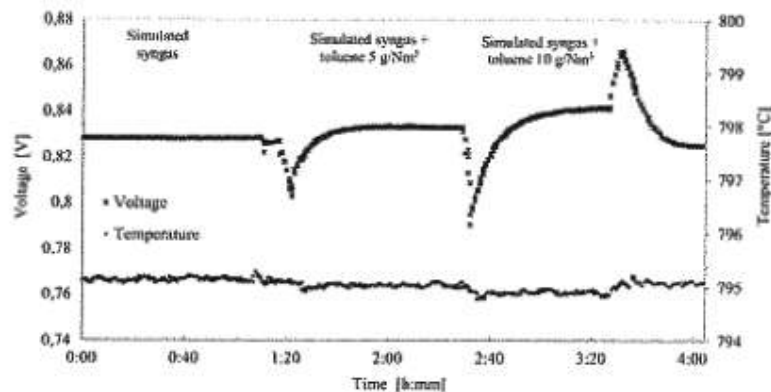

Fig. 8. Voltage and temperature experimental data throughout constant load (j = 250 mA/cm²) run on syngas (test 2.1) and toluene-enriched syngas (test 2.2a–2.2b). Current density, cell housing temperature, anode feeding overall flow rate and moisture content were kept constant for all the test duration.
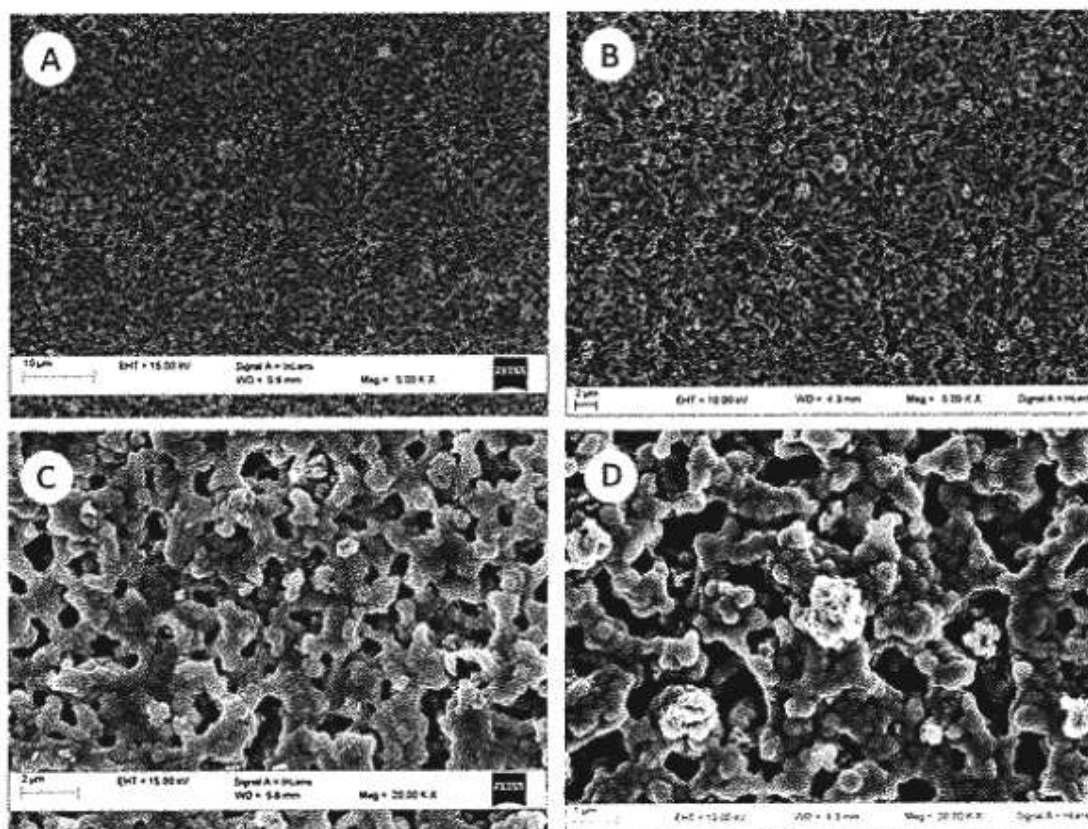
Fig. 9. SEM image of cell anode surface before and after the exposure to simulated syngas with model tar. On the left, pictures A and C are related to the specimen exposed to toluene-laden simulated syngas, while on the right, pictures B and D refer to a reference reduced NiYSZ anode.

measured for a constant current density of 250 mA/cm²) was 0.828 V, which does not differ substantially from test 1 outcome. It is recalled that during the operation on real wood syngas from the pilot gasifier, average voltage was 0.826 V. Model tar is added by means of a carrier gas. Test 2.2a and 2.2b voltage and temperature measurements are reported in Fig. 8. When the carrier gas flow rate is controlled to achieve the desired model tar concentration, cell voltage had a transient behaviour because of anode feeding line pressure variations. As soon as the pressure transient ends, cell voltage reaches stability. With regard to test 2.1 performance, cell voltage measured during test 2.2a (toluene fraction is 5 g/N m³) exhibits a slight increase (from 0.828 V to 0.834 V). Then, voltage increase (up to.842 V) is more evident in test 2.2b, when toluene concentration is risen to 10 g/N m³. By adding toluene to simulated syngas, anode feeding lower heating value grows. Even though toluene concentration is quite low, LHV gain is not negligible. All results are shown in Table 6, where anode feeding LHV and voltage variations are displayed for every test of part 2. The explanation of cell voltage increase could be found in equilibrium reactions on the anode surface. Hence, toluene decomposition is likely to take place according to the reforming path (Eq. (6)). Initial anode feeding steam-to-carbon ratio is very low, but constant load operation at 250 mA/cm² provides water which drives the reaction equilibrium towards the formation of the products.

$$C_7H_8 + 7H_2O \rightarrow 11H_2 + 7CO \qquad (6)$$

Moreover, the reforming of toluene explains temperature reduction observed during the test. Since reforming is an endothermic process, toluene decomposition to hydrogen and carbon monoxide

(Eq. (6)) acts as a heat sink, lowering temperature measured close to the cell active surface. However, temperature variations are in the range of 0.5 °C and because of that they should be considered qualitatively. Finally, while restoring simulated syngas without model tar as anode feeding, voltage decreases and temperature increases again up to their initial values.

3.2.1. Post-analysis

Short operation test 2.1 did not reveal any fast performance loss while supplying simulated syngas to the SOFC. This is true in the case of toluene-laden simulated syngas as well (tests 2.2a/2.2b). Besides simple observations based on performances measurements, in order to investigate material degradation on the microscale, SEM images of tested specimen were compared with a reference specimen. To provide a reference, a reduced NiYSZ-anode cell was analysed using the same procedure. Fig. 9 reports toluene-exposed cell SEM images on the left, while on the right there are SEM pictures of reference cell (A and C are taken at 5 k magnitude, B and D are taken at 20 k magnitude).

From SEM analysis, it resulted that no solid deposits which can be related to carbon nanotubes or graphitic carbon were observed on the anode surface (A and C, Fig. 9), especially on the central part of the specimen that was exposed directly to the fuel flow. Then, comparing images A and C with SEM image of the reference cell (B and D in Fig. 9), it appears that no change in material morphology happened.

4. Conclusions

This work investigated the coupling of a pilot downdraft gasifier with a commercial SOFC. During the first part of the experimental

activity, real wood syngas was used as fuel in the SOFC, achieving successful operation. Wood chips were the primary feedstock and gasification was performed using air as oxidizing medium. In the second part of the work, wood syngas was simulated with technical gases, reproducing the average composition observed at the gasifier outlet. The occurrence of tars on the simulated gas was considered, assuming toluene to be a good model compound and setting a toluene concentration overestimating the typical tar load of similarly produced wood syngas. Measured voltage was stable during the test, however lower than the voltage produced when the cell was fed with pure hydrogen or carbon monoxide, owing to poor heating value of the mixture, which contains a great amount of inert gases (nitrogen and carbon dioxide). Model tar increased hydrogen partial pressure at the cell anode, because of inner tar decomposition. Consequently cell performances were higher with regard to the same fuel mixture without toluene. After the exposure to simulated syngas and toluene-laden simulated syngas, no carbon deposition was observed on the commercial NiYSZ-anode cell. Hence, it can be concluded that wood syngas is suitable for SOFCs. Toluene loads slightly overestimating downdraft bio-syngas typical tar concentrations (within $10 \, g/N \, m^3$) cause a small increase in voltage (about +3.8% with regard to the same fuel mixture without tar), acting as a fuel: furthermore, they do not lead to typical deterioration mechanisms driven by high carbon content.

Thus, considering a syngas matrix similar to wood syngas from an air downdraft gasifier, tar are neither causing fast degradation, nor producing carbon deposition. It can be concluded that, after short-time exposure and within the concentration levels assumed for the current investigation, SOFC materials tolerate tars. This guarantees SOFC correct operation even in the event of tar removal failure. However, to fully understand whether tar removal could be completely avoided, longer duration tests are required.

References

[1] Al Arni Saleh, Bosio Barbara, Arato Elisabetta. Syngas from sugarcane pyrolysis: an experimental study for fuel cell applications. Renew Energy 2010;35 (1):29–35.

[2] Zhang Xiongwen, Chan SH, Li Guojun, Ho HK, Li Jun, Feng Zhenping. A review of integration strategies for solid oxide fuel cells. J Power Sources 2010;195 (3):685–702.

[3] Corradetti A, Desideri U. Analysis of biomass integrated gasification fuel cell plants in industrial CHP applications, ASME 2006 4th international conference on fuel cell science, engineering and technology. p. 605–13.

[4] Colantoni S, Corradetti A, Desideri U, Fantozzi F. Thermodynamic analysis and possible applications of the integrated pyrolysis fuel cell plant (IPFCP), in ASME turbo expo 2007: power for land, sea, and air. p. 427–36.

[5] Jia Junxi, Abudula Abuliti, Wei Liming, Sun Baozhi, Shi Yue. Thermodynamic modeling of an integrated biomass gasification and solid oxide fuel cell system. Renew Energy 2015;81:400–10.

[6] Campitelli G, Cordiner S, Gautam M, Mariani Al, Mulone V. Biomass fueling of a SOFC by integrated gasifier: study of the effect of operating conditions on system performance. Int J Hydrogen Energy 2013;38(1):320–7.

[7] Colpan C Ozgur, Hamdullahpur Feridun, Dincer Ibrahim, Yoo Yeong. Effect of gasification agent on the performance of solid oxide fuel cell and biomass gasification systems. Int J Hydrogen Energy 2010;35(10):5001–9.

[8] Aravind PV, Schilt C. Thermodynamic model of a very high efficiency power plant based on a biomass gasifier, SOFCs, and a gas turbine. Int J Renew Energy Develop 2012;1(2):51–5.

[9] Toonssen Richard, Sollai Stefano, Aravind PV, Woudstra Nico, Verkooijen Adrian HM. Alternative system designs of biomass gasification SOFC/GT hybrid systems. Int J Hydrogen Energy 2011;36(16):10414–25.

[10] Bellomare Filippo, Rokni Masoud. Integration of a municipal solid waste gasification plant with solid oxide fuel cell and gas turbine. Renew Energy 2013;55:490–500.

[11] Bang-Moller C, Rokni M. Thermodynamic performance study of biomass gasification, solid oxide fuel cell and micro gas turbine hybrid systems. Energy Convers Manage 2010;51(11):2330–9.

[12] Bain, Graham. Biomass gasification: hot gas clean-up. Technical report. Ensyn Technologies/NREL; 1993.

[13] Din Zia Ud, Zainal ZA. Biomass integrated gasification–SOFC systems: technology overview. Renew Sustain Energy Rev 2016;53:1356–76.

[14] W. Y. Lee, J. Hanna, and A. F. Ghoniem, On the predictions of carbon deposition on the nickel anode of a SOFC and its impact on open-circuit conditions. J. Electrochem. Soc., vol. 160, no. 1, pp. 94–105, 2012.

[15] Kim T, Liu G, Boaro M, Lee S-I, Vohs JM, Gorte RJ, et al. A study of carbon formation and prevention in hydrocarbon-fueled SOFC. J Power Sources 2006;155(2):231–8.

[16] Lv Pengmei, Yuan Zhenhong, Ma Longlong, Wu Chuangzhi, Chen Yong, Zhu Jingxu. Hydrogen-rich gas production from biomass air and oxygen/steam gasification in a downdraft gasifier. Renew Energy 2007;32(13):2173–85.

[17] Iaquaniello G, Mangiapane A. Integration of biomass gasification with MCFC. Int J Hydrogen Energy 2006;31(3):399–404.

[18] Hofmann Ph, Schweiger A, Fryda L, Panopoulos KD, Hohenwarter U, Bentzen JD, et al. High temperature electrolyte supported Ni-GDC/YSZ/LSM SOFC operation on two-stage Viking gasifier product gas. J Power Sources 2007;173 (1):357–66.

[19] Hofmann P, Panopoulos K, Fryda L, Schweiger A, Ouweltjes J, Karl J, et al. Integrating biomass gasification with solid oxide fuel cells: effect of real product gas tars, fluctuations and particulates on Ni-GDC anode. Int J Hydrogen Energy 2008;33(11):2834–44.

[20] Hofmann Ph, Panopoulos KD, Aravind PV, Siedlecki M, Schweiger A, Karl J, et al. Operation of solid oxide fuel cell on biomass product gas with tar levels >10 g N m⁻³. Int J Hydrogen Energy 2009;34(22):9203–12.

[21] Molino Antonio, Chianese Simeone, Musmarra Dino. Biomass gasification technology: the state of the art overview. J Energy Chem 2016;25(1): 10–25.

[22] T. A. Milne, R. J. Evans, and N. Abatzoglou, "Biomass Gasifier ' Tars": Their Nature, Formation, and Conversion," NREL technical report, Golden, Colorado, 1998.

[23] Basu P. Biomass gasification and pyrolysis: practical design and theory. Elsevier; 2010.

[24] Stevens Don J. Hot gas conditioning: recent progress with larger-scale biomass gasification systems update and summary of recent progress hot gas conditioning: recent progress with larger-scale biomass gasification systems update and summary of recent progress. Technical report; August 2001.

[25] Reed T. Handbook of biomass downdraft gasifiers engine systems. Colorado: Golden; 1998.

[26] Jayah TH, Aye Lu, Fuller RJ, Stewart DF. Computer simulation of a downdraft wood gasifier for tea drying. Biomass Bioenergy 2003;25(4):459–69.

[27] Pedroso DT, Aiello RC, Conti L, Mascia S. Biomass gasification on a new really tar free downdraft gasifier. Rev Cienc Exatas Taubaté 2005;11:59–62.

[28] Simone Marco, Barontini Federica, Nicolella Cristiano, Tognotti Leonardo. Gasification of pelletized biomass in a pilot scale downdraft gasifier. Bioresource Technol 2012;116:403–12.

[29] Mermelstein J, Millan M, Brandon NP. The impact of carbon formation on Ni-YSZ anodes from biomass gasification model tars operating in dry conditions. Chem Eng Sci 2009;64(3):492–500.

[30] Lorente E, Millan M, Brandon NP. Use of gasification syngas in SOFC: impact of real tar on anode materials. Int J Hydrogen Energy 2012;37(8):7271–8.

[31] Mermelstein Joshua, Millan Marcos, Brandon Nigel. The impact of steam and current density on carbon formation from biomass gasification tar on Ni/YSZ and Ni/CGO solid oxide fuel cell anodes. J Power Sources 2010;195 (6):1657–66.

[32] Mermelstein J, Millan M, Brandon NP. The interaction of biomass gasification syngas components with tar in a solid oxide fuel cell and operational conditions to mitigate carbon deposition on nickel-gadolinium doped ceria anodes. J Power Sources 2011;196(11):5027–34.

[33] Aravind PV, Ouweltjes JP, Woudstra N, Rietveld G. Impact of biomass-derived contaminants on SOFCs with Ni/Gadolinia-doped ceria anodes. Electrochem Solid-State Lett 2007:24–8.

[34] Hauth Martin, Lerch Werner, König Karlheinz, Karl Jürgen. Impact of naphthalene on the performance of SOFCs during operation with synthetic wood gas. J Power Sources 2011;196(17):7144–51.

[35] Liu M, Millan MG, Aravind PV, Brandon N. Influence of operation conditions on the carbon deposition of SOFC fuelled by gasified-syngas with tar included. Meet Abstr 2011;34:9212.

[36] Doyle Tygue S, Dehouche Zahir, Aravind PV, Liu Ming, Stankovic Sinisa. Investigating the impact and reaction pathway of toluene on a SOFC running on syngas. Int J Hydrogen Energy 2014;39(23):12083–91.

[37] Liu Ming, van der Kleij A, Verkooijen AHM, Aravind PV. An experimental study of the interaction between tar and SOFCs with Ni/GDC anodes. Appl Energy 2013;108:149–57.

[38] C. M. Chun, J. D. Mumford, and T. A. Ramanarayanan, Carbon-induced corrosion of nickel anode, J. Electrochem. Soc., vol. 147, no. 10, pp. 3680–3686, 2000.

[39] Namioka Tomoaki, Naruse Taichi, Yamane Ryosuke. Behavior and mechanisms of Ni/ScSZ cermet anode deterioration by trace tar in wood gas in a solid oxide fuel cell. Int J Hydrogen Energy 2011;36(9):5581–8.

[40] Namioka Tomoaki, Nagai Yuki, Yoshikawa Kunio, Min Taijin. A tolerance criterion for tar concentration in a model wood gas for a nickel/scandia-stabilized zirconia cermet anode in a solid oxide fuel cell. Int J Hydrogen Energy 2012;37(22):17245–52.

[41] Tao Jun, Lu Qiang, Dong Changqing, Du Xiaoze, Dahlquist Erik. Effects of electric current upon catalytic steam reforming of biomass gasification tar model compounds to syngas. Energy Convers Manage 2015; 100:56–63.

[42] Gai Chao, Dong Yuping, Fan Pengfei, Zhang Zhaoling, Liang Jingtui, Xu Pengju. Kinetic study on thermal decomposition of toluene in a micro fluidized bed reactor. Energy Convers Manage 2015;106:721–7.

[43] Sarker Shiplu, Nielsen Henrik Kofoed. Assessing the gasification potential of five woodchips species by employing a lab-scale fixed-bed downdraft reactor. Energy Convers Manage 2015;103:801–13.

[44] Abatzoglou N, Deutch S, Greil C, Buffinga GJ, Brage C, Suomalainen M. Guideline for sampling and analysis of tar and particles in biomass producer gases, Energy project ERK6-CT 1999–20002, 1999.

[45] Poling, Pausnitz, O'Connell. The properties of gases and liquids, 5th ed. New York: McGrawHill; 2001.
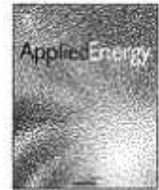
An experimental and kinetic modeling study of glycerol pyrolysis

F. Fantozzi [a], A. Frassoldati [b], P. Bartocci [a,*], G. Cinti [a], F. Quagliarini [c], G. Bidini [a], E.M. Ranzi [b]

[a] Department of Engineering, University of Perugia, Via G. Duranti 67, 06125 Perugia, Italy
[b] Politecnico di Milano, Dipartimento di Chimica, Materiali e Ingegneria Chimica, Giulio Natta, Piazza Leonardo da Vinci 32, Milano, Italy
[c] FAIST Components Spa, Via dell'Industria 2, 06014 Montone, Perugia, Italy

HIGHLIGHTS

- Glycerol pyrolysis can produce about 44–48%v hydrogen at 750–800 °C.
- A simplified 452 reactions kinetic model of glycerol pyrolysis has been developed.
- The model has good agreement with experimental data.
- Non condensable gas yields can reach 70%.

ARTICLE INFO

ABSTRACT

Pyrolysis of glycerol, a by-product of the biodiesel industry, is an important potential source of hydrogen. The obtained high calorific value gas can be used either as a fuel for combined heat and power (CHP) generation or as a transportation fuel (for example hydrogen to be used in fuel cells). Optimal process conditions can improve glycerol pyrolysis by increasing gas yield and hydrogen concentration. A detailed kinetic mechanism of glycerol pyrolysis, which involves 137 species and more than 4500 reactions, was drastically simplified and reduced to a new skeletal kinetic scheme of 44 species, involved in 452 reactions. An experimental campaign with a batch pyrolysis reactor was properly designed to further validate the original and the skeletal mechanisms. The comparisons between model predictions and experimental data strongly suggest the presence of a catalytic process promoting steam reforming of methane. High pyrolysis temperatures (750–800 °C) improve process performances and non-condensable gas yields of 70%w can be achieved. Hydrogen mole fraction in pyrolysis gas is about 44–48%v. The skeletal mechanism developed can be easily used in Computational Fluid Dynamic software, reducing the simulation time.

© 2016 Elsevier Ltd. All rights reserved.

1. Introduction

EU goals for biofuels, as set out in the RED 2009/28/EC (see mandatory goals) [1], have promoted the use and production of biodiesel. The EU Energy and Climate Change Package (CCP) became operative on April 6, 2009. The Renewable Energy Directive (RED), which is part of this package, came into effect on June 25, 2009. The CCP includes the "20/20/20" goals for 2020: a reduction of 20% in greenhouse gas (GHG) emissions compared to 1990; an improvement of 20% in energy efficiency (compared to forecasts for 2020) and a 20% share of renewable energy in the total European energy mix. Part of this last 20% share is represented by a 10% minimum target for biofuels in the transport sector to be achieved by all Member States. This percentage was slightly modified by a proposal of Indirect Land Use Change (ILUC). Given this framework, the current biofuels scenario will bring to a stable production of first generation biofuels, that will hardly increase, and a slight increase in second generation biofuels (second generation bioethanol mainly). New European targets should be still fixed.

The 2014 USDA Foreign Agriculture Service statistics [2], show that a production of biodiesel equal to 10,890 Ml was reached in Europe in 2014, this means a production of 916,000 t per year of glycerol. This product has an interesting energy content and can be used to provide heat and electricity to the same transesterification plant, as it is reported in D'Alessandro et al. [3]. The analyses proposed by Fantozzi et al. [4], Manos et al. [5] and Manos et al. [6] describe how integrating CHP technologies inside a biofuel plant is part of the "agroenergy district" promotion strategy. Authayanun et al. [7] have performed experiments feeding directly glycerol in

a high-temperature polymer electrolyte membrane fuel cell (HT-PEMFC). Beatrice et al. [8] have tested in a compression engine a bio-derivable glycerol-based ethers mixture (GEM). Besides Beatrice et al. [9] have also synthesized an oxygenated fuel additive (glycerol alkyl-ether) suitable for blending with diesel and biodiesel. Martín and Grossmann [10] have performed fermentation tests on glycerol. Nanda et al. [11] have designed and tested a continuous-flow reactor for the conversion of glycerol to solketal, through ketalization with acetone. Pedersen et al. [12] have performed hydrothermal co-liquefaction of aspen wood and glycerol with water phase recirculation.

Pyrolysis of glycerol and reforming are interesting techniques that can be used to produce hydrogen for transportation, see Wulf and Kaltschmitt [13].

Several works in literature take into account pyrolysis or gasification of glycerol. Experimental works can be classified based on reactor typology and process parameters.

Encinar et al. [14] used a cylindrical tube of stainless steel 316, set in vertical position. In the upper part of the reactor a thermocouple was used to control the temperature. A second reactor was placed under the first one, aiming at increasing the residence time of the material at a fixed reaction temperature. A solution of water and glycerol is inserted inside the reactor with the help of a pump.

In the work of Fernandez et al. [15] pyrolysis of glycerol was performed in an electrically heated furnace and in a microwave reactor. Glycerol was supplied to the upper part of the reactor through an injector, and activated charcoal was used as a catalyst for the reaction.

Peres et al. [16] have performed continuous pyrolysis tests in a steel reactor that was filled with alumina oxide. A pump used for liquid gas chromatography was employed to supply glycerol in the reactor. The reactor was heated using an electrical furnace. The produced gas was sampled in tedlar bags. Vallyiappan [17] and Vallyiappan et al. [18] used a packed fixed bed reactor full of quartz and silicon carbide, to simulate a plug flow reactor. Packing material was contained inside a plug of quartz wool, which was inserted on a supporting mesh at the center of reactor. Vallyiappan obtained interesting yields of hydrogen (about 50% in volume), performing pyrolysis at 800 °C. Baker-Hemings et al. used these sets of experimental data [19] to develop and validate a detailed kinetic model of glycerol pyrolysis.

A detailed CFD model of the above hinted reactors has never been reported in literature, for this reason this work has two main goals. One is to provide new experimental data, aimed at further validating a detailed kinetic mechanism for glycerol pyrolysis. The second goal is to develop a simplified skeletal kinetic mechanism, suitable for CFD simulations. This new and simplified skeletal mechanism, which represents a novelty in the state of the art of glycerol pyrolysis simulation, is the added value of this work and it is available in the supplementary material. The new tool can be used for reactor design and optimization.

The paper presents the analysis and optimization of an energy process (pyrolysis of glycerol), to compare its performance with other alternative processes (such as steam reforming or steam gasification), this indicates that the results presented are interesting for the scientific and technical community involved in the development of processes to produce hydrogen from glycerol and to use it in different cogeneration devices (among them fuel cells).

The originality of the work is based on a new skeletal model. This has the advantages to be enough simplified to be used in CFD modeling for reactor optimization. It is the first step in the development of a new process in which a unique reactor can reform glycerol using biochar as a catalyst and achieve an increase of biochar porosity (so partially activating it).

2. Materials and methods

All the analyses of the samples were performed at the Biomass Research Centre of the University of Perugia, see the analysis protocols described in Bidini et al. [20]. The proximate analysis of the raw materials and of the char and tar were determined using the thermogravimetric analyzer Leco TGA-701 according to the CEN/TS 14774-14775 [21,22]. The amounts of chemical elements like nitrogen, hydrogen and carbon were characterized by the Leco TruSpec CHN analyzer, according to the UNI EN 15104:2011 [23]. The calorific value of the sample and products was determined with an LECO AC-350 analyzer, according to the UNI EN 14918:2009 [24].

Pyrolysis gas composition was determined by Micro-GC 490, Varian, using a Thermal Conductivity Detector (TCD). The Micro GC includes a heated injector, backflush and Genie membrane filter to remove particles and liquids from analyzed gas samples. The Micro-GC contains two analytical modules: Molecular Sieve capillary column with Argon as carrier gas used for the analysis of CH_4, CO, H_2, O_2, N_2 and Pora Plot Q capillary column with Helium for the analysis of CO_2, C_1-C_3 gaseous species.

A batch reactor used in the laboratory of CRB was employed to perform pyrolysis (see Fig. 1). This was already described in Bartocci et al. [25], Paethanom et al. [26] and Bidini et al. [20]. It is a plant in which it was possible to perform pyrolysis of solid/liquid samples and to characterize the products from different experiments. The experimental setup used in the laboratory during this study is shown in previous works, see Bidini et al. [20]. Pyrolysis tests were carried out in a reactor with a height of 30 cm and the inner diameter of 15 cm. At the top of the reactor there is a nitrogen inlet pipe (N_2), a valve to feed the glycerol, one thermocouple connected to the P.I.D device to maintain the programmed temperature inside the reactor (T1), one thermocouple to measure the temperature inside the reactor (T2), a pressure sensor (p). The heating system is made of two semi-spherical electric heaters, each with a power of 4.8 kW.

Before the experimental test, nitrogen was fed into the reactor to remove air and create inert atmosphere conditions for the pyrolysis process. The reactor was heated from ambient temperature to 600 °C at a heating rate of about 20 °C/min. When the reactor reached the desired temperature, the sample (of a total mass of 100 g) was gradually inserted into the reactor, with an average mass flow of 3 g/min. Volatiles exited from a pipe and passed through the tar sampling line. The gas sampling line cooled the volatiles, which reached ambient temperature values. The portion
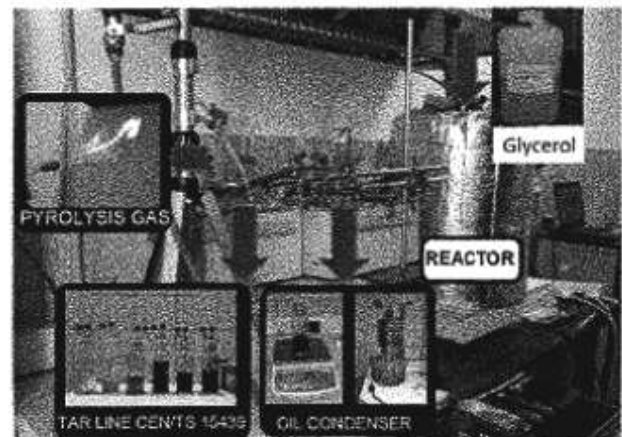

Fig. 1. Batch reactor description and tar sampling methodology.

of the non-condensable gas was sampled in Tedlar bags and analyzed in a Micro-GC 490. After 30 min the pyrolysis process was completed.

Fig. 2 reports the layout of the batch pyrolysis plant, where it is shown the DAQ (Data Acquisition) system and the position of the thermocouple used. On the left, two different sampling lines are shown: one (sampling line number 1) with a condenser, which is not filled with a solvent and separates condensable gases based on temperature decrease, another (sampling line number 2) to condense the gases in isopropanol, through adsorption and cooling. The first one was used to sample pyrogas in tedlar bags and then to measure its composition (without having traces of tars in the bags, which could harm the micro-GC). The second one was used to measure mass balance, because when the condensable gases are absorbed in isopropanol it is difficult to separate them (in fact some condensed compounds have the same temperature of evaporation of isopropanol). This means that two kinds of tests were performed: one to measure the gas composition and one to measure condensable gases and non-condensable gases masses.

In both the sampling lines presented in Fig. 2, there is no extraction pump for pyrogas, but it flows through the sampling line, due to the internal pressure of the reactor. The average charge in the reactor was about 36 mg each 22 s.

Concluding, it should be stressed that the experimental conditions of the reactor were quite close to ideal conditions, for the following reasons: the mass of the reactor is greater respect to the mass of the raw material which is fed into it; the reactor has been already heated up and has reached a steady temperature; time of reaction is very short. Another aspect which has to be taken into account is the fact that in this case a liquid biomass is used, which vaporizes in a very short period and so undergoes to pyrolysis reaction also very quickly. All these facts make an assumption of a Perfectly Stirred Reactor (PSR) reasonable. This is also a great advantage of glycerol, respect to solid biofuels.

The fact that the working conditions were quite close to ideal conditions implies that kinetics is predominant on heat transfer effect. This was an advantage in the experimental campaign. It was noticed also that the fast heating rates and the high temperatures avoid polymerization and char formation. Small quantities of char, were formed at low temperatures, but they couldn't be weighed, so it was assumed that these were not significant.

The internal heating rate can be calculated based on the average retention time of about 22 s. This implies heating rates of about 17 °C/s, 22 °C/s, 26 °C/s, 28 °C/s and 31 °C/s, respectively for temperatures of 400 °C, 500 °C, 600 °C, 650 °C and 700 °C (considering an ambient temperature of 20 °C). A fully batch test was made at the beginning of the experimental campaign. With an average heating rate, typical of the batch reactor (i.e. 20 °C/min), the result was to have glycerol evaporation, instead of its pyrolysis. For this reason, it was chosen to heat up the reactor and then to insert glycerol in an already heated environment. In this case, the reactor can be used in a continuous way and can be directly coupled to an internal combustion engine or a fuel cell. This is another advantage of glycerol pyrolysis if compared with biomass pyrolysis.

Char yield (CY) is expressed as the weight ratio between the solid residue (SR) and the raw material (RM). Gas yield (GY), always referred to the raw material, was measured by the flowmeter and converted in mass knowing the gas composition and its exit temperature. Finally, Tar Yield (TY) is simply obtained by difference. Control tests were performed to check data obtained, using a condenser to control the results on tar.

In literature there are different methods for tar sampling, some have been presented by Paethanom et al. [26], Phuphuakrat et al. [27] and Michailos and Zabaniotou [28]. In this study, the sampling line was designed on the basis of CEN/TS 15439:2006 [29]. Volatiles produced by pyrolysis passed through a series of six impinger bottles where tar is collected by condensation and absorption. The last bottle is empty. The total volume of isopropyl alcohol used as sampling solvent in the first five bottles is 500 ml (100 ml on the each bottle). The series of impinger bottles was placed in two separate baths. Bottles 1, 2 and 3 are placed in an electrically heated water bath at +35 °C, while bottles 4, 5 and 6 are cooled with NaCl/ice eutectic mixture in a proportion of 3:1 to obtain −20 ± 1 °C. It took about 15 min to reach final temperature. The sampling train was connected with a gas flow meter. After the test all the content of impinger bottles was gathered in a unique flask and evaporated with a rotary evaporator, to separate the solvent from tar in accordance with CEN/TS 15439:2006 [29]. The residue in the flask was weighed to determine the quantity of gravimetric tar. Tar or biooil produced from glycerol pyrolysis was measured both using the above mentioned tar line and a condenser. The advantage of using the condenser was to avoid tar mixing with iso-

LEGENDA:
1- GLYCEROL INLET 2- ELECTRICAL HEATERS 3- THERMOCOUPLES 4- REACTOR 5- INERT GAS (N₂)
6- DATA ACQUISITION SYSTEM 7- PRESSURE SENSOR 8- IMPINGERS - HOT BATH
9- IMPINGERS - COLD BATH 10- FLOW METER 11- GAS SAMPLING BAG
12- THERMOCOUPLE (GAS OUTLET) 13- CONDENSER

Fig. 2. Gas sampling procedures (left) and batch pyrolysis plant layout (right).

ANALYSIS PROCEDURE

Fig. 3. Pyrolysis products characterization methodology.

Table 1
Glycerol characterization.

	Pure glycerol	Standard deviation
Moisture (%w)	0	0.3
Ash (%w)	0	0.2
Volatiles (%w)	100	0.5
Fixed carbon (%w)	0	0.1
HHV (kJ/kg)	19,000	515
Carbon (%w)	39.13	0.3
Hydrogen (%w)	8.70	0.1
Nitrogen (%w)	–	0.05
Oxygen (%w)	52.17	0.3

In Fig. 4 a bar chart reporting mass yields of non-condensable and condensable gases is shown, being the production of a solid fraction negligible, the mass balance is closed by the two gaseous components.

The standard deviation of gas composition and gas yields values is due to the difficulty of the experimental apparatus to regulate precisely the mass flow of glycerol inside pyrolysis reactor; this implies a slight variation in residence time.

4. Kinetic scheme and numerical methods

4.1. Numerical methods

The software DSMOKE, developed by the CRECK modeling group of the Politecnico di Milano, was used for the simulation reported in this work. It is an easy platform to launch a simulation using detailed kinetic schemes developed and available online in [30]. An isothermal PSR reactor was assumed and simulations were performed at different temperatures between 823 K and 1073 K. Once reaction temperature was fixed, the effective residence time of reactants inside the reactor volume (5 l) was evaluated accounting for the mass flow of glycerol inserted into the reactor (3 g/min) and an effective and average density of reacting mixture.

4.2. Glycerol pyrolysis modeling

The major radical reaction steps in the pyrolysis of glycerol are the initiation and the H-abstraction reactions, which refer to the different types of hydrogen atoms available in the glycerol molecule. As already discussed by Barker-Hemings et al. [19], molecular dehydrations are interesting reaction pathways as well. Fig. 5 summarizes both these radical and molecular reaction paths. The primary propagation reactions of glycerol, coupled with a general kinetic scheme of hydrocarbon pyrolysis and oxidation (Ranzi et al. [30]), were also tested against several sets of experimental data, offering good agreement between predicted and measured values.

Fig. 6 shows the concentration profiles of the major species involved in the reaction system. Acetol and 3-hydroxypropanal are very reactive intermediates rapidly decomposing to form the most stable species, such as acetaldehyde and acrolein. Successive pyrolysis of these species further contributes to syngas formation. CO and H_2 profiles clearly indicate that they are only successive decomposition products.

The overall kinetic scheme POLIMI_BIO1407, already validated by Barker-Hemings et al. [19], used in these simulations is constituted by 137 species and 4500 reactions and it is not adequate for CFD simulations. For this reason, it is necessary to develop a reduced mechanism that can be used for this purpose.

4.3. Development of a skeletal scheme of glycerol pyrolysis

The skeletal kinetic scheme of glycerol pyrolysis has been obtained with the RFA (Reacting Flux Analysis), successively com-

propanol. Fig. 3 shows pyrolysis products characterization methodology.

As already mentioned, pyrogas is collected in tedlar bags and analyzed with a micro-GC 490, Varian. Tar is sampled both using a tar line and a condenser. In a first test, the tar line is used to absorb all the tar and avoid it going in the tedlar bags, in this way the microGC is protected. In a second test, it was used a condenser to collect all the tar in purity, without mixing it with the isopropanol contained in the tar line. Then tar was characterized using a thermogravimetric balance to perform proximate analysis an LECO Truespec CHN analyser and a bomb calorimeter. No important quantities of char were found inside the reactor after the tests. All tests were performed in triplicate.

3. Experiments: glycerol pyrolysis in a batch reactor

3.1. Glycerol characterization and pyrolysis experimental tests

The results of pure glycerol characterization analysis (see Table 1) show that it has a slightly higher LHV, compared to biomass and a similar concentration of carbon, hydrogen, and oxygen. Hydrogen content is also a little higher.

The results of pyrolysis tests are shown in Table 2. It can be seen that increasing temperature non-condensable gas yield increases, especially for temperatures higher than 500 °C. Table 2 also shows the composition of non-condensable gases, always as a function of the pyrolysis temperature. Hydrogen concentration increases with the increase of temperature, carbon monoxide, and carbon dioxide concentrations decrease, while methane has a nearly constant behavior. Ethylene concentration decreases also with the increase of temperature.

Table 2
Yields of condensable and non-condensable gases and molar gas compositions.

	400 °C		500 °C		600 °C		650 °C		700 °C	
	Yields	Standard deviation	Yields	Standard deviation	Yields	Standard deviation	Yields	Standard deviation	Yields	Standard deviation
Non condensable gas yields (%w)	**19**	1.1	**51**	1.5	**60**	1.3	**63**	1.4	**67**	2
Condensable gas yields (%w)	**81**	1.8	**49**	1.6	**40**	2.1	**37**	1.2	**33**	1.1
Molar gas composition (%v)										
H_2	**15**	2.1	**18**	2.3	**25**	2.1	**30**	2.7	**35**	2.5
CO	**45**	2.8	**45**	2.5	**42**	2.3	**40**	1.9	**39**	2.3
CO_2	**10**	1.1	**7**	0.9	**3**	0.5	**3**	0.2	**2**	0.1
CH_4	**12**	3.2	**14**	3.1	**16**	2.8	**15**	2.5	**15**	2.1
C_2H_4	**18**	2.5	**16**	2.3	**14**	2.1	**12**	1.5	**9**	1.2
TOT	**100**	–	**100**	–	**100**	–	**100**		**100**	

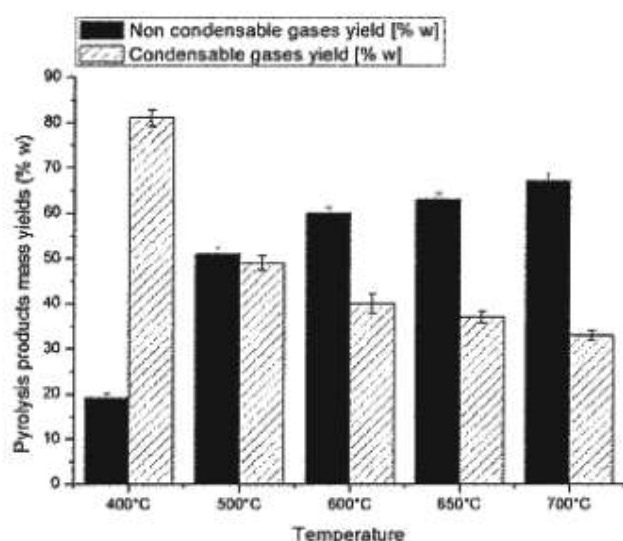Bold numbers indicate pyrolysis product yields.

Fig. 4. Bar chart reporting pyrolysis products yields.

plemented with a sensitivity analysis by Stagni et al. [31]. The RFA reduction technique analyses the behavior of the original mechanism in ideal reactors. The importance of each species is evaluated according to the production and consumption rates throughout the whole reactor. The total fluxes of each reactor are then normalized with respect to the local maximum value, and according to the required size and precision of the reduced mechanism, only the first *n* species are kept in the skeletal model. The reduced kinetic scheme of glycerol pyrolysis, derived from the whole POLIMI_-BIO1407 mechanism, is constituted by only 44 species reported in Table 3 and is thus suitable for CFD simulations. This skeletal kinetic scheme, involving 452 elementary and lumped reactions, is reported in the Supplemental Material of this paper, where 4 files are proposed with the following extensions: CKI, NAM, CKT, TRC; indicating respectively the kinetic scheme, the nomenclature, the thermodynamic data and the species transport data.

5. Validation of the model: comparison with experimental data

As already mentioned, Stein et al. [32] studied the pyrolysis of glycerol in steam using a tubular, laminar flow quartz reactor. Table 4 reports a comparison between these experimental results and the predicted values obtained with both POLIMI_BIO1407 and the new skeletal mechanism proposed in this work. It is possible to observe that the predictions of the two mechanisms are very

similar and in good agreement with experimental data. The kinetic mechanisms are able to characterize the effect of the temperature on the conversion of glycerol and also to predict the yields of the different products. As already discussed by Barker-Hemings et al. [19], and shown in Fig. 6, the major species obtained in glycerol pyrolysis are acrolein and acetaldehyde. Moreover, the deviation observed between experimental measurements and model predictions for CO and H_2 could be explained assuming the complete decomposition of formaldehyde, which was not experimentally detected.

Valliyappan [17] studied the pyrolysis of glycerol at various temperatures (650–800 °C) and varying flow rates (30–70 ml/min) in a tubular reactor using different packing materials. The major observed product was syngas with traces of CO_2, CH_4, and C_2H_4. Table 5 shows a comparison between the predictions of the kinetic mechanisms and the measured values. In this case, too, the skeletal scheme provides predictions very close to the ones of the detailed model and in good agreement with the experimental results, especially at low temperatures.

The major deviation for CH_4 and C_2H_4 at 800 °C suggests that their decomposition is not accounted for in the kinetic scheme. Moreover, the increase in the syngas yield also suggests that the steam reforming of methane and ethylene may occur within the reactor. A possible explanation for this discrepancy is supported by a thermodynamic equilibrium calculation, which indicates that at 800 °C the stable products in the system are CO and H_2, whereas methane and other hydrocarbons should decompose. This reactivity cannot be explained by a gas phase reaction at these temperatures. As already discussed by Barker-Hemings et al. [19], experimental evidence of analogous concerted heterogeneous–homogeneous processes are reported in literature Donazzi et al. [33]. Similar effects were also observed in the study of other oxygenated fuels (ethanol and methyl formate) by Lefkowitz et al. [34]. A catalytic effect inside the reactor could promote these steam reforming reactions of methane and justify the lack of reactivity:

$$CH_4 + H_2O \rightarrow CO + 3H_2 \tag{1}$$

In a similar way, it is possible to expect some catalytic interactions between ethylene and steam to form oxygenated species, here simply assumed as ethanol.

$$C_2H_4 + H_2O \rightarrow C_2H_5OH \tag{2}$$

Table 5 also presents the final product distribution obtained by simply including in the skeletal kinetic scheme the two apparent catalytic reactions. Results show a more satisfactory agreement with the experimental data also at high temperatures.

Fig. 7 shows a satisfactory comparison of experimental measurements of Valliyappan et al. [17] and model simulations in
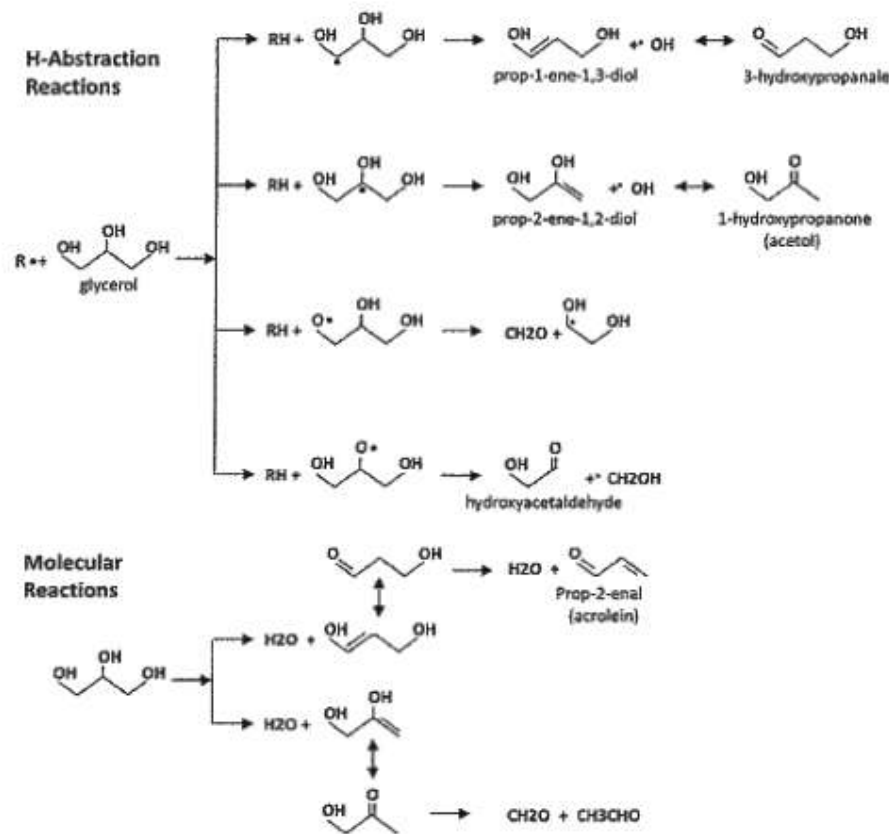
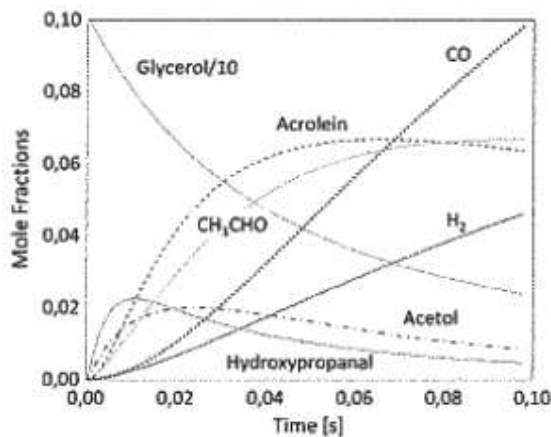Fig. 5. Primary reactions of glycerol pyrolysis.

Fig. 6. Primary and successive reaction products of glycerol pyrolysis at 700 °C and 1 atm (model predictions).

terms of total gas and liquid yields. The carbonaceous residue found experimentally is probably due to the successive polymerization of tar products that stick to the packing materials within the reactor. Acrolein, for instance, is well known for its polymerization propensity. These phenomena are not included in the gas phase kinetic scheme. These reactions have a negligible effect on the total gas and liquid mass yields but increase significantly the syngas production at high temperature, as already shown in Table 5.

Kawasaki and Yamane [35] studied the effect of reaction temperature of the pyrolysis of reagent glycerol in N_2 inside a quartz flow reactor at atmospheric pressure. Fig. 8 shows a comparison between these experimental measurements and model predictions. Since glycerol is injected as a liquid, the residence time in the plug flow reactor simulation is assumed to be a fraction (50%) of the nominal residence time reactor to take into account the non ideal behavior of the system. It is possible to observe that the model is able to predict the effect of temperature on the gas conversion efficiency and on the relative yields of the major gas

Table 3
List of species contained in the skeletal mechanism for glycerol pyrolysis studied in this work.

N_2	O_2	H	OH	H_2	H_2O	CO	CO_2
HCO	CH_2O	CH_3	CH_2OH	CH_3O	CH_4	CH_3OH	C_2H_2
CH_2CO	$C_2H_2O_2$	C_2H_3	CH_3CO	C_2H_4	CH_3CHO	$C_2H_4O_2$	C_2H_5
C_2H_4OH	C_2H_6	C_2H_5OH	C_2H_3CHO	C_3H_6	C_2H_5CHO	ACETOL	$C_3H_6O_2$
C_3H_8	GLYCEROL	C_4H_4	C_4H_8	SC_4H_7	$CH_2C_3H_4$	CYC_5H_5	CYC_5H_6
C_5H_7	C_6H_6	C_7H_7	C_7H_8				

Table 4
Pyrolysis of glycerol in steam at 650, 700 °C and atmospheric pressure. Comparison between the complete kinetic mechanism of Barker-Hemings et al. [19], the skeletal model of glycerol pyrolysis and the experimental data of Stein et al. [32].

Temperature	650 °C			700 °C			
	Exp. This work	Predicted Detailed bio1407	Predicted Skeletal mechanism	Exp. Stein et al. [32]	Exp. This work	Predicted Detailed bio1407	Predicted Skeletal mechanism
Glycerol (mol%)	1.69	1.69	1.69	1.04	1.04	1.04	1.04
Conversion (%)	17.6	18	18.2	25	24	23.8	24
Residence time (s)	0.13	0.13	0.13	0.048	0.05	0.05	0.05
Products yield (%)							
CO	30	38	38	58	35	40	40
CO_2	3	4	4	1	2	4	4
Hydrogen	40	29	29	44	39	29	29
Methane	15	9	9	11	15	10	10
Ethylene	12	19	19	17	9	17	17

Table 5
Effect of temperature on gas product composition during pyrolysis of glycerol at carrier gas flow rate 50 ml/min and atmospheric pressure. Experimental data of Valliyappan [17].

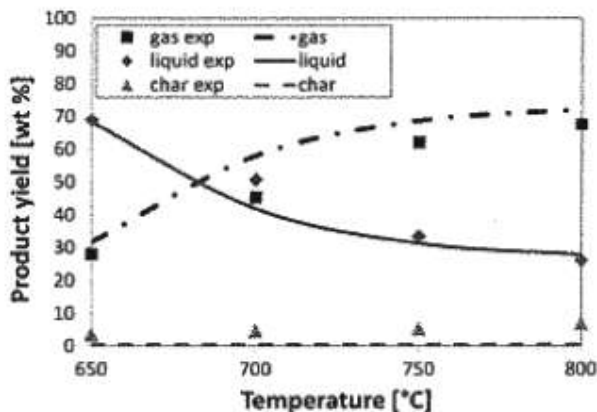| Temperature	650 °C		800 °C		
Species (dry mol%)	Valliyappan [17]	Skeletal scheme	Valliyappan [17]	Skeletal scheme	Skeletal (including catalytic effect)
H_2	17	19.0	48.6	23.9	37.7
CO	54	46.5	44.9	45.8	45.5
CO_2	0.2	2.6	1	2.5	1.7
CH_4	14.2	16.2	3.3	16.1	8.2
C_2H_4	10.1	11.4	2	9.4	4.8
C_2H_6	2.2	2.4	0.1	0.7	0.6
C_3H_6	2.4	0.0	0.1	0.2	0.1
$H_2 + CO$	71	65.5	93.5	69.7	83.1

Fig. 7. Effect of temperature on product yields during pyrolysis of glycerol at an effective residence time of 1.2 s and 1 atm. Symbols are experimental data taken from Valliyappan [17], model predictions of the skeletal kinetic model are the lines.
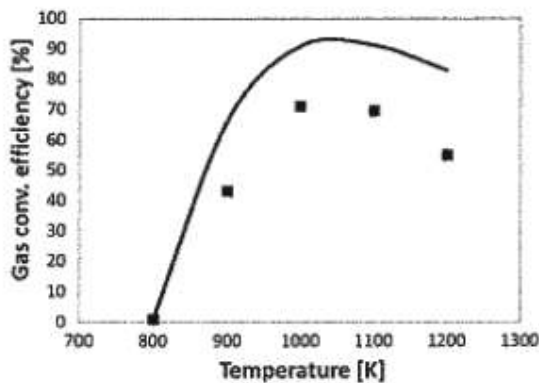
phase species. The gas conversion efficiency is defined by the authors [35] using the measured molar flow rates:

$$\eta_{gas} = (\dot{n}_{CO} + \dot{n}_{CO_2} + \dot{n}_{CH_4} + 2\dot{n}_{C_2H_4} + 2\dot{n}_{C_2H_6})/3\dot{n}_{Glycerol} \qquad (3)$$

The increasing formation of acetylene, C4 species and aromatics explains the reduction of the efficiency moving towards higher temperatures. The formation of gases and syngas, in particular, tends to be overestimated by the model. This deviation is the opposite of the one already discussed in Table 5.

6. Discussion

It is important in this section to present the comparison between the performances of glycerol pyrolysis and glycerol steam gasification. In fact, both the processes can be used to produce hydrogen [36–38]. As it can be seen from Tables 2, 4 and 5 in this paper, hydrogen production through pyrolysis (in a non-catalyzed environment) has acceptable yields only at temperatures above
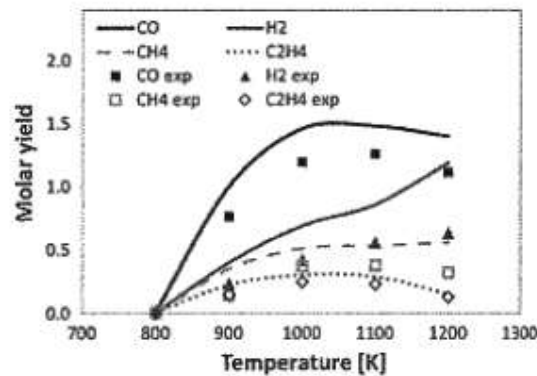

Fig. 8. Effect of temperature on gaseous product yields during pyrolysis of glycerol at 1 atm and an effective time equal to half of the nominal residence time in the flow reactor. Symbols are experimental data taken from [35]. Lines represent model predictions of the skeletal kinetic scheme.

Table 6
Comparison between the energy performance of pyrolysis and steam gasification of glycerol.

Parameter		Pyrolysis at 800 °C [17]	Steam gasification at 800 °C [17]
Gas conversion		67.3%w	90.60%w
Average gas composition	H_2	48.6%v	58.90%v
	CO	44.9%v	30.30%v
	CO_2	1.0%v	4.40%v
	CH_4	3.3%v	4.80%v
Gas higher heating value		18,600 kJ/kg	21,500 kJ/kg
Energy required	Steam	/	3,943 kJ/kg
	Glycerol	5,950 kJ/kg	2,625 kJ/kg
	Total	5,950 kJ/kg	6,568 kJ/mol
Net energy gain (kJ/kg glycerol)		6,568 kJ/kg	12,911 kJ/kg
Ratio between energy in input and energy in output (referred to 1 kg of raw material)		0.50	0.76

700–800 °C. To compare pyrolysis performances with those of steam gasification of glycerol, two energetic indexes were chosen: the net energy gain and the process efficiency.

The net energy gain is defined in Eq. (4):

$$NEG = HHVgas * GY - ER \qquad (4)$$

where NEG represents the Net Energy Gain (expressed in kJ/kg glycerol), HHVgas represents the Higher Heating Value of pyrolysis Gas (expressed in kJ/kg), GY represents pyrogas yield (expressed in mass fraction) and ER is the Energy Required to promote pyrolysis or gasification processes (expressed in kJ/kg of glycerol). The process efficiency is defined in Eq. (5):

$$PE = HHVgas * GY/(HHVgl + ER) \qquad (5)$$

where PE represents Process Efficiency (a dimensionless quantity), HHVgas, ER and GY have been already explained, HHVgl is the Higher Heating Value of glycerol (expressed in kJ/kg). The results of the calculation of the two indexes are proposed in Table 6.

It can be seen from Table 6 that: the net energy gain of the steam gasification process is almost twice that of pyrolysis. Besides the efficiency of the steam gasification process (given by the ratio of the energy in output and the energy in input) is about 0.76 while pyrolysis has an efficiency of 0.50. If the gas will be used in fuel cells this efficiency should be multiplied by the efficiency of the fuel cell itself. These results imply that more efficient pyrolysis processes are needed, which can compete with reforming and steam gasification.

An optimized pyrolysis process should:

– introduce a packed bed of biochar to improve volatile yields and their cracking reactions and so hydrogen production;
– in this way, on the one hand, the biochar produced from pyrolysis of biomasses will work as a catalyst;
– on the other hand, it is very probable that using mixtures of glycerol and water as feed material, these will increase biochar bed porosity by flowing through it.

The possibility to use char as a catalyst to promote volatiles cracking is shown by several works and among them those of Prof. Kunio Yoshikawa and coworkers, see [39–42]. New pyrolysis processes are in development, as shown in [43]. Water-glycerol mixtures can be a promising material to be used in thermal processes, see [44]. In this way, pyrolysis can become competitive, also compared to the reforming process. Eventually, pyrolysis can be also coupled with steam reforming to improve its performance, see [45]. This is also confirmed by the latest progress on pyroreforming or Thermo-Catalytic Reforming, see [46].

7. Conclusions

Glycerol pyrolysis can be a relevant process to produce hydrogen to be used either as a biofuel for transport purposes or in CHP. Several plants have been proposed to pyrolyze glycerol (fixed beds, pyro-reforming plants, etc.) and a zero dimensional model for glycerol pyrolysis has been already developed. In this study, a skeletal kinetic model of glycerol pyrolysis is developed and it allows possible CFD applications for plant optimization and scale up. This is an added value, with respect to the state of the art of pyrolysis modeling, as recently shown by Anca-Couce [47]. Starting from a detailed kinetic mechanism of more than 4500 reactions involving 137 species, a significant reduction was obtained through the RFA (Reaction Flux Analysis) and the skeletal model simply involves 44 species. The predictions of the skeletal and detailed mechanisms are very similar and in a reasonable agreement with experimental data. The agreement of model predictions improves with the increase of pyrolysis temperature. The new experimental data confirm the increase of non-condensable gases yields, particularly of hydrogen, with the increasing temperatures. Model predictions also confirm that gas yields of 70%w can be achieved at 750–800 °C, with hydrogen concentrations up to 44–48%v. These results don't show still an advantage of the pyrolysis process on reforming or steam gasification, because they can achieve yields of gasses above 90%w; so further research will be done on catalytic pyrolysis processes.

Appendix A. Supplementary material

Supplementary data associated with this article can be found, in the online version, at http://dx.doi.org/10.1016/j.apenergy.2016.10.018.

References

[1] Directive 2009/28/EC of the European Parliament and of the Council of 23 April 2009 on the promotion of the use of energy from renewable sources. Off J Eur Union. <http://eur-lex.europa.eu/legal-content/EN/ALL/?uri=CELEX:32009L0028> [accessed 17/09/2016].
[2] USDA Foreign Agriculture Service. Gain Report number: NL4025, EU Biofuels Annual 2014. <http://gain.fas.usda.gov/Recent%20GAIN%20Publications/Biofuels%20Annual_The%20Hague_EU-28_7-3-2014.pdf> [accessed 7/1/2015].

[3] D'Alessandro B, Bartocci P, Fantozzi F. Gas turbines CHP for bioethanol and biodiesel production without waste streams. Proceedings of ASME turbo expo, vol. 1. p. 691–700.

[4] Fantozzi F, Bartocci P, D'Alessandro B, Arampatzis S, Manos B. Public-private partnerships value in bioenergy projects: economic feasibility analysis based on two case studies. Biomass Bioenergy 2014;66(July):387–97.

[5] Manos B, Partalidou M, Fantozzi F, Arampatzis S, Papadopoulou O. Agro-energy districts contributing to environmental and social sustainability in rural areas: evaluation of a local public-private partnership scheme in Greece. Renew Sustain Energy Rev 2014;29:85–95.

[6] Manos B, Bartocci P, Partalidou M, Fantozzi F, Arampatzis S. Review of public-private partnerships in agro-energy districts in Southern Europe: the cases of Greece and Italy. Renew Sustain Energy Rev 2014;39(November):667–78.

[7] Authayanun S, Mamlouk M, Scott K, Arpornwichanop A. Comparison of high-temperature and low-temperature polymer electrolyte membrane fuel cell systems with glycerol reforming process for stationary applications. Appl Energy 2013;109:192–201. doi: http://dx.doi.org/10.1016/j.apenergy.2013.04.009.

[8] Beatrice C, Di Blasio G, Guido C, Cannilla C, Bonura G, Frusteri F. Mixture of glycerol ethers as diesel bio-derivable oxy-fuel: impact on combustion and emissions of an automotive engine combustion system. Appl Energy 2014;132:236–47. doi: http://dx.doi.org/10.1016/j.apenergy.2014.07.006.

[9] Beatrice C, Di Blasio G, Lazzaro M, Cannilla C, Bonura G, Frusteri F, et al. Technologies for energetic exploitation of biodiesel chain derived glycerol: oxy-fuels production by catalytic conversion. Appl Energy 2013;102:63–71. doi: http://dx.doi.org/10.1016/j.apenergy.2012.08.006.

[10] Martin M, Grossmann IE. Design of an optimal process for enhanced production of bioethanol and biodiesel from algae oil via glycerol fermentation. Appl Energy 2014;135:108–14. doi: http://dx.doi.org/10.1016/j.apenergy.2014.08.054.

[11] Nanda MR, Yuan Z, Qin W, Ghaziaskar HS, Poirier MA, Xu CC. A new continuous-flow process for catalytic conversion of glycerol to oxygenated fuel additive: catalyst screening. Appl Energy 2014;123:75–81. doi: http://dx.doi.org/10.1016/j.apenergy.2014.02.055.

[12] Pedersen TH, Grigoras IF, Hoffmann J, Toor SS, Daraban IM, Jensen CU, et al. Continuous hydrothermal co-liquefaction of aspen wood and glycerol with water phase recirculation. Appl Energy 2016;162:1034–41. doi: http://dx.doi.org/10.1016/j.apenergy.2015.10.165.

[13] Wulf C, Kaltschmitt M. Life cycle assessment of biohydrogen production as a transportation fuel in Germany. Bioresour Technol 2013;150:466–75.

[14] Encinar JM, Gonzalez JF, Martinez G, Sanchez N, Sanguino IM. Hydrogen production by means pyrolysis and steam gasification of glycerol. In: International conference on renewable energies and power quality. Las Palmas de Gran Canaria (Spain): 13–15 Aprile 2010.

[15] Fernandez Y, Arenillas A, Diez MA, Pis JJ, Menendez JA. Pyrolysis of glycerol over activated carbons for syngas production. J Anal Appl Pyrol 2009;84:145–50.

[16] Peres APG, de Lima DR, de Lima da Silva N, Wolf Maciel MR. Syngas production and optimization from glycerol pyrolysis. Int Rev Chem Eng – Rapid Commun 2010;2(2):305.

[17] Valliyappan T. Hydrogen or syngas production from glycerol using pyrolysis and steam gasification processes. A Thesis Submitted to the College of Graduate Studies and Research in partial fulfillment of the requirements for the degree of Master of Science in the Department of Chemical Engineering University of Saskatchewan Saskatoon, Saskatchewan; 2004.

[18] Valliyappan T, Bakhshi NN, Dalai AK. Pyrolysis of glycerol for the production of hydrogen or syngas. Bioresour Technol 2008;99:4476–83.

[19] Barker-Hemings E, Cavallotti C, Cuoci A, Faravelli T, Ranzi E. A detailed kinetic study of pyrolysis and oxidation of glycerol (propane-1,2,3-triol). Combust Sci Technol 2012;184(7–8):1164–78.

[20] Bidini G, Fantozzi F, Bartocci P, D'Alessandro B, D'Amico M, Laranci P, et al. Recovery of precious metals from scrap printed circuit boards through pyrolysis. J Anal Appl Pyrol 2015;111:140–7.

[21] UNI 14774-2:2010 Solid biofuels – determination of moisture content – OvenDry method – Part 2: Total moisture – simplified method. Rome (Italy): Italian Organization for Standardization.

[22] UNI 14775:2010 Solid biofuels – determination of ash content. Rome (Italy): Italian Organization for Standardization.

[23] UNI 15104:2011 Solid biofuels. Determination of total content of carbon, hydrogen and nitrogen. Instrumental methods. Rome (Italy): Italian Organization for Stan-dardization.

[24] UNI 14918: Solid biofuels – determination of calorific value. Rome (Italy): Italian Organization for Standardization.

[25] Bartocci P, Slopiecka K, Testarmata F, D'Amico M, Moriconi N, Fantozzi F. Batch pyrolysis reactor: design. Proceedings of the 20th European biomass conference and exhibition. Milan, Italy, 2012.

[26] Paethanom A, Bartocci P, D'Alessandro B, D'Amico M, Testarmata F, Moriconi N, et al. A low-cost pyrogas cleaning system for power generation: scaling up from lab to pilot. Appl Energy 2013;111:1080–8.

[27] Phuphuakrat T, Namioka T, Yoshikawa K. Tar removal from biomass pyrolysis gas in two-step function of decomposition and adsorption. Appl Energy 2010;87:2203–11.

[28] Michailos S, Zabaniotou A. Simulation of olive kernel gasification in a bubbling fluidized bed pilot scale reactor. J Sustain Bioenergy Syst 2012;2:145–59.

[29] CEN/TS 15439:2006. Biomass gasification. Tar and particles in product gases. Sampling and analysis.

[30] Ranzi E, Frassoldati A, Grana R, Cuoci A, Faravelli T, Kelley AP, et al. Hierarchical and comparative kinetic modeling of laminar flame speeds of hydrocarbon and oxygenated fuels. Prog Energy Combust Sci 2012;38:468–501. BIO_1311 mechanism, available at: <http://creckmodeling.chem.polimi.it/>.

[31] Stagni A, Cuoci A, Frassoldati A, Faravelli T, Ranzi E. A fully coupled, parallel approach for the post-processing of CFD data through reactor network analysis. Comput Chem Eng 2014;60(10):197–212.

[32] Stein YS, Antal MJ, Jones M. A study of the gas-phase pyrolysis of glycerol. J Anal Appl Pyrol 1983;4(4):283–96.

[33] Donazzi A, Livio D, Maestri M, Beretta A, Groppi G, Tronconi E, et al. Synergy of homogeneous and heterogeneous chemistry probed by in situ spatially resolved measurements of temperature and composition. Angew Chem Int Ed 2011;50(17):3943–6.

[34] Lefkowitz JK, Heyne JS, Won SH, Dooley S, Kim HH, Haas FM, et al. A chemical kinetic study of tertiary-butanol in a flow reactor and a counterflow diffusion flame. Combust Flame 2012;159:968–78.

[35] Kawasaki K, Yamane K. Thermal decomposition of waste glycerol. In: Proceedings of the international conference on power engineering-09 (ICOPE-09): November 16–20, 2009, Kobe, Japan.

[36] Authayanun S, Mamlouk M, Scott K, Arpornwichanop A. Comparison of high-temperature and low-temperature polymer electrolyte membrane fuel cell systems with glycerol reforming process for stationary applications. Appl Energy 2013;109:192–201.

[37] Park D, Lee C, Ju Moon D, Kim T. Novel macro-micro channel reactor for reforming glycerol produced from biodiesel productions. Energy Proc 2014;61:2075–8.

[38] Guo Y, Azmat MU, Liu X, Wang Y, Lu G. Effect of support's basic properties on hydrogen production in aqueous-phase reforming of glycerol and correlation between WGS and APR. Appl Energy 2012;92:218–23.

[39] Shen Y, Zhao P, Shao Q, Takahashi F, Yoshikawa K. In situ catalytic conversion of tar using rice husk char/ash supported nickel–iron catalysts for biomass pyrolytic gasification combined with the mixing-simulation in fluidized-bed gasifier. Appl Energy 2015;160:808–19.

[40] Shen Y, Chen M, Sun T, Jia J. Catalytic reforming of pyrolysis tar over metallic nickel nanoparticles embedded in pyrochar. Fuel 2015;159:570–9.

[41] Shen Y, Wang J, Ge X, Chen M. By-products recycling for syngas cleanup in biomass pyrolysis – an overview. Renew Sustain Energy Rev 2016;59:1246–68.

[42] Shen Y. Chars as carbonaceous adsorbents/catalysts for tar elimination during biomass pyrolysis or gasification. Renew Sustain Energy Rev 2015;43:281–95.

[43] Shirazi Y, Viamajala S, Varanasi S. High-yield production of fuel- and oleochemical-precursors from triacylglycerols in a novel continuous-flow pyrolysis reactor. Appl Energy 2016;179:755–64.

[44] Setyawan HY, Zhu M, Zhang Z, Zhang D. An experimental study of effect of water on ignition and combustion characteristics of single droplets of glycerol. Energy Proc 2015;75:578–83.

[45] Namioka T, Saito A, Inoue Y, Park Y, Min T, Roh S, et al. Hydrogen-rich gas production from waste plastics by pyrolysis and low-temperature steam reforming over a ruthenium catalyst. Appl Energy 2011;88:2019–26.

[46] Neumann J, Binder S, Apfelbacher A, Gasson JR, Garcia PR, Hornung A. Production and characterization of a new quality pyrolysis oil, char and syngas from digestate – introducing the thermo-catalytic reforming process. J Anal Appl Pyrol 2015;113:137–42.

[47] Anca-Couce A. Reaction mechanisms and multi-scale modelling of lignocellulosic biomass pyrolysis. Prog Energy Combust Sci 2016;53:41–79,
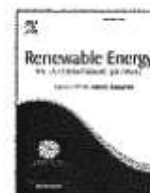
A system approach in energy evaluation of different renewable energies sources integration in ammonia production plants

CrossMark

D. Frattini [a, b], G. Cinti [c, *], G. Bidini [c], U. Desideri [d], R. Cioffi [a, b], E. Jannelli [b]

[a] INSTM Research Group Naples Parthenope, Centro Direzionale Napoli, Isola C4, 80143 Naples, Italy
[b] Department of Engineering, University of Naples 'Parthenope', Centro Direzionale Napoli, Isola C4, 80143 Naples, Italy
[c] Department of Engineering, University of Perugia, Via G. Duranti 67, 06125 Perugia, Italy
[d] Department of Energy, Systems, Territory and Constructions Engineering, University of Pisa, Largo L. Lazzarino, 56122 Pisa, Italy

ARTICLE INFO

ABSTRACT

A sustainable pathway for ammonia synthesis by means of the Haber-Bosch process should reduce or zero out the use of fossil fuels, taking advantage of renewable sources. Using renewable energy systems, hydrogen can be obtained from biomass gasification, biogas reforming or electrolysis of water with electricity generated by solar or wind energy. The scale-up of the concept is not an easy issue. From a theoretical point of view there is no limit to multiply single units but on a practical way, chemical companies are hardly reaching the size of 100 kW, due to energy, economic and sustainability problems. Hydrogen, from high-temperature water electrolysis, from biomass gasification and from biogas reforming, has been considered as the most promising solutions for ammonia production plants, based on the Haber-Bosch process. In this study the impact of three different strategies, for renewables integration and scale-up sustainability in the ammonia synthesis process, was investigated using thermochemical simulations. The study is finalized to compare the energy efficiency and sustainability of those three strategies. For a complete evaluation of the benefits of the overall system, the balance of plant, the use of additional units and the equivalent greenhouse gas emissions have been considered.

© 2016 Published by Elsevier Ltd.

1. Introduction

Ammonia is the most produced chemical worldwide and it is directly synthesized using gaseous hydrogen and nitrogen as reactants, without precursors or by-products. In its gaseous state, nitrogen is largely available in nature, as N_2, and it is normally produced by separating it from air [1,2]. Production of hydrogen, H_2, is still challenging and, for industrial synthesis of ammonia, it is usually obtained from Steam Methane Reforming (SMR) of natural gas. Moreover, when air is used for reforming processes, N_2 is also introduced, thus avoiding the need for air separation unit, but a clean-up process is necessary to remove oxygen-containing species such as O_2, CO, CO_2, H_2O, in order to prevent the catalysts from being poisoned in the ammonia reactor tank [3]. Carbon dioxide is a product of SMR and can be separated and recovered inside the plant, in Carbon Capture and Storage (CCS) systems or, more commonly, flashed into air [4,5]. Hydrogen production is therefore a critical process in ammonia synthesis and a sustainable production of ammonia is desirable to reduce the consumption of a primary source, such as natural gas, and to avoid CO_2 emissions from the process [6,7].

World ammonia production is estimated to be 140 Mt (2012) [8]. CO_2 from ammonia production plant is normally 2.07 tCO_2 eq/t NH_3 [9]. A total of 289.8 Mt of CO_2 can be estimated as global emission from ammonia production plants. In order to achieve a greener solution, a sustainable contribution to the process comes from a reliable replacement of hydrogen in the synthesis. The production of hydrogen by a renewable source allows to replace fossil fuels in all the steam reforming units and relative ancillaries. In the last decade, several studies in the literature focused on efficient hydrogen production from electrolysis of water [10], alternative pathways to combine electrolysis with solar or wind energy [11,12], or H_2-rich syngas production using different types of biomass in gasification and co-gasification processes [13,14].

High temperature electrolysers are an efficient way to produce hydrogen from water. In addition, the use of electrolyzers may also contribute to solve the problem of energy storage of intermittent sources such as solar and wind energy. The direct electro-synthesis of ammonia in high temperature electrolyzers is possible, but it is

* Corresponding author.
E-mail addresses: domenico.frattini@uniparthenope.it (D. Frattini), giovanni.cinti@unipg.it (G. Cinti), umberto.desideri@unipi.it (U. Desideri), raffaele.cioffi@uniparthenope.it (R. Cioffi), elio.jannelli@uniparthenope.it (E. Jannelli).

still at a very early stage of development, with unacceptable levels of reactants conversion into the products [15].

The biomass gasification path is a more versatile way to convert different types of biomass, derived from agricultural wastes [16], forestry residues [17] or plastic and solid wastes [18] into syngas, using air, steam or a combination of both, as gasifying agent [19]. This technology is very promising in terms of flexible use of alternative sources, pollutant emissions reduction and energy efficiency [20,21]. However, the quality of hydrogen from a biomass gasification plant is a critical issue in this kind of approach. In fact, hydrogen produced from biomass or biogas is usually rich of contaminant species with carbon and oxygen atoms, which have to be removed. Hydrogen from electrolyzers just needs a dehumidification step in order to achieve a high level of purity [22,23]. Thus, any evaluation and optimization to produce hydrogen using renewable energy sources requires a preliminary study in order to adjust process parameters and to assess a feasible and sustainable approach.

Currently, the scale-up of the concept is the major issue to be addressed for industrial applications in large plants. The most limiting aspects in this field are the negligible interest of large companies for the implementation of alternative solutions, technology transfer of scientific results, reliability and profitability of the integration of renewables, so that there are few examples of applications [24–26]. A scale-down of ammonia production plants can reduce current uncertainties related to the above mentioned pathways and their economic feasibility [27]. Within this framework, it is possible to propose a distributed production of ammonia that might produce the following benefits: 1) to reduce the environmental and economic cost of distribution, 2) to enhance direct use of renewable sources which are distributed on the territory [28], 3) to give to final customers the direct control of production, 4) to reduce environmental and economic cost of transportation [29]. In addition to the fertilizers' industry, ammonia can also be used directly as a fuel to feed power electrical system or for automotive application and agriculture machinery [30–33]. Rural area can then benefit from an ammonia based system in a complex, sustainable and efficient way, with a lower environmental impact than fossil fuels [34,35].

Within this framework, this study investigates potential pathways for green ammonia production. Starting from renewable energy sources such as biomass or electricity from solar or wind energy, three systems were designed and modeled in Aspen Plus. The concept was implemented considering all processes for gas supply and ammonia synthesis. Considering the most common and consolidated technologies the systems were designed and the chemical equilibrium analysis allowed to evaluate the amount of renewable energy necessary to supply one unit of NH_3, demonstrating the feasibility of a green and sustainable path for green ammonia that can contribute to a reduction of the environmental impact of this chemical opening new scenarios for a diffused production of ammonia and novel applications such as the utilization of ammonia as a fuel.

2. Technological background

2.1. Ammonia production process

Ammonia is mainly produced in thermo-chemical plants where a gas mixture of hydrogen and nitrogen is synthesized [36]. An ammonia plant can be divided in two main subsystems: the gas supply and the ammonia synthesis system. The gas supply system is necessary to provide the synthesis plant with the correct $H_2:N_2$ mixture. Ammonia synthesis is based on following exothermal reaction:

$$\frac{1}{2}N_2 + \frac{3}{2}H_2 \rightarrow NH_3 \quad \Delta H_0 = -45.64 \, kJ/mol \quad (1)$$

The reaction takes place at high temperatures (500–600 °C) and is enhanced by the presence of an iron catalyst. In the majority of cases a complex plant is designed around the reactor, with a recycling loop and the following units:

- A gas clean-up unit, to purify the raw syngas coming from upstream processes for H_2/N_2 production. This block is of fundamental importance to remove from the syngas unwanted gases or oxygen containing species that have poisoning effects on ammonia catalyst (SO_x, CO, CO_2, etc.).
- A compression unit, including one or more high efficiency compressors, to compress reacting gasses to the synthesis loop pressure.
- A conversion unit, including one or more catalytic synthesis reactors, equipped with temperature control and the recovery of reaction heat.
- A heat removal unit, for product gas separation, further heat recovery and condensation of ammonia.
- One or more units for purging inert gases out of the loop and recirculating unconverted hydrogen and nitrogen to the conversion block.

The most important process parameters are [3]:

- Operating pressure in the ammonia reactor;
- Gas separator temperature in flash drums;
- The recycle ratio (the ratio between the recycled stream and loop feeding stream);
- The conversion per pass (reactants converted into ammonia for single pass in the reactor).

Depending on the values of such parameters it is possible to identify the most commonly used processes for NH_3 production (Table 1).

Within this work the Haber-Bosch (HB) process has been considered due to the fact that is the most diffused and studied. Several plant modifications, described in the next paragraph, have been introduced in the basic plant layout to optimize the above mentioned parameters.
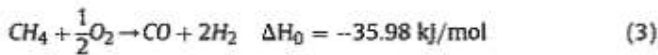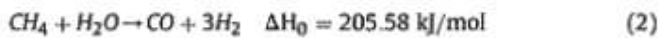
2.2. The biogas path

Biogas is the product of biomass digestion plants and of water waste treatment processes were biological matter is decomposed at anaerobic condition. The efficiency off the process is strongly related to the system design, the inlet biomass and the decomposition temperature. Also gas composition depends on the same parameters but it is usually a mixture of methane and carbon dioxide with a $CH_4:CO_2$ concentration ratio of 60:40% by volume [37]. Biogas contains traces of contaminants such as sulphur oxides, chlorine compounds and others substances depending on the starting substrate. For the purpose of this study, biogas is considered as a mixture of methane and carbon dioxide only. The clean-up system that removes contaminant is considered part of the biogas plants, due to the fact that the gas is normally treated in the plant. Common biogas purification systems are not enough to reach the purity and the composition required by the Haber-Bosch process. The biogas production plant therefore need a reforming reactor, a water gas shift reactor, an Acid Gas Removal unit (AGR), a methanator and, finally, a condenser to upgrade the biogas to feed a Haber-Bosch process. Such design is the typical NH_3 plants with the

Table 1
Most commonly used ammonia synthesis processes [36].

| Process	Op. Pressure [bar]	Temperature [°C]	Conversion [%]	Recycle [Y/N]
Haber-Bosch	250	550	15–20	Y
Kellogg	300	500	20–30	Y
Uhde	300	500	18–22	Y
Claude	1000	600	40–85	N
Casale	600	600	20–22	Y
Fauser	300	530	18–20	Y
Mont Cenis	100	400	10–20	Y

significant difference that the inlet stream also contains carbon dioxide that may affect the equilibrium conditions. In an ammonia production plants reforming usually takes place in an autothermal reactor and both air and steam are mixed with the fuel in order to enhance steam methane reforming (SMR) and partial oxidation reactions:

$$CH_4 + H_2O \rightarrow CO + 3H_2 \quad \Delta H_0 = 205.58 \text{ kJ/mol} \tag{2}$$

$$CH_4 + \frac{1}{2}O_2 \rightarrow CO + 2H_2 \quad \Delta H_0 = -35.98 \text{ kJ/mol} \tag{3}$$

Both reactions occur at high temperatures (~650 °C) allowing an energetic optimization because steam reforming is an endothermal reaction while partial oxidation is exothermal. It is therefore possible to balance the heat and use an adiabatic reactor with no need of an external heat source. In addition, the nitrogen, which is necessary for the NH_3 synthesis, is introduced into the process by air. Carbon monoxide is removed from the gas mix in a water gas shift (WGS) reactor. The reaction is the following:

$$CO + H_2O \rightarrow CO_2 + H_2 \quad \Delta H_0 = -41.33 \text{ kJ/mol} \tag{4}$$

The reaction is exothermal and takes place at lower temperatures (~350 °C) than in the SMR. Temperature of the reactor and concentration of steam, that can be added in this section, can enhance the reaction to achieve a complete transformation of CO. The Acid Gas Removal unit and the methanator are designed together to remove CO_2 and adjust the H_2/N_2 ratio reducing H_2 concentration. Methanation reaction is the following:

$$CO_2 + 3H_2 \rightarrow CH_4 + 2H_2O \quad \Delta H_0 = -164.40 \text{ kJ/mol} \tag{5}$$
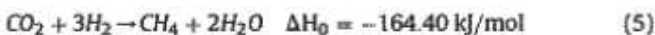
This reaction allows to adjust the hydrogen concentration by increasing the methane concentration, that is inert in the HB loop, and the steam concentration that can be easily separated by condensation. The removal of CO_2 is required by the HB loop and is achieved in the AGR where more than 90% CO_2 is separated [38]. The remaining part of CO_2 is chemically transformed in the methanator reactor. The last component of the gas processing is the condenser. Water is removed to eliminate the risk of condensation in the compressor unit, to reduce the energy consumption of the compressor and to mitigate its negative effect on the HB reactor.

2.3. The gasification path

Gasification of biomass is a thermochemical process that decomposes the biological matter and produces a mixture of pure gases, called syngas, that can be used to feed the Haber Bosch loop. An oxidizing agent, usually air or steam, is used to partially oxidize the solid biomass and pressurize the system so that the produced gas can be flashed out to its final use. The gasification process usually includes a clean-up unit that removes particulate matter and tars from the gas stream. The product is, thus, a clean mixture of H_2, CO, CO_2, CH_4 N_2 and steam that can be processed and used in the ammonia production plant. The composition of the mix depends on the biological substrate used as inlet feed and on the gasification design. Gasification typology is usually related to the flow directions of inlet biomass, gasification agent and off gases. Four types of gasifier are the most diffused: updraft, downdraft, fluidized bed (FB) and entrained bed (Fig. 1).

Each technology is characterized by an operational temperature and pressure. The combination of biomass source, gasifier typology, oxidizing agent and gasification thermodynamic parameters (temperature and pressure) affect syngas composition. Examples of syngas composition are reported in Table 2 from the literature [14,18,19,39].

Syngas obtained from gasification is a gaseous mixture which needs a complete clean up and treatment to produce the N_2/H_2 mixture required by the ammonia synthesis plants. In details, WGS, a AGR, a methanator and a condenser are used to transform the syngas into a suitable mixture for the ammonia synthesis.

The main difference lies in the gas compositions. The eight compositions reported in Table 2 where initially tested in the gas processing with the result that not all of them where suitable. This is mainly caused by the wrong H_2/N_2 ratio, that, even after WGS, does not reach the minimum value of 3. The methanator reactor can help to adjust composition only reducing amount of H_2 but not increasing it and the WGS is limited to the total amount of CO. The optimal syngas composition is not the one with a correct H_2/N_2 ratio but the one with a suitable $(CO + H_2)/N_2$ ratio. Such values are reported in Table 2 showing that only compositions 2, 4 and 8 achieved the required conditions. Composition 8 was selected because it is the closer to the required target of 3.

2.4. The synthesis path from H_2 and N_2

Both hydrogen and nitrogen can be obtained by non-carbonaceous source. In particular hydrogen can be obtained by water electrolysis and nitrogen can be produced from air and then mixed with reforming products [1,2]. The main source of nitrogen as chemical product is air due to its high concentration, ~79% by volume, and availability. There are three industrial ways to separate nitrogen from air: cryogenic, adsorption and permeation generation. Cryogenic distillation is the first to be historically developed but, due its high capital cost and power requirement, it is usually developed in large and centralized plants from where it is distributed via pipelines or trucks. Pressure swing adsorption is used with carbon molecular sieves that selectively adsorb oxygen, allowing nitrogen to pass through at the desired purity level. PSA operates at ambient temperature and adsorption pressure is in the range of 10 bar. The net cost of nitrogen produced via PSA is lower that cryogenic one. Selective gas permeation is realized in membrane systems to separate nitrogen from air. The technological principle is based on the difference of velocity of the gas mixture at the two side of the membrane so that the different partial pressure causes gas separation. Compared to PSA this technology cannot reach high purity levels, in particular with high flowrates. the main drawback
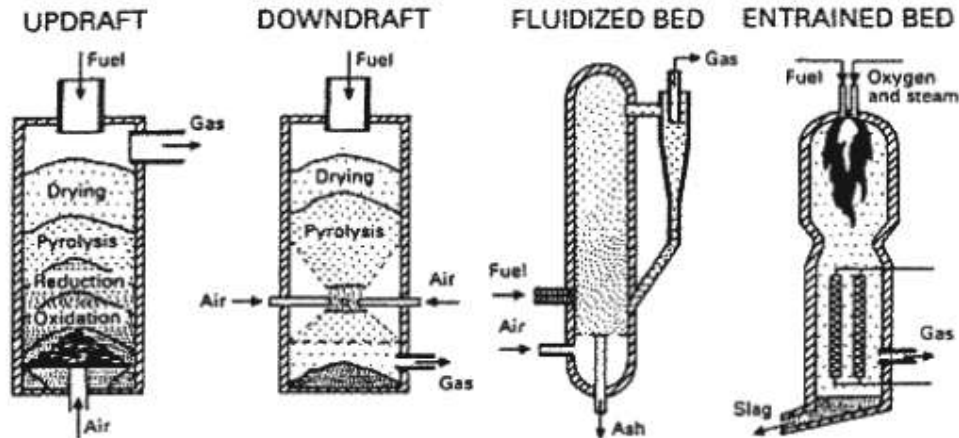
Fig. 1. Different gasifier concepts.

Table 2
Typical syngas compositions from biogas gasifiers (FB = fluidized bed, BFB = bubbling fluidized bed).

Biomass type	N.	Oxidizing agent	Reactor type	H_2 [% v/v]	CO [% v/v]	CO_2 [% v/v]	CH_4 [% v/v]	N_2 [% v/v]	H_2O [% v/v]	$(CO + H_2)/N_2$ [−]
Dry wood	1	Air	FB Downdraft	13.9	17.2	10.7	0.8	39.4	18.0	0.78
Dry wood	2	O_2	FB Downdraft	28.7	43.0	13.4	1.8	2.7	10.4	26.55
Dry wood	3	Air	BFB	7.5	14.1	10.6	3.5	42.8	21.5	0.51
Dry wood	4	Steam	BFB	20.7	10.4	8.1	3.2	2.6	55.0	11.96
Dry wood	5	Air/Steam	BFB	14.3	7.9	9.1	1.2	24.5	43.0	0.91
Olive husk	6	Air/Steam	BFB	11.7	10.6	6.9	2.7	23.6	44.5	0.94
Dry wood/plastic	7	Air/Steam	BFB	19.5	8.4	9.6	2.4	20.1	40.0	1.38
Olive husk/plastic	8	Air/Steam	BFB	21.0	11.5	8.2	3.5	7.8	48.0	4.16

of this technology is the purity level when flowrate increases over 10 l/min. Fig. 2 reports the best nitrogen production technology depending on the two main factors: nitrogen purity and production requirements. For this study the PSA process, with commercial carbon molecular sieves as adsorbent [40], was selected.

Hydrogen can be obtained from water and electricity via electrolysis:

$$H_2O \rightarrow H_2 + \frac{1}{2}O_2 \quad \Delta H_0 = 241.57 \text{ kJ/mol} \tag{6}$$
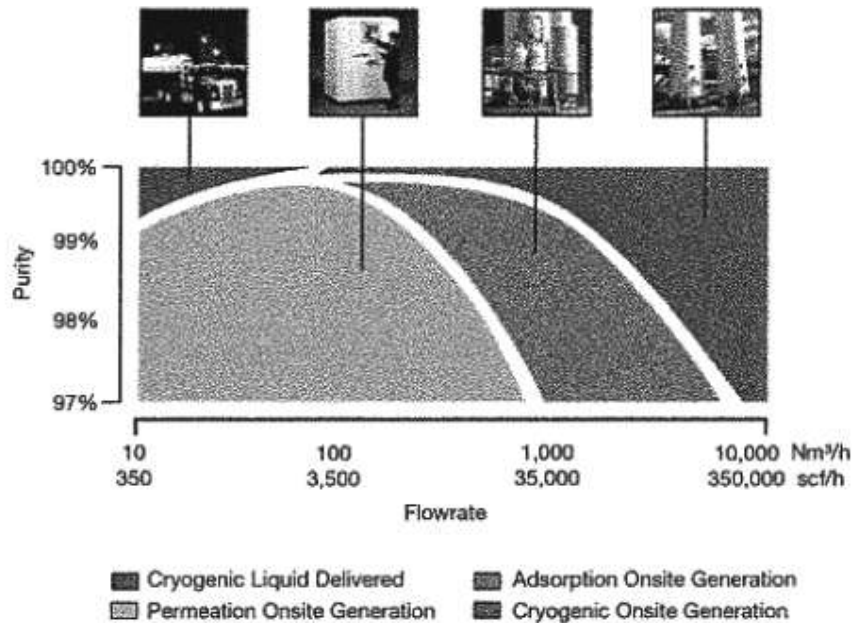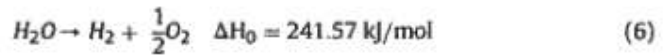

Fig. 2. Best nitrogen production technology depending on purity and flowrate [41].

When electricity is generated by renewable energy sources hydrogen can be considered as a green fuel. Electrolysis is a well knows process and is industrially realized in electrochemical devices where electricity supplied to the two electrodes (anode and cathode), flows through the electrolyser and decomposes the water. Hydrogen is produced at the cathode and oxygen at the anode. There are two main commercial technologies distinguished by the type of electrolyte [41]: alkaline (liquid electrolyte) and Proton Exchange Membrane (PEM) electrolyzers. In addition, anion exchange membranes (AEM) were recently introduced into the market and high temperature solid oxide electrolyzers (SOE) are promising but still at an early stage of development. The main parameters for the selection of this technology are the system size and hydrogen purity. Alkaline electrolyzers are the ones that can be built in larger sizes, up to 5000 kW–760 Sm^3_{H2}/h and are also less expensive than those based on the PEM technology. On the other hand, PEM electrolyzers can achieve higher purity of hydrogen [42]. As far as the efficiency is concerned, such systems are strongly dependent on the design and operational strategies. Both technologies may reach 50%–80% efficiencies. An additional important parameter is the H_2 output pressure. If H_2 is already produced at high pressure, less energy is required by the compressor. Common electrolyzer's pressure ranges from atmospheric up to 30 bar. Table 3 summarizes the main characteristics with the addition of system cost where alkaline system are still more convenient mainly due to a more mature and diffused technology and to the scale benefits.

2.5. Steam methane reforming

The main traditional benchmarking process for production of H_2 and N_2 is the steam methane reforming. This process applied to natural gas is the basic process with which all others proposed above are compared.

3. Model development

In this section, the model development and operating parameters used for simulations, in the Aspen Plus environment, are described. Following the approach described in the previous paragraphs, three system concepts have been designed, all based on the Haber Bosch (HB) process. In the first system (case A), the HB process has been coupled with a syngas clean-up unit. The syngas itself comes from a biomass gasifier, as explained before. In the second one (case B), the feeding gas for HB loop has been obtained from an electrolyser and an air separator unit. In the third case (case C), a biogas is fed to a steam reforming unit and then treated in a clean-up section, before entering the HB loop. A reference benchmark system (case 0), based on steam reforming of natural gas has also been developed as a comparison. To perform an equivalent comparison between the technologies, the system units were operated at the best performing condition, according to the technological background exposed above. Thermodynamic parameters such as temperatures and pressures were not varied in the simulations.

3.1. Haber Bosch synthesis loop: layout and model parameters

The HB loop layout was implemented in Aspen Plus and then integrated in the three complete models. Fig. 3 shows the HB loop flowsheet developed in Aspen Plus. The purified feed gas is compressed to the operating pressure by means of a multistage intercooled compressor (COMP01), and then introduced into the synthesis loop. The "MCompr" block type was used with the rigorous ASME method for efficiency, heat and power consumption calculation. Intercooling temperature after each stage, namely 40, 70 and 150 °C, and the final discharge pressure, namely 250 bar, were specified for this block. The compressed feed gas was adiabatically mixed (MIXER01) with the recycled gas stream, containing unreacted H_2 and N_2, a large amount of inerts and ammonia to a smaller extent. To remove the residual ammonia, after MIXER01, the feed stream was first sent to a counter current shell-and-tube heat exchanger (EVA01) and pre-cooled by the cold product gas stream coming from the ammonia removal section (MIXER03, EXPANDER). EVA01 is modelled with a "HeatX" block type and the cold stream outlet temperature is fixed at 20 °C as block specification. Afterwards, the feeding stream is directed to the first flash separator (SEP01) at 0 °C: in this equipment, part of the residual ammonia liquefies and is separated from gases, which pass through the purge valve (SPLIT01) and then fed to the ammonia conversion section.

At this point, the reactant gas stream is pre-heated using the hot product gas coming from the synthesis reactor (REACTOR) in a counter current heat exchanger (HEATER04), and then a recirculation compressor (COMP02) adjusts the inlet gas pressure to the nominal value. The "RGibbs" reactor block is used to model ammonia synthesis and the built-in PENG-ROB method, based on Peng-Robinson cubic equation of state, is applied throughout the HB loop for thermodynamic properties, physical and chemical equilibrium calculations [26]. The reactor is considered isothermal and at thermodynamic equilibrium, with a temperature of 550 °C and a pressure of 250 bar, so that the exothermal reaction released a heat flux. Cooled products are then fed to the second flash separator, downstream to the reactor (SEP02), operated at 20 °C and at high pressure, so that the ammonia heat of condensation is lower and the largest part of produced ammonia is here separated from the other gases. The resulting gas from SEP02 represents the recycle stream of the HB loop. The liquid stream from SEP02 is mixed (MIXER02) with the liquid stream from SEP01 and sent to an adiabatic throttling flash drum (EXPANDER) which operates at atmospheric pressure and therefore at a temperature lower than −30 °C. Pure liquid ammonia is thus obtained as the main product of the plant. The small fraction of vapors obtained in EXPANDER, consisting of ammonia and the non-condensable gases, i.e. CH_4, N_2 and H_2, are collected and mixed again with a small amount of liquid ammonia (MIXER03), resulting in the cold gas inlet stream for EVA01, thus subtracting heat to the feed stream. The outlet gas stream from EVA01 is mainly composed of NH_3 with a little presence of other gases and is the secondary product available from the plant. The rigorous vapour-liquid equilibrium flash drum model "Flash2" is the block used for SEP01, SEP02 and EXPANDER. The following Table 4 summarizes the specifications used for these blocks:

Table 3
Summary of main alkaline and PEM electrolyzer parameters.

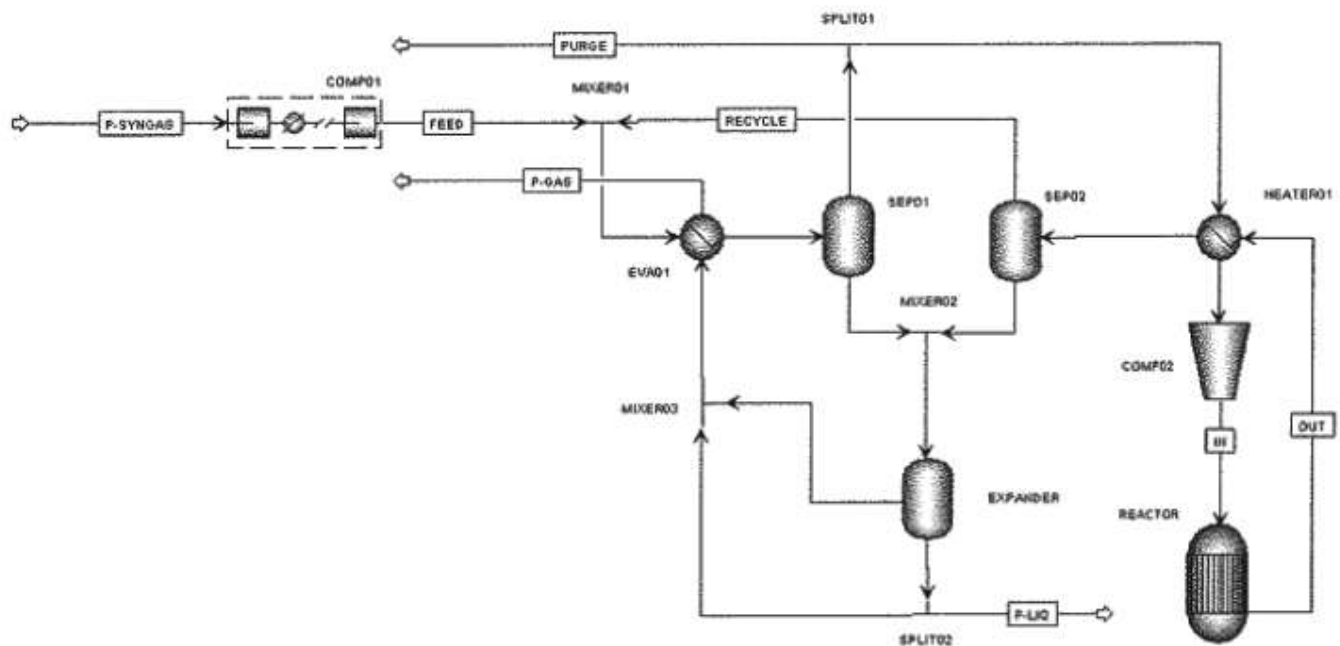|	System size		Hydrogen purity	Efficiency	Cost
Alkaline	0.25–760 Sm^3_{H2}/h	1.8–5300 kW	99.5–99.9998%	50–78	1000–1200 €/kW
PEM	0.01–240 Sm^3_{H2}/h	0.2–1150 kW	99.5–99.9999%	50–83	1900–2300 €/kW

Fig. 3. HB loop developed in Aspen Plus.

Table 4
Specifications of the HB loop blocks.

Specification	REACTOR	SEP01	SEP02	EXPANDER
Temperature (°C)	550	0	20	–
Pressure (bar)	250	250	250	1
Heat Duty (kW)	–	–	–	0

For each block, only two specifications are required because the third one is the result of flowsheet simulation. The HB loop thus described produces ammonia both in liquid and gaseous forms.

3.2. Reforming and clean-up unit: layout and model parameter

In this subsection, the reference case, namely case 0, and the relative layout is explained. The HB loop previously described is coupled with a CH_4 steam reforming and clean-up unit to obtain the purified syngas for ammonia synthesis. Natural gas and air, at room temperature, are fed to an adiabatic combustor (BURNER), after pre-heating, and are burnt by the oxygen introduced with nitrogen. The amount of oxygen is not sufficient to oxidize all the fuel and a partial gasification occurs with H_2 and CO formed together with CO_2. In the next reformer block (REFORMER), a steam stream is fed with the burnt gas, with a Steam-to-Carbon ratio (S/C) of 2, and the endothermal SMR reaction takes place at 650 °C. Afterwards, three reactors are used (WGSR1, WGSR2, WGSR3) to complete the Water Gas Shift reaction (WGS). In those blocks, CO reacts with steam to produce H_2 thus increasing hydrogen content in the syngas for ammonia production. Fig. 4 accounts for the complete flowsheet layout.

After each reactor, a counter current heat exchanger (HEATER01, HEATER02, HEATER03, and HEATER04) is used to cool down the syngas for the next WGS stage and to produce the steam required for reforming. WGS reactors are operated at decreasing temperature since the shift reaction is a slightly exothermal equilibrium reaction, favored at low temperature but kinetically limited [38], thus proper catalysts are required in real plants to achieve chemical

equilibrium at the set temperature. The reactor block used to model those units is "RGibbs" and the built-in NRTL property method is set as the thermodynamic model for this section. For a clearer understanding, Table 5 shows the operating conditions for those reactors.

The Acid Gas Removal unit (AGR) is devoted to CO_2, CO and partial H_2O separation and removal, after the WGS section. According to the technological background described in the previous paragraph, in order to simplify the model, a "Sep" block is used with standard specifications, concerning temperature (≈ 50–80 °C) and separation efficiency (>90%), in agreement with the literature. Finally, in order to complete CO_2 and H_2O removal, a methanator (METH) and a condenser (COND) block are placed in series. The methanator has the double function of chemically converting residual CO_2 into CH_4 and adjusting the final H_2/N_2 ratio for the HB loop by means of reaction (5). An "RStoic" reactor block is used to model METH at adiabatic conditions. COND is a "Flash2" block type, operated at 15 °C to allow the complete liquefaction of H_2O and gas/liquid separation. Table 6 summarizes the specifications of those last three blocks. The purified syngas obtained is thus fed to the HB loop described above.

The first system proposed, case A, is an alternative layout to the CH_4 reforming one explained above. A real syngas composition was implemented and the layout was modified as shown in Fig. 5.

The most relevant difference is that a raw syngas from biomass gasification is directly used as primary source. The BURNER, REFORMER and relative ancillaries' streams have been removed. The specifications of remaining block are the same as stated above, while for case C, where a standard biogas composition was used, no modifications on the flowsheet layout are necessary. Table 7 shows in details the gas stream composition, used in case 0, A and C, as a primary source.

3.3. H_2 and N_2 generation unit: layout and model parameter

The last system proposed, case B, is completely different from the previous ones. The feeding streams to the plant are air and water, at room condition, as primary source for H_2 and N_2. The
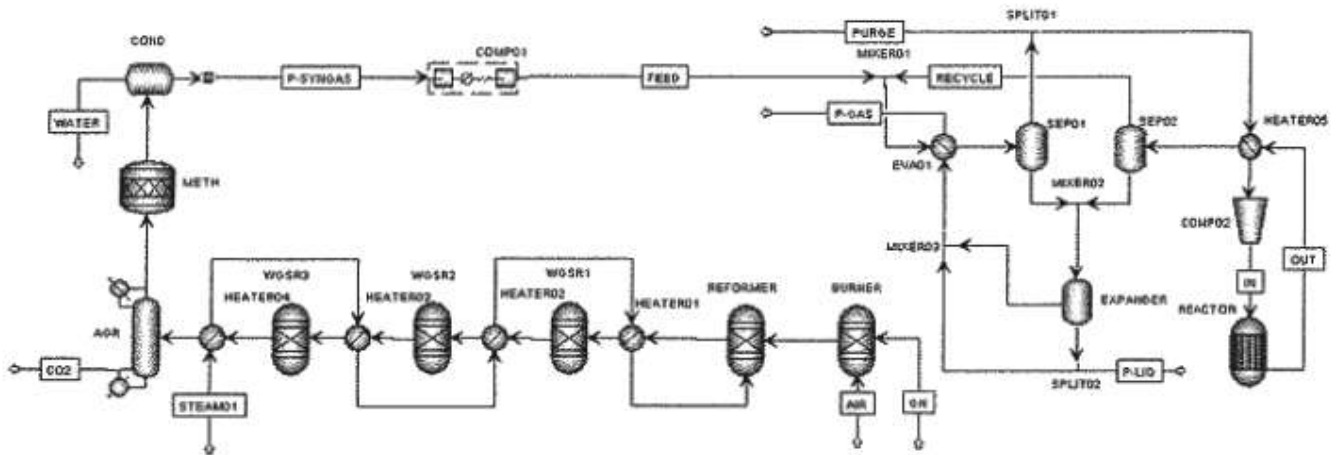
Fig. 4. Complete SMR and HB loop flowsheet.

Table 5
Operating conditions for the case 0 reactors.

Specification	BURNER	REFORMER	WGSR1	WGSR2	WGSR3
Temperature (°C)	–	650	500	350	250
Pressure (bar)	1	1	1	1	1
Heat Duty (kW)	0	–	–	–	–

Table 6
Blocks specifications of case A.

Specification	AGR	METH	COND
Temperature (°C)	50	–	15
Pressure (bar)	1	1	1
Heat Duty (kW)	–	0	–

Table 7
Inlet gas stream composition used in Case 0, A and C parameter.

Component	Case 0 (NG)	Case A (R-SYNGAS)	Case C (R-BIOGAS)
N_2 (% mol/mol)	–	7.80	–
H_2 (% mol/mol)	–	21.00	–
CH_4 (% mol/mol)	100.00	3.50	62.00
H_2O (% mol/mol)	–	48.00	–
CO_2 (% mol/mol)	–	8.20	33.00
CO (% mol/mol)	–	11.50	5.00

relative flowsheet is shown in Fig. 6.

Feedwater is compressed in a hydraulic pump (PUMP01) and heated in a counter current heat exchanger (HEATER01) to the electrolyzer (ELECTR) operating conditions, namely 80 °C and

30 bar. The built-in "Pump" block has been used to model PUMP01, HEATER01 is a "HeatX" block type and ELECTR is an "RGibbs" reactor block. In agreement with the actual water electrolyzers performance, a hydrogen purity of 99.9% and an electrical efficiency of 64.4% have been specified for this block. The air separation unit is based on a PSA standard process, which can be modelled in Aspen Plus as a compressor (COMP03) and a separator (PSA) in series. They are operated at 30 bar and room temperature. The heat available from compression is partially used to heat up feedwater coming out from PUMP01. The nitrogen purity, as reported in the
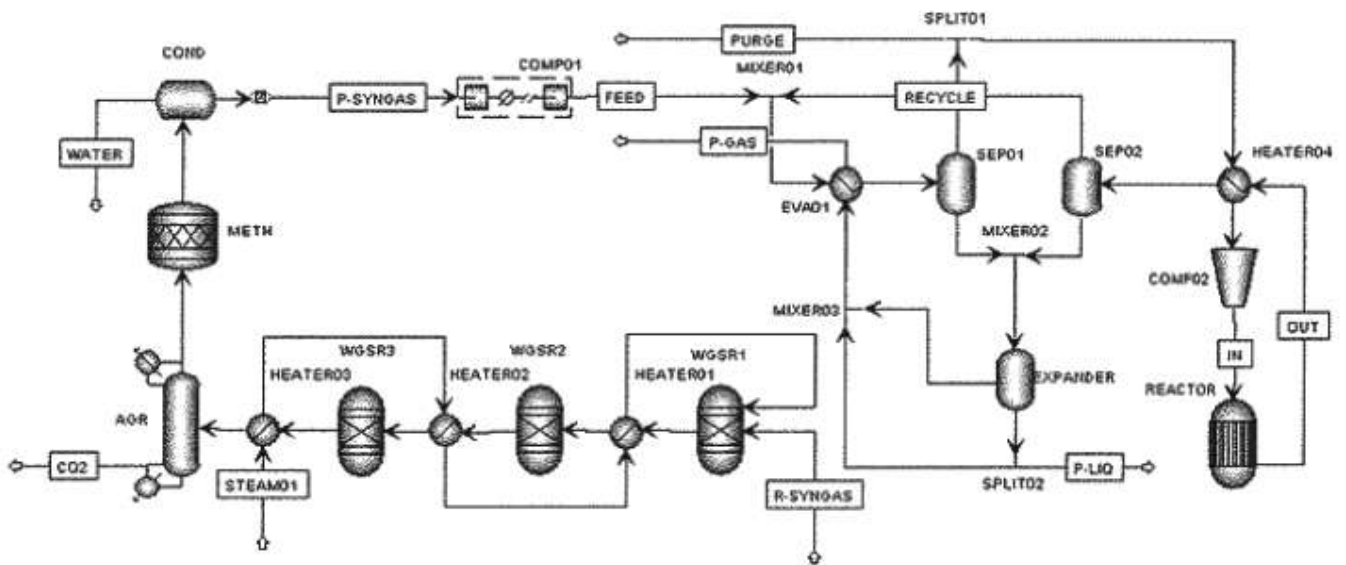

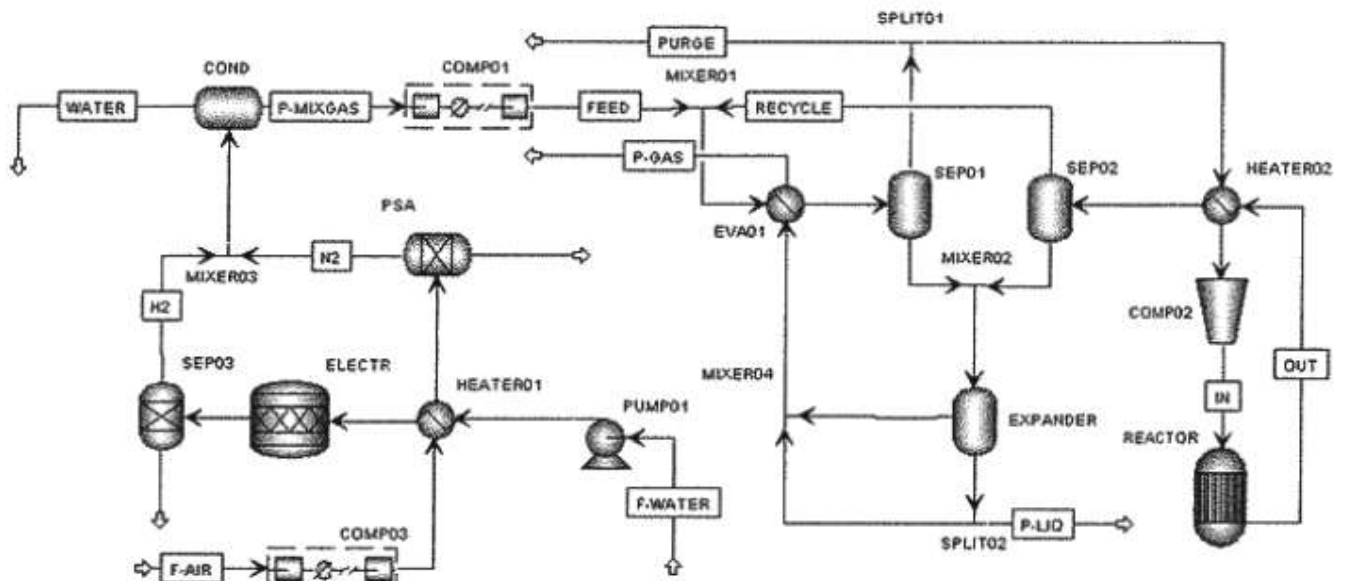
Fig. 5. System scheme of case A.

Fig. 6. Case B system layout.

technical literature, is set at 99.9%. After these blocks, produced gases are adiabatically mixed (MIXER03) in a controlled way in order to achieve the desired H_2/N_2 ratio for ammonia production. A "Flash2" block type (COND), at 30 bar and 20 °C, was used again to remove the eventual traces of water from feeding streams, after mixing. The purified mixture of gases is thus fed to the HB loop. The property method used in this section was the NRTL built-in Aspen model.

4. Results

Model results are mainly in terms of gas and energy flows. Each of the three new concepts allows to produce ammonia in a novel way and simultaneously reducing the impact on the environment. Inlet energy source are deeply different: case 0 is based on a fossil fuel, case B on sustainable electricity (wind or sun) and case A and C are base of biomass. In details case A is based on syngas coming from a gasification process of solid matter while case C is biogas from anaerobic digestion of degradation of liquid biomass. Table 8 reports the main results relative to HB loop for different cases. The first parameter $(H_2/N_2)_{FEED}$ is the stoichiometric ratio between hydrogen and nitrogen entering into the HB unit. In all cases, as expected, values were close to stoichiometric ones. The $(H_2/N_2)_{IN}$ parameter is the gas ratio at reactor inlet. Also in this case all values are close to three.

With reference to the recirculation ratio, in Case A it is slightly bigger than in the other ones. This is caused by the big amount of CH_4, which is inert in the process. A larger recirculation ratio has an effect on the total inlet reactor flow and, consequently, on the compressor energy consumption. The purge ratio, namely the

molar ratio between purge stream and feed stream, in all cases with the exception of electrolysis, is in the 0.4–0.5 range. This is mainly related to the absence of inert in case B. However, a little part has to be purged out of the system for calculation convergence requirements, due to the architecture of HB loop. Finally, Fig. 7 reports the reaction efficiency in terms of percentage of completed reaction and also the percentage of inerts (y_{inerts}) in the reactor inlet stream.

In details, efficiency is calculated as the amount of nitrogen reacting with respect to the inlet one. Such value can be calculated at reactor level (η_{react}) and global level (η_{glob}). The results show that
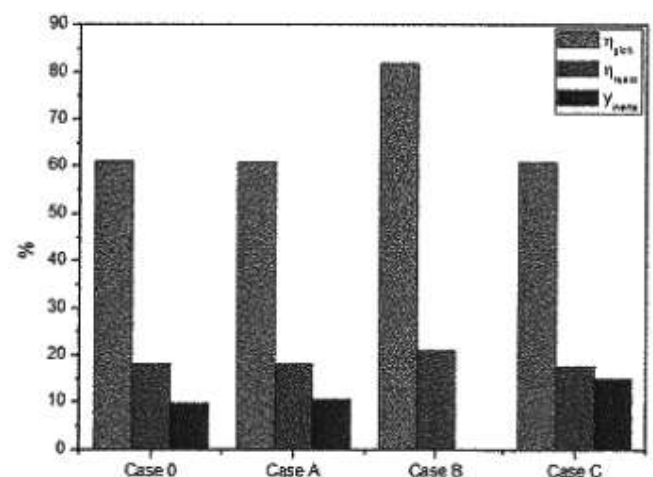

Fig. 7. HB loops efficiency and inerts concentration.

Table 8
Main results relative to HB loops for different cases.

Loop	$(H_2/N_2)_{FEED}$ (mol/mol)	$(H_2/N_2)_{IN}$ (mol/mol)	Rec. Ratio (mol/mol)	Purge ratio (mol/mol)
Case 0	3.07	3.17	3.33	0.44
Case A	3.06	3.12	3.44	0.47
Case B	3.01	3.02	3.29	0.18
Case C	3.09	3.19	3.40	0.45

case B is still the most interesting one achieving up to 81% of global reaction efficiency. Case C, differently, has a very low reactor efficiency due to the inerts concentration. The efficiency achieves acceptable values at global level only because of the high recirculation and high purge ratio in all cases.

Fig. 8 reports the specific energy consumption of the four designs. Energy flows are normalized for each kg of NH_3.

Overall consumption of primary energy is very similar in all cases: electrolyzer has the lower consumption while biogas has the higher one due to high methane inlet content and relative chemical energy. As expected, the reference case, together with biogas and syngas, is the case with a higher energy consumption, while the electrolysis case only demands 14.36 kW/kg$_{NH3}$ of electricity. Table 9 shows other energy indicators and the CO_2 equivalent emissions for the four layouts proposed.

Specific heat consumption is negative for all cases because the overall process is exothermal in all configurations. An additional energy flow of the system is the purge gas. The table reports the LHV of the purge gas. Case A and case C have the higher values due to the methane still present in the off gases. Finally, the table reports the specific emissions in terms of CO_2/NH_3 mass ratio. With the exclusion of case B, where no emissions are produced, the lower amount of emissions are in the reference case. This value is tricky because such emissions come from a fossil fuel while biogas and syngas come from a biomass and are, for the well-known reason, not a source of GHG emissions. It is worth noting that GHG emission of case 0 is in perfect agreement with reference value of 2.07 [6,9]. Such result can be also considered as an overall validation of the system design and of model numeric results. As stated in the introduction section, ammonia is one of the most produced chemical worldwide but its production is associated to a net CO_2 emission of 290 Mt. This emission is exclusively ascribed to the carbon present in the feedstock and is not directly related to the ammonia itself, which is composed only by nitrogen and hydrogen. In fact for the case B, with electrolyzer and PSA, the GHG emission is virtually zero because carbon-free feedstock were used. On the other hand, when a syngas or a biogas are used as feedstock, the total CO_2 emissions are 534.8 Mt and 502.6 Mt, respectively, higher than the 290 Mt from natural gas, but the process can be considered carbon neutral due to the renewable feature of the feedstock. However, the main environmental result is that, from the qualitative point of view, the alternative layouts proposed can effectively reduce the impact of ammonia production plants and that are a feasible way to increase the sustainability of this industry in order to achieve a green chemistry.
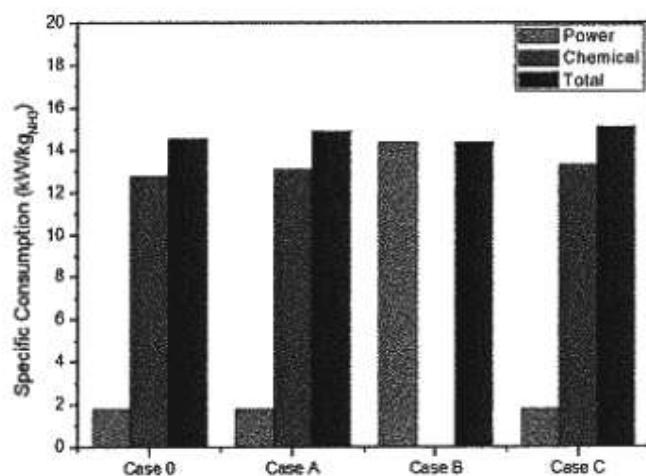
Finally, Fig. 9 shows the detailed energy balance of plant for all cases, using Sankey diagrams, in order to evaluate the relative distribution of energy fluxes, i.e. chemical, heat and power, around each system unit and so their influence on the overall balance. In order to specify the quality of the thermal energy available from the HB loop, the temperature of each heat flux outgoing the system is also indicated. This energy can be considered as a positive contribution to balance once a useful application is found (cogeneration, residential heating, domestic hot water, thermal storage, etc.), according to the temperature. Relative to this latter issue a distributed production of NH_3 could permits an easier valorization of heat, e.g. residential use. For all the layout in Fig. 9, the largest energy flow is represented by the chemical energy inside the purge gas. This flow can be used as a secondary fuel for reacting in a combustor and obtain additional heat or power for other industrial processes. In fact its LHV, as reported in the previous Table 9, together with the high energy percentage confirmed in Sankey diagrams, is of interest in all cases. From this point of view, a particular discussion is needed for case B, when the electrolysis/air separation path is chosen: from the diagram it is possible to observe that the energy input of this layout is represented only by electricity and that the output is essentially the chemical energy associated to purge gas and ammonia, with a small amount of waste heat from single units, except from reactor, which is the largest exothermal source of waste heat at high temperature (6.22% at 550 °C). This result confirm the profitability and the advantages associated to this layout because, globally, it is possible to conclude that the electric energy is quite completely converted, i.e. stored, into two type of useful chemicals, such as ammonia and the purge gas. In addition, due to the absence of high temperature treatments, as methanation, water gas shift and burning/reforming, the cooling requirements are low and also the heat losses related to low temperature operations, i.e. without the possibility to recover high temperature heat (AGR, water separation, ammonia condensation), are limited. In conclusion, the case B is the most convenient, not only from the chemical point of view, due to the high conversion efficiencies, and from the environmental one, due to the potential absence of GHG emissions, but also from the energy point of view because, among the renewable energy sources integration scenarios proposed in this work, it is the only layout that could allow the complete use and storage of electricity from renewables into energy vectors like hydrogen (in form of the purge gas) and ammonia.

As far as the waste heat from the other HB Loop layouts is concerned, two sources of waste heat are eligible for recovery. Such heat comes mainly from the ammonia reactor and from multistage compressor cooling. In fact, from the diagrams, these two fluxes can represent more than 10% of the available energy. Even if the waste heat from the WGSR is available at higher temperatures, 500-250 °C depending on the shift stage, this flux is <2% of the total energy output so that it is unworthy to recover it. On the contrary, in the reference case and in the case C with biogas, the waste heat from reactor is around the 5% of the total, and is available at a temperature of 550 °C, which is suitable for cogeneration, while the waste heat from compressors is only 8% but is available at a lower temperature, namely 150 °C, which is in agreement to heating and domestic hot water requirements.

5. Conclusions

A renewable path for ammonia synthesis was studied and modelled for the first time in this paper. This study demonstrates that ammonia can be produced in an efficient way from renewable energy sources. Three different plants were designed and studied

Fig. 8. Specific energy consumption for the different cases.

Table 9
Energy and emissions indicators.

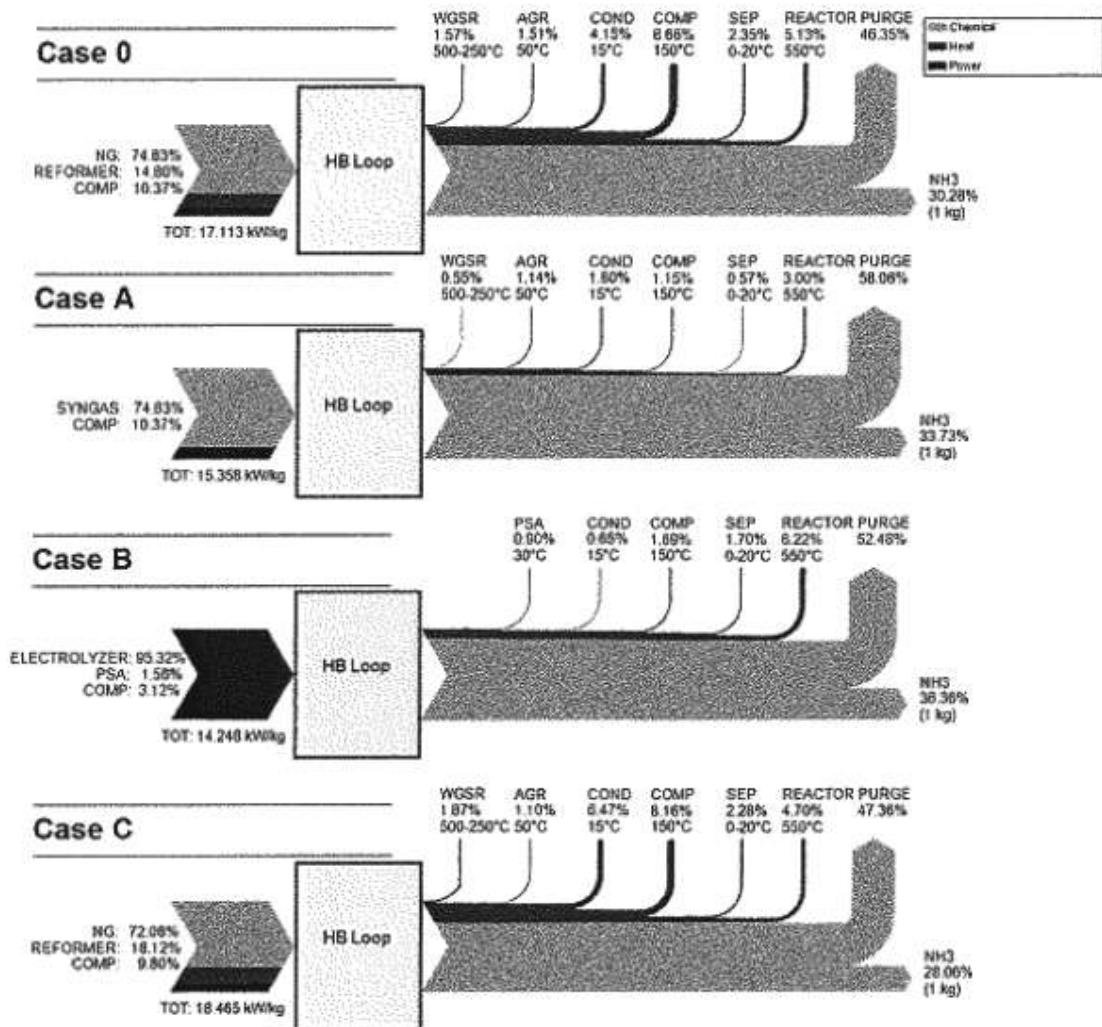|	Spec. Heat consumption (kW$_{th}$/kg$_{NH3}$)	LHV of purge gas (MJ/kg)	GHG emissions (kg$_{CO2}$/kg$_{NH3}$)
Case 0	−1.47	26.76	2.05
Case A	−1.26	27.15	3.82
Case B	−1.59	21.35	0
Case C	−1.19	27.25	3.59

Fig. 9. Sankey diagrams for energy fluxes.

using a thermochemical model developed in Aspen Plus. The results of the study reveals the option of a distributed, efficient and sustainable ammonia production. Energy flows show that all the system have the same primary energy consumption in the order of 14–15 kW/kg$_{NH3}$ with no impact of the new designs on the amount of primary energy used to produce NH$_3$. This means that the introduction of renewable energy do not limit the efficiency of the plan even if the large amount of inerts limits the total ammonia production. The design can be integrated in the overall plant considering also peculiarity of the three energy sources considered: solar/wind electricity, biogas from anaerobic digestion and syngas from biomass gasification. Such results open to a novel concept for distributed ammonia production that permits reducing of CO$_2$ emissions and costs and increase the security of supply. In addition considering a future application of NH$_3$ as a fuel, such concepts permits to store renewable energy into an energy vector with high energy density and low emission. Distributed storage reduces grid losses of electricity and permits to use produced energy in transportation field with the development and diffusion of vehicles powered by NH$_3$.

References

[1] C. Linde, (1903). U.S. Patent No. 727,650. Washington, DC: U.S. Patent and Trademark Office.
[2] S. Ivanova, R. Lewis, Producing nitrogen via pressure swing adsorption, Chem. Eng. Prog. 108 (6) (2012) 38–42.
[3] I. Dybkjaer, Ammonia production processes, in: Ammonia, Springer Berlin Heidelberg, 1995, pp. 199–327.
[4] S. Weitemeyer, D. Kleinhans, T. Vogt, C. Agert, Integration of Renewable

Energy Sources in future power systems: the role of storage. Renew. Energy 75 (2015) 14–20.

[5] P. Gilbert, S. Alexander, P. Thornley, J. Brammer, Assessing economically viable carbon reductions for the production of ammonia from biomass gasification. J. Clean. Prod. 64 (2014) 581–589.

[6] S. Wood, A. Cowie, A review of greenhouse gas emission factors for fertiliser production, in: IEA Bioenergy Task, vol. 38 No. 1, 2004, June, pp. 1–20.

[7] J. Tallaksen, F. Bauer, C. Hulteberg, M. Reese, S. Ahlgren, Nitrogen fertilizers manufactured using wind power: greenhouse gas and energy balance of community-scale ammonia production. J. Clean. Prod. 107 (2015) 626–635.

[8] http://minerals.usgs.gov/minerals/pubs/commodity/nitrogen/mcs-2014-nitro.pdf (accessed 17.07.2016).

[9] http://www.blonkconsultants.nl/wp-content/uploads/2016/06/fertilizer_production-D03.pdf (accessed 17.07.2016).

[10] T.E. Mallouk, Water electrolysis: divide and conquer, Nat. Chem. 5 (5) (2013) 362–363.

[11] M. Wang, Z. Wang, X. Gong, Z. Guo, The intensification technologies to water electrolysis for hydrogen production—A review, Renew. Sustain. Energy Rev. 29 (2014) 573–588.

[12] M. Granovskii, I. Dincer, M.A. Rosen, Greenhouse gas emissions reduction by use of wind and solar energies for hydrogen and electricity production: economic factors, Int. J. Hydrogen Energy 32 (8) (2007) 927–931.

[13] P. Parthasarathy, K.S. Narayanan, Hydrogen production from steam gasification of biomass: influence of process parameters on hydrogen yield—A review, Renew. Energy 66 (2014) 570–579.

[14] G. Ruoppolo, P. Ammendola, R. Chirone, F. Miccio, H₂-rich syngas production by fluidized bed gasification of biomass and plastic fuel, Waste Manag. 32 (4) (2012) 724–732.

[15] S. Giddey, S.P.S. Badwal, A. Kulkarni, Review of electrochemical ammonia production technologies and materials, Int. J. Hydrogen Energy 38 (34) (2013) 14576–14594.

[16] S. Heidenreich, P.U. Foscolo, New concepts in biomass gasification, Prog. Energy Combust. Sci. 46 (2015) 72–95.

[17] S. Caro, D. Torres, M. Toledo, Syngas production from residual biomass of forestry and cereal plantations using hybrid filtration combustion, Int. J. Hydrogen Energy 40 (6) (2015) 2568–2577.

[18] P. Brachi, R. Chirone, F. Miccio, M. Miccio, A. Picarelli, G. Ruoppolo, Fluidized bed co-gasification of biomass and polymeric wastes for a flexible end-use of the syngas: focus on bio-methanol, Fuel 128 (2014) 88–98.

[19] P. Lv, Z. Yuan, C. Wu, L. Ma, Y. Chen, N. Tsubaki, Bio-syngas production from biomass catalytic gasification, Energy Convers. Manag. 48 (4) (2007) 1132–1139.

[20] G. Ruoppolo, F. Miccio, R. Chirone, Fluidized bed cogasification of wood and coal adopting primary catalytic method for tar abatement, Energy & Fuels 24 (3) (2010) 2034–2041.

[21] J. Duscomb, A. Kouthapalli, R. Fakhrai, Thermal conversion efficiency of producing hydrogen enriched syngas from biomass steam gasification, Int. J. Hydrogen energy 38 (27) (2013) 11790–11798.

[22] P.J. Woolcock, R.C. Brown, A review of cleaning technologies for biomass-derived syngas, Biomass Bioenergy 52 (2013) 54–84.

[23] S.D. Sharma, M. Dolan, D. Park, L. Morpeth, A. Ilyushechkin, K. McLennan, K.V. Thambimuthu, A critical review of syngas cleaning technologies—fundamental limitations and practical problems, Powder Technol. 180 (1) (2008) 115–121.

[24] E. Morgan, J. Manwell, J. McGowan, Wind-powered ammonia fuel production for remote islands: a case study, Renew. Energy 72 (2014) 51–61.

[25] S.S. Beerbühl, M. Fröhling, F. Schultmann, Combined scheduling and capacity planning of electricity-based ammonia production to integrate renewable energies, Eur. J. Op. Res. 241 (3) (2015) 851–862.

[26] P. Trop, D. Goricanec, Comparisons between energy carriers' productions for exploiting renewable energy sources, Energy (2015), http://dx.doi.org/10.1016/j.energy.2015.07.013, ISSN 0360-5442.

[27] M. Huberty, L. Schmidt, E. Cussler, Small-scale production of renewable ammonia, in: S. Kong (Ed.), 5th Ammonia Fuel Conference, Minneapolis, Combustion Efficiency and Exhaust Emissions of Ammonia Combustion in Diesel Engines." Papers of the 5th Ammonia Fuel Conference, Minneapolis, vol. 1, 2008, September.

[28] A. Patil, L. Laumans, H. Vrijenhoef, Solar to ammonia—via Proton's NFuel units, Procedia Eng. 83 (2014) 322–327.

[29] C. Zamfirescu, I. Dincer, Using ammonia as a sustainable fuel, J. Power Sources 185 (1) (2008) 459–465.

[30] C. Zamfirescu, I. Dincer, Ammonia as a green fuel and hydrogen source for vehicular applications, Fuel Process. Technol. 90 (5) (2009) 729–737.

[31] J.H. Lee, S.I. Lee, O.C. Kwon, Effects of ammonia substitution on hydrogen/air flame propagation and emissions, Int. J. Hydrogen Energy 35 (20) (2010) 11332–11341.

[32] A.J. Reiter, S.C. Kong, Combustion and emissions characteristics of compression-ignition engine using dual ammonia-diesel fuel, Fuel 90 (1) (2011) 87–97.

[33] A.A. Boretti, Novel heavy duty engine concept for operation dual fuel H₂–NH₃, Int. J. Hydrogen Energy 37 (9) (2012) 7869–7876.

[34] I. Pérez, M. Garfí, E. Cadena, I. Ferrer, Technical, economic and environmental assessment of household biogas digesters for rural communities, Renew. Energy 62 (2014) 313–318.

[35] N.B. Esteves, A. Sigal, E.P.M. Leiva, C.R. Rodriguez, F.S.A. Cavalcante, L.C. de Lima, Wind and solar hydrogen for the potential production of ammonia in the state of Ceará–Brazil, Int. J. Hydrogen Energy 40 (32) (2015) 9917–9923.

[36] Max Appl, Ammonia: Principles and Industrial Practice, Springer Berlin Heidelberg, 1999.

[37] J.B. Holm-Nielsen, T. Al Seadi, P. Oleskowicz-Popiel, The future of anaerobic digestion and biogas utilization, Bioresour. Technol. 100 (22) (2009) 5478–5484.

[38] P. Mondal, G.S. Dang, M.O. Garg, Syngas production through gasification and cleanup for downstream applications—Recent developments, Fuel Process. Technol. 92 (8) (2011) 1395–1410.

[39] N. Couto, A. Rouboa, V. Silva, E. Monteiro, K. Bouziane, Influence of the biomass gasification processes on the final composition of syngas, Energy Procedia 36 (2013) 596–606.

[40] http://www.linde-engineering.com/internet.global.lindeengineering.global/en/images/HA_N_1_1_e_08_150dpi19_6131.pdf (accessed 17.07.2016).

[41] http://www.fch.europa.eu/sites/default/files/study%20electrolyser_0-Logos_0_0.pdf (accessed 17.07.2016).

[42] M. Carmo, D.L. Fritz, J. Mergel, D. Stolten, A comprehensive review on PEM water electrolysis, Int. J. Hydrogen Energy 38 (12) (2013) 4901–4934.
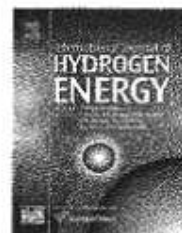
SOFC operating with ammonia: Stack test and system analysis

CrossMark

G. Cinti [a,*], G. Discepoli [a], E. Sisani [a], U. Desideri [b]

[a] Department of Engineering, Università degli Studi di Perugia, Via G. Duranti 93, 06125 Perugia, Italy
[b] Department of Energy, Systems, Territory and Constructions Engineering, Università di Pisa, Largo L. Lazzarino, 56122 Pisa, Italy

ARTICLE INFO

ABSTRACT

Ammonia has been studied as a potential energy vector and suitable fuel for Solid Oxide Fuel Cells (SOFCs). The use of ammonia could guarantee high electrical efficiency, with a carbon free and high energy density fuel. This study analyzes the potential of a power generation system based on a SOFC fueled by NH_3. Experimental tests on a SOFC short stack were developed using both pure and diluted ammonia. The tests demonstrated the operation of the concept and highlighted possible advantages in terms of thermal equilibrium. Decomposition of ammonia introduces an endothermic reaction that permits heat absorbance in the anode and a better control of stack temperature. Based on tests results, a thermodynamic model of a complete system was designed and studied. The results demonstrate that the ammonia fueled SOFC is more efficient than an equivalent hydrogen fueled one, due to the cooling effect of internal reactions that reduces ancillaries energy consumptions related to cathode air flow.

© 2016 Hydrogen Energy Publications LLC. Published by Elsevier Ltd. All rights reserved.

Introduction

Ammonia is the most produced chemical worldwide and its production is based on a well-known and efficient technology. Moreover, ammonia is widely distributed, due to its utilization as fertilizer in agriculture and a logistic network is already present. Those aspects, along with a high energy density and a carbon free status, make ammonia a potential green and sustainable energy vector, especially if renewable energy is used to produce the basic chemicals (hydrogen and nitrogen) necessary for its synthesis [1]. Ammonia has a higher density than other energy vectors, since it can be stored as a liquid phase at low pressure (20 bar) and it can be easily and efficiently transported [1,2]. During its combustion, ammonia reacts with oxygen producing only nitrogen and water, without CO_2 emissions.

Additional advantages can be obtained if hydrogen and nitrogen are produced using carbon free energy sources following the so called path to Green Ammonia [3]. Currently, almost the entire worldwide ammonia stock is made using hydrogen produced by natural gas reforming, which does not make ammonia a carbon free fuel [4], even though, in this plants, carbon dioxide is usually recovered and commercialized as a pure technical gas for other purposes (gaseous soft drinks and production of other chemicals), and it is not directly emitted in the atmosphere.

Table 1 reports physical and energy properties of a variety of fuels, including hydrogen, pure ammonia and ammonia diluted into water. Diluted ammonia, compared to pure one, is not toxic and, consequently, is widely diffused in different industrial markets (cleaning, chemicals, etc.). Two levels of dilution for ammonia were considered: 0.4 and 0.3 M concentration (X), both available in commerce and with an acceptable energy density. Table 1 shows how ammonia has very interesting gravimetric and volumetric densities compared to other fuels. With respect to pure ammonia, diluted mixtures are strongly penalized, especially for their low gravimetric density, but they are significantly less dangerous in terms of toxicity and flammability.

Ammonia can be utilized as fuel in different energy systems. The oxidation reaction is exothermic and produces heat, thus all internal and external combustion technologies could be fueled by ammonia [6-10]. However, in such applications, characterized by high combustion temperature, the emissions of NO_x cannot be avoided and they even increase, due to the presence of nitrogen in the fuel. Another potential path for the use of ammonia in energy systems is the decomposition of ammonia into hydrogen and nitrogen and, consequently, the use of hydrogen as a well-known fuel in combustion systems or in low temperature fuel cells [11].

An innovative and very promising application is the direct use of NH_3 in high temperature fuel cells, such as SOFCs [12]. In commercial SOFCs the anode is based on nickel, that is an excellent catalyst of ammonia cracking reaction. Consequently, ammonia is directly cracked in the cell into hydrogen and nitrogen, resulting in a suitable mixture for the operation of the cell. In addition, such reaction is endothermal and keeps the cell at a lower temperature than with pure hydrogen. This is very interesting at system level, because all endothermal reactions take part of the heat generated by the cell that should, otherwise, be collected by the cathode air stream. Such stream has to be heated and pressurized to get into the cell with relevant losses in terms of exergy efficiency and any reduction of the temperature in the fuel cell is beneficial. The use of ammonia permits a smaller air flow rate with reduced consumption of electricity in the blower.

The operation of SOFC with ammonia was first observed in 1980, studying an innovative technology to produce NO_2 where electricity was a byproduct. Since then, the experimentation was focused particularly on the risk of NO_x production; this aspect is not interesting anymore and represents, on the contrary, a limiting factor for the use of this technology for energy applications. The research activity in

that field was mainly focused on the optimization of anodic composition to reduce operational temperature and increase power density. Maffei at al. focused their efforts on studying intermediate temperature SOFCs [13-16] operating with NH_3 and on the electrolyte typology, either ionic or electronic, achieving acceptable operational temperatures as low as 450 °C [15]. Similarly, Ma et al. developed and tested innovative electrodes and electrolytes to obtain maximum power density from a SOFC fed by ammonia operating in the temperature range 550-700 °C [17-20]. Literature reports also experimental tests performed with SOFCs made of standard commercial materials [21-27]. All results show that ammonia completely cracks in the cell anode and the electrochemical reaction occurs in a two stage process. No NO_x production is reported, demonstrating that there is no risk of emitting this undesired gas during fuel cell operation.

At system level, very little is reported in literature, mainly related to theoretical system studies [22,28] and system components [29]. There is no paper in the literature showing a complete study on the advantages of heat balancing when ammonia is used as fuel. This study aims to cover this aspect, developing a system model based on experimental study on a SOFC short stack fueled by ammonia. In addition, the study also analyzes the use of diluted ammonia that can offer interesting prospective due to its easy handling, fewer risks of toxic compounds release, improved fire safety and even wider distribution.

Methodology

The study is based on the experimental results on a short stack directly fed by pure and diluted ammonia. Such results were used in a thermodynamic model simulating a system designed to operate with NH_3. The following paragraphs describe the experimental and modeling methodologies.

Experimental tests

The experimental tests were developed on a short stack supplied by Forschungszentrum Jülich based on 4 single Anode Supported Cells (ASC) planar cells. Stack details are reported in Table 2. The stack and the test rig used were already described in previous studies [30-33]. The stack was equipped with voltage sensors for each cell and two thermocouples were placed close to the anode (T1) and cathode inlet (T2).

Fuel	Storage		Molar mass [g/mol]	Density [kg/m³]	Gravimetric energy density [MJ/kg]	Volumetric energy density [GJ/m³]
	T [°C]	P [bar]				
Liquid ammonia (NH_3)	20	10	17.03	610.33	18.65	11.38
Gaseous hydrogen (H_2)	20	250	2.016	17.86	120.21	2.15
Methanol (CH_3OH)	20	1	32.04	790.95	19.7	15.58
Natural Gas (CH_4)	20	250	16.04	195.36	50	9.77
Gasoline (C_8H_{18})	20	1	114.23	702.31	43.6	30.62
Diluted ammonia X = 0.4 (NH_3)	20	1		870.65	7.22	6.29
Diluted ammonia X = 0.3 (NH_3)	20	1		894.41	5.37	4.80

Table 1 – Physical and energy properties of different fuels [5].

The experimental activity focused on measuring polarization curves. Such tests were performed varying the current at constant steps of 25 mA/cm^2. Each current condition was kept for two minutes and the lowest voltage was set at 0.6 V. Voltage and temperatures were calculated as mean values during each step. Inlet gas composition and furnace temperature were kept constant during the polarization curve.

The test campaign was developed in three phases. The first phase focused on the comparison between the stack operating with three compositions: pure hydrogen, simulated craked ammonia (H_2/N_2), and pure NH_3. Hydrogen flow rate was set at 60 Stl/h for pure H_2, simulated craked mixture was obtained with 60 Stl/h of H_2 and 20 Stl/h of N_2, and, finally, ammonia flow rate was calculated considering the complete cracking of ammonia via the reaction:

$$NH_3 = \frac{3}{2}H_2 + \frac{1}{2}N_2 \qquad (1)$$

Table 3 reports gas flow rates used in the first phase of the experimental tests. The results are three gas flows that have the same amount of hydrogen, considering also ammonia complete decomposition.

Each composition was tested at three different furnace temperature: 700, 750 and 800 °C. For all tests air flow was kept constant at 400 Stl/h.

A second phase aimed at quantifying the thermal effect of ammonia introduction. With such objective, air variation study was performed. To evaluate the contribution of the ammonia cracking reaction to the temperature equilibrium, the test was performed with pure H_2 varying the air flow rate. In detail, the air flow rate was varied at Open Circuit Voltage (OCV) conditions and reduced down to 50% of its nominal value (400 Stl/h). OCV condition was chosen to isolate the effect of the chemical reaction from the thermal contribution coming from the polarization losses. Furnace temperature was kept constant at 800 °C.

In the third phase, the experimental tests were designed to evaluate the performance of diluted ammonia. A mix of water and ammonia was used to feed the stack with two concentrations, namely 0.3 and 0.4 M ratio of NH_3/H_2O. Used flows are reported in Table 4. Air flow was kept constant at nominal 400 Stl/h. The tests were performed at 750 °C.

Table 3 – Gas compositions tested in first phase.

	H_2 [Stl/h]	N_2 [Stl/h]	NH_3 [Stl/h]
H_2	60	0	0
H_2/N_2	60	20	0
NH_3	0	0	40

Model

To perform a study at system level, a 0-dimensional thermodynamic model was developed. The model uses the FluidProp Library for thermodynamic parameters. The model was developed with the main scope of evaluating energy equilibrium and, at system level, the effect of ammonia on cathode inlet flow. The system schematic is shown in Fig. 1. The SOFC stack model is based on experimental results. Equilibrium is calculated by varying air inlet flow rate in order to have a stack exhaust gas temperature 100 °C higher than the inlet one. Inlet gas temperature is set at 700 °C for both anode and cathode, in order to have a stack average operating temperature of 750 °C and outlet temperature of 800 °C. Electrochemical characteristic were derived from experimental values as described in the following paragraph. The model calculates the current density from fuel inlet flow rate and fuel utilization (U_f) using Equation (2):

$$J = \frac{U_f * F * n * n_{fuel}}{A * n_{cell}} \qquad (2)$$

where F is the Faraday constant, n_{fuel} is the molar fuel gas flow, A the cell area, n_{cell} the number of cells and n the mole of electron available for each mole of inlet fuel (for hydrogen n = 2).

Both cathode air and anode fuel are heated up to the stack temperature recovering the heat available in SOFC exhaust. Inlet flows undergo a two stage heating. High temperature heat exchangers, HE-2 (anode) and HE-3 (cathode) in Fig. 1, are heated up by recovering the exhaust heat from the cell. This is always possible because SOFC outlet temperature is higher than the inlet one and the total mass flow composition (from cathode to anode) does not compensate the temperature increase. Design conditions of high temperature heat exchanger are set by an outlet exhaust temperature of 330 °C. Products of combustion are used in a low temperature heat exchanger to heat up cathode air (HE-4) and fuel (HE-1) from ambient conditions. Whenever diluted ammonia was added to the fuel, the first heat exchanger (HE-1) also acts as evaporator. The afterburner (AB) was designed with the assumption of a complete combustion of inlet fuel. According to literature [34], the afterburners operate with an inlet temperature of 330 °C and a maximum outlet temperature of 900 °C. Stack's thermal losses were modeled as 10% of the electrical power. The model calculates the energy balance of the stack, of the after burner

Table 2 – Stack characteristics.

Anode substrate	Ni/8YSZ cermet 1500 μm
Anode functional layer	Ni/8YSZ cermet 7–10 μm
Electrolyte	8YSZ 8–10 μm
Cathode functional layer	LSM/8YSZ 10–15 μm
Cathode current collector	LSM 60–70 μm
Stack design	F-design
Interconnect/cell frame	Crofer22APU
Anode contact layer	Ni-mesh
Cathode contact layer	perovskite type oxide (LCC10)
Sealing	glass-ceramic (87YSZ20)
Number of cells	4
Size of cells	100 × 100 mm^2
Active area per cell	80 cm^2
Total active area	320 cm^2

Table 4 – Gas compositions used during the third phase.

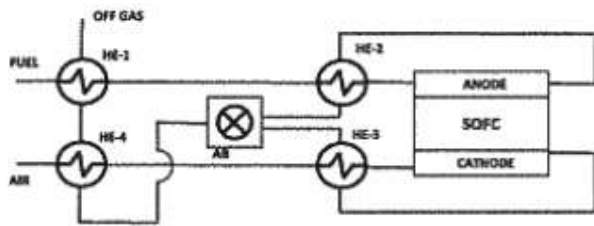|	H_2O [g/h]	NH_3 [Stl/h]
X03	75	40
X04	48	40

Fig. 1 – Schematic of the system model.

Table 5 – Maximum voltage differences between polarization curves.

	700 °C	750 °C	800 °C
H_2/N_2 Vs H_2	−1.3%	−2%	0.3%
NH_3 Vs H_2	−0.1%	−2%	−1.9%

maximum voltage differences between the same temperature curves in the order of 0.1–2%. Such results shows how ammonia can perfectly feed a SOFC stack as expected from
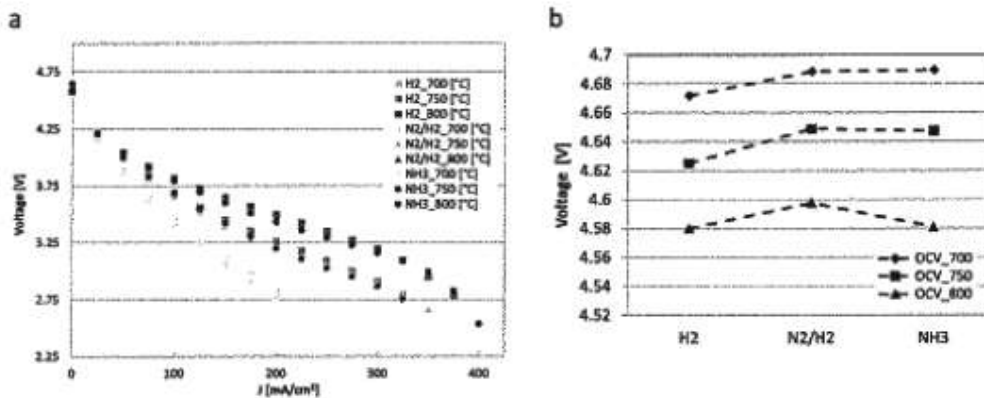

Fig. 2 – Polarization curves (a) and OCV (b) relative to the first phase.

and of the heat exchangers. A total pressure loss of 100 mbar was assumed in the cathode gas line and 90% heat exchangers efficiency was considered for all devices. In order to evaluate the overall system efficiency, air blower was assumed to operate with an isentropic efficiency of 0.8.

Results and discussion

Polarization curves and OCV values of the first phase are shown in Fig. 2. In such phase, nine curves were measured (3 compositions for 3 temperatures). The polarization curves show that stack performance is almost unchanged with the three tested compositions, even when the reduction of temperature causes an expected fall of performance. A more detailed investigation (reported in Table 5) shows the

single cells studies. In addition a study of OCV values was performed (Fig. 2 – b). All compositions featured an increase of OCV values at lower temperatures. This phenomenon was already discussed at cell level and is here confirmed in the stack. Considering the OCV values at 750 and 700 °C the N_2/H_2 mixture shows higher values than pure hydrogen and at the same level of ammonia. The dilution effect of nitrogen, that seems in contrast with Nernst law, was already discussed in many studies and has to be related to a positive effect due to gas distribution and inlet gas speed. The equivalence of ammonia and N_2/H_2 mix is an additional indication of ammonia decomposition in the stack.

Fig. 3 shows the average temperature (between T1 and T2) during the tests. As expected, the temperature of the ammonia mixture is always lower due to the effect of endothermal cracking reaction. Such temperature difference is
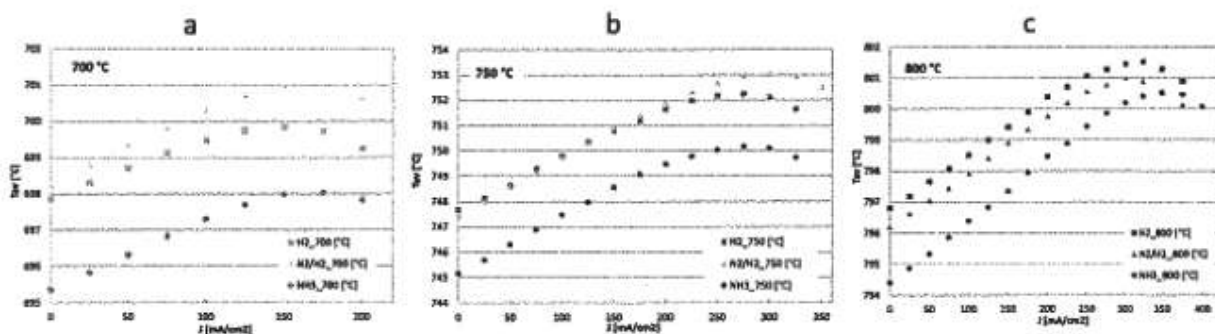

Fig. 3 – Average temperature variation during polarization curves at 700 °C (a), 750 °C (b) and 800 °C (c).
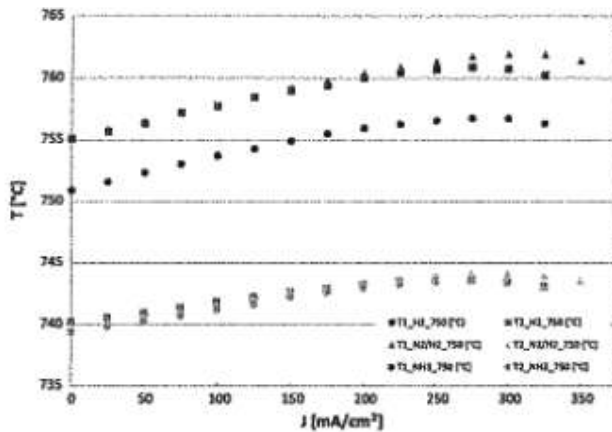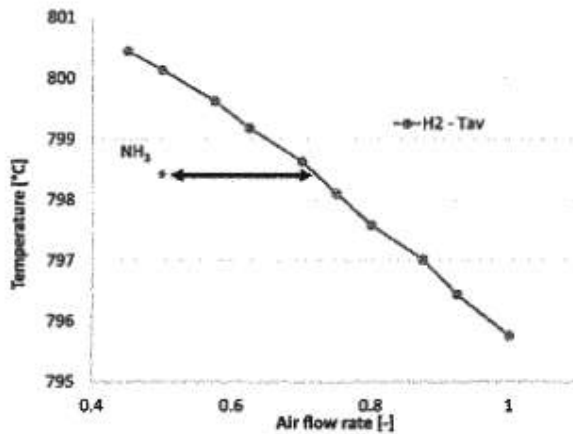
Fig. 4 – T1 and T2 variation at 750 °C.

Fig. 5 – OCV test with different air flow rate at 800 °C.

relatively constant at different temperatures and at all current values and is in the range of 3 °C.

Fig. 4 shows the values of T1 and T2 for the 750 °C polarizations. The cathode temperature (T2) does not change between tests due to the constant value of air inlet. T1, close to anode inlet, is the one that in NH₃ case brings the cooling contribution to the stack obtaining two effects: the average temperature of the stack is lower compared to the other
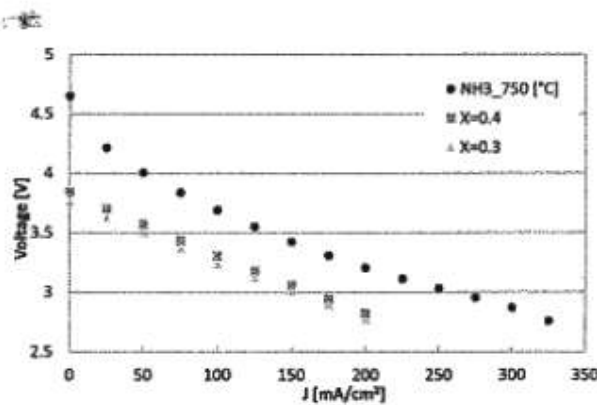

Fig. 6 – Test results with diluted ammonia at 750 °C.
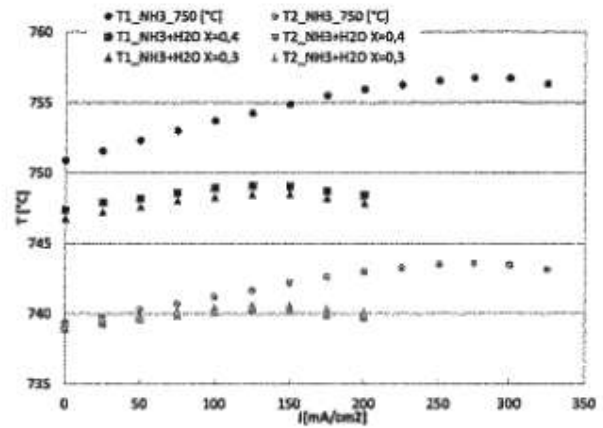

Fig. 7 – Temperature variation in the stack during diluted tests.

compositions and also the difference between T1 and T2 is reduced. Both those effects have to be considered as positive for the thermal stability of the stack and the reduction of thermal stresses. Similar curves were obtained at 700 and 850 °C.

The results of the first phase confirms main results already obtained at single cell level [21]: the use of ammonia does not reduce SOFC performances and a two stage reaction can be predicted with a preliminary ammonia cracking and a consequent electrochemical reaction of hydrogen. In addition, the analysis of the temperature shows a cooling effect in the stack related to decomposition reaction.

In order to better evaluate the effect of cracking reaction on the equilibrium, the second phase of experimental activity investigates the equilibrium temperature when varying the air flow. The aim of these tests is to quantify, with experimental measurements, the reduction of air flow rate that can be obtained when using ammonia. Fig. 5 shows the stack average temperature at OCV with H_2, when varying the inlet air flow rate. Air flow is plotted as the fraction of the nominal value of 400 Stl/h. An almost linear behavior relates air flow rate with the stack average temperature at OCV. The graph reports also the temperature at OCV with NH_3 pure gas flow rate and air flow rate of 0.50 of the nominal value. That temperature is the equivalent of H_2 test with the air flow rate of 0.73 of the nominal value. Thus, such temperature can be obtained by increasing the air flow rate or by changing hydrogen with ammonia. This test demonstrates that ammonia operation requires a smaller air flow rate (0.5) than the one necessary using hydrogen (0.72). Such reduction in the air flow rate allows to increase the system efficiency due to a reduced air compressor energy consumption.

Table 6 – Fitted values of the linear regression of polarization curves at 750 C.

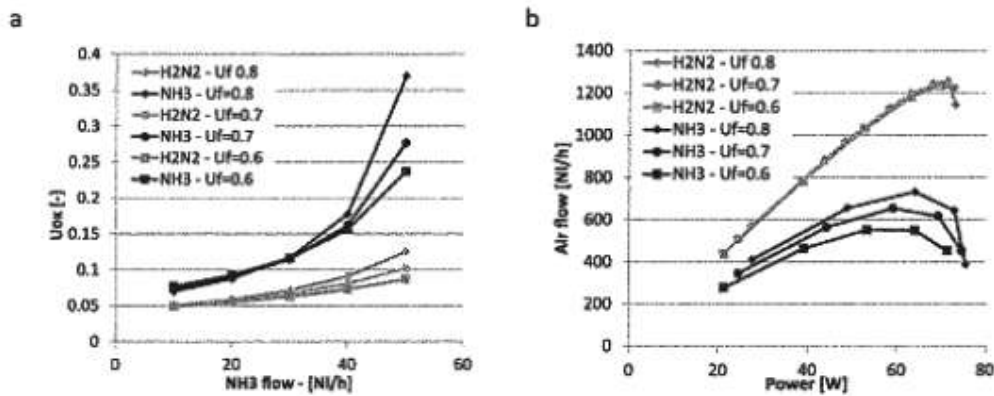| Fuel	m	q
H_2/N_2	−0.00514	4.274
NH_3	−0.00503	4.293
X = 0.4	−0.00508	3.833
X = 0.3	−0.00492	3.746

Fig. 8 − Model results of air flow reduction as function of ammonia flow (a) and power rate (b).

Finally the tests with diluted ammonia (third phase) were performed. As expected, the steam content strongly affects OCV values and, consequently, the polarization curve. Steam acts as an inert gas in the anode, lowering hydrogen concentration in the total flow. A reduction of 19% and 17%, with respect to pure ammonia, was measured at OCV for ammonia/water fractions of 0.3 and 0.4 respectively (Fig. 6). Those reductions become 12% and 10% at 50 mA/cm² (after activation losses) and remain constant at higher currents. The steam dilution also affects the temperature. Fig 7 shows T1 and T2 variations. In general, steam, being inert at the anode and increasing total heat capacity, reduces temperature changes caused by the increase of current density. In the ammonia-water mixtures, both T1 and T2 are more stable with the increase of current density. In addition, the anodic temperature (T1) is smaller because of a larger mass flow rate and heat capacity, compared to pure ammonia.

Experimental results were used to develop the theoretical model. The model was operated at 750 °C. Consequently, the temperature boundary conditions for the model were 700 and 800 °C for gas inlet and outlet, respectively. The electrochemical model is based on the polarization results, and, taking advantage of the reduced activation losses of the measured curves, typical of SOFCs, a linear regression was performed for each polarization curve in the form $V = mJ + q$.

The fitted values of m and q are listed in Table 6. This approach does not bring to the validation of an electrochemical model but a model itself is derived from the regression of experimental results.

To evaluate system performance the model was studied varying two main parameters: utilization of fuel and inlet fuel flow. For all simulations air inlet flow is calculated so to obtain average stack temperature at design value (750 °C). Fuel utilization was varied in the range $U_f = 0.6, 0.7$ and 0.8, while inlet gas flow was varied considering inlet NH_3 quantity (pure hydrogen or considering ammonia decomposition) in the range 10–50 Stl/h with steps of 10 Stl/h. Main parameter outputs of the study are electrical power, stack and system efficiency, inlet air flow and utilization of oxygen. Here below the definition of each parameter:

Stack efficiency	$\eta_S = \frac{P_{el}}{LHV_{fuel} \cdot m_{fuel}}$	(1)
System efficiency	$\eta_S = \frac{P_{el}-P_{anc}}{LHV_{fuel} \cdot m_{fuel}}$	(2)
Utilization of oxygen	$U_{ox} = \frac{I}{n \cdot F \cdot m_{O_2}}$	(3)

where P_{el} is stack power, P_{anc} is ancillaries power adsorption, LHV_{fuel} is fuel lower heating value and m_{fuel} is fuel molar flow. Additional thresholds introduced for the correct operation of the system are: minimum voltage value of 0.5 V (each
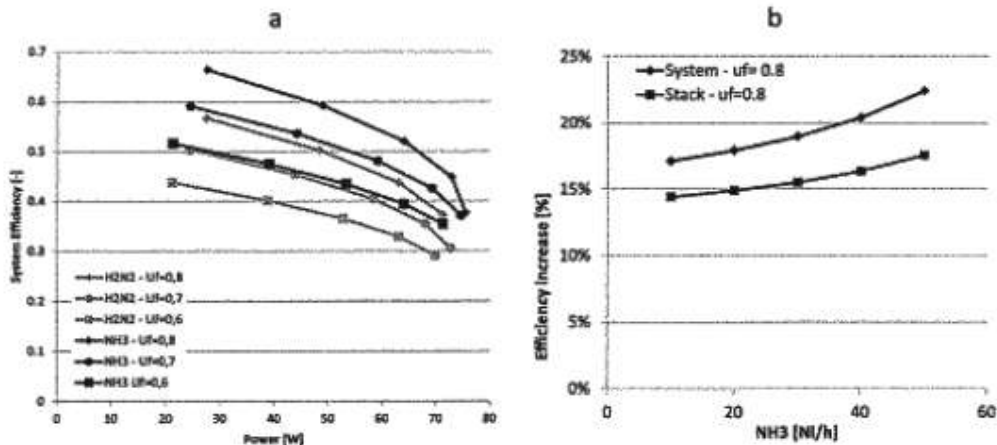

Fig. 9 − Model results of system efficiency of NH_3 and H_2N_2 based model.

cell) and maximum afterburner temperature of 900 °C. Whenever such conditions were not respected, results were not considered for the study.

Inlet fuels studied were H_2/N_2 mixture, pure NH_3 and diluted NH_3. The relation between hydrogen and ammonia flows is the same already presented in the experimental phase.

Model results operating with pure NH_3 and H_2/N_2 mixture as a fuel are reported in Fig. 8 and Fig. 9. Fig. 8 reports results of air study analysis while in Fig. 9 the efficiencies are reported. Fig. 8 (a) depicts U_{ox} values variation as function of inlet fuel for the three U_f studied. Ammonia requires higher U_{ox} (less air) compared to equivalent H_2/N_2 mixture. The increase of U_f produces an increase of U_{ox} for both fuels. The latter effect is mainly related to the increase of efficiency (see Fig. 9) and consequently a reduction of heat produced in form of irreversibility.

The same results are differently reported in Fig. 8 (b), where air flow is plotted as function of stack power. Similar curves are obtained for H_2/N_2 flows while, in the case of NH_3, differences are evident varying U_f. This peculiarity is related to the fact that fuel flow and system power are not directly related.

Fig. 9 (a) reports stack efficiencies as function of power. Such curves show the typical behavior of SOFC, with an increase of efficiency when power is rated. All curves related to simulation using NH_3 as a fuel are higher than the equivalent N_2/H_2. Such increase is close to 0.1 points for each U_f and does not have significant variations with power. The increase of performance was deeply commented in the experimental part, used as input in the model, and a similar trend is reported. In addition, the model permits to study additional effect at system level due to air flow reduction. In particular, Fig. 9 (b) reports the increase of efficiency, in terms of percentage, obtained with NH_3 compared to the equivalent mix. The two curves reported are both for the case $U_f = 0.8$ and differ for using in calculations system or stack efficiency. The graph shows how the main contribution (15%) comes from the increase of stack efficiency while an additional contribution (3-5%) comes from system level.
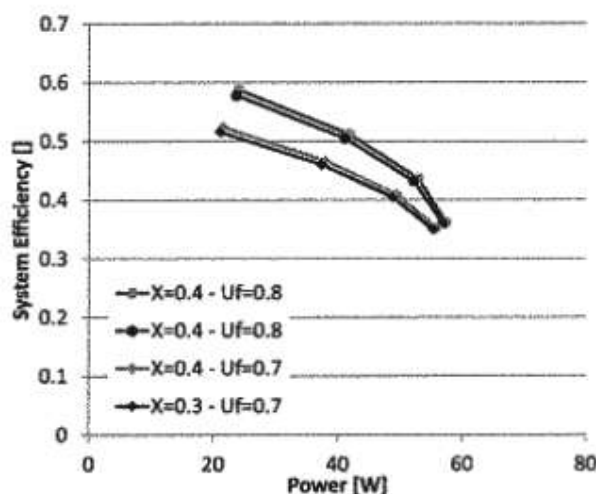
The model was also operated with diluted ammonia with concentration of 0.3 and 0.4. Results of stack efficiency calculations with the ammonia/water mixture are depicted in Fig. 10.

The operational range of power output is smaller due to the reduced performance and to the large amount of steam entering the after burner, with consequent increase of exhaust temperature. The difference between the two diluted compositions is minimal. As expected, higher concentrations allow to achieve higher values. Despite reduced performance, system reaches values higher than 50% at utilization of fuel 0.8.

Conclusion

The study succeeded on evaluating, both experimentally and theoretically, the advantage of operating a SOFC system with ammonia. Because of cathode air flow rate reduction, caused by the different heat balance due to internal ammonia cracking, the efficiency increases up to 22% when the system is fed with ammonia compared with a gaseous mixture with the same amount of hydrogen and nitrogen. In addition, the operation of SOFC with diluted ammonia was assessed and the efficiency was found to be as high as 50%. Such result is extremely interesting considering that diluted ammonia is not toxic, not flammable and can be easily handled. The authors imagine that a potential application of this latter situation could be in the field of auxiliary power units (APU), which could be easily fueled producing electricity with high efficiency and zero emissions.

Acknowledgments

Fig. 10 – Efficiency of system operating with diluted ammonia.

REFERENCES

[1] Zamfirescu C, Dincer I. Using ammonia as a sustainable fuel. J Power Sources 2008;185:459–65. http://dx.doi.org/10.1016/j.jpowsour.2008.02.097.

[2] Morgan E, Manwell J, McGowan J. Wind-powered ammonia fuel production for remote islands: a case study. Renew Energy 2014;72:51–61. http://dx.doi.org/10.1016/j.renene.2014.06.034.

[3] Zamfirescu C, Dincer I. Ammonia as a green fuel and hydrogen source for vehicular applications. Fuel Process Technol 2009;90:729–37. http://dx.doi.org/10.1016/j.fuproc.2009.02.004.

[4] Tallaksen J, Bauer F, Hulteberg C, Reese M, Ahlgren S. Nitrogen fertilizers manufactured using wind power: greenhouse gas and energy balance of community-scale ammonia production. J Clean Prod 2015. http://dx.doi.org/10.1016/j.jclepro.2015.05.130.

[5] Linstrom PJ, W.G. Mallard. NIST Chemistry WebBook, NIST Standard Reference Database Number 69, Eds. n.d.

[6] Frigo S, Gentili R, Doveri N. Ammonia plus hydrogen as fuel in a S.I. Engine: experimental results. SAE Tech Pap 2012;4. http://dx.doi.org/10.4271/2012-32-0019.

[7] Duynslaegher C, Jeanmart H, Vandooren J. Ammonia combustion at elevated pressure and temperature conditions. Fuel 2010;89:3540–5. http://dx.doi.org/10.1016/j.fuel.2010.06.008.

[8] Lee JH, Lee SI, Kwon OC. Effects of ammonia substitution on hydrogen/air flame propagation and emissions. Int J Hydrogen Energy 2010;35:11332–41. http://dx.doi.org/10.1016/j.ijhydene.2010.07.104.

[9] Reiter AJ, Kong S-C. Combustion and emissions characteristics of compression-ignition engine using dual ammonia-diesel fuel. Fuel 2011;90:87–97. http://dx.doi.org/10.1016/j.fuel.2010.07.055.

[10] Karabeyoglu A, Evans B. Selection of NH3 for gas turbine use. In: 8th NH3 Conf – Portl; 2011.

[11] Alagharu V, Palanki S, West KN. Analysis of ammonia decomposition reactor to generate hydrogen for fuel cell applications. J Power Sources 2010;195:829–33. http://dx.doi.org/10.1016/j.jpowsour.2009.08.024.

[12] Afif A, Radenahmad N, Cheok Q, Shams S, Kim JH, Azad AK. Ammonia-fed fuel cells: a comprehensive review. Renew Sustain Energy Rev 2016;60:822–35. http://dx.doi.org/10.1016/j.rser.2016.01.120.

[13] Maffei N, Pelletier L, Charland J, McFarlan A. An intermediate temperature direct ammonia fuel cell using a proton conducting electrolyte. J Power Sources 2005;140:264–7. http://dx.doi.org/10.1016/j.jpowsour.2004.08.020.

[14] Maffei N, Pelletier L, Charland JP. McFarlan a. An ammonia fuel cell using a mixed ionic and electronic conducting electrolyte. J Power Sources 2006;162:165–7. http://dx.doi.org/10.1016/j.jpowsour.2006.06.056.

[15] Maffei N, Pelletier L. McFarlan a. A high performance direct ammonia fuel cell using a mixed ionic and electronic conducting anode. J Power Sources 2008;175:221–5. http://dx.doi.org/10.1016/j.jpowsour.2007.09.040.

[16] Pelletier L, McFarlan A, Maffei N. Ammonia fuel cell using doped barium cerate proton conducting solid electrolytes. J Power Sources 2005;145:262–5. http://dx.doi.org/10.1016/j.jpowsour.2005.02.040.

[17] Ma Q, Peng R, Lin Y, Gao J, Meng G. A high-performance ammonia-fueled solid oxide fuel cell. J Power Sources 2006;161:95–8. http://dx.doi.org/10.1016/j.jpowsour.2006.04.099.

[18] Ma Q, Peng R, Tian L, Meng G. Direct utilization of ammonia in intermediate-temperature solid oxide fuel cells. Electrochem Commun 2006;8:1791–5. http://dx.doi.org/10.1016/j.elecom.2006.08.012.

[19] Meng G, Jiang C, Ma J, Ma Q, Liu X. Comparative study on the performance of a SDC-based SOFC fueled by ammonia and hydrogen. J Power Sources 2007;173:189–93. http://dx.doi.org/10.1016/j.jpowsour.2007.05.002.

[20] Xie K, Ma Q, Lin B, Jiang Y, Gao J, Liu X, et al. An ammonia fuelled SOFC with a BaCe0.9Nd0.1O3−δ thin electrolyte prepared with a suspension spray. J Power Sources 2007;170:38–41. http://dx.doi.org/10.1016/j.jpowsour.2007.03.059.

[21] Cinti G, Desideri U, Penchini D, Discepoli G. Experimental analysis of SOFC fuelled by ammonia. Fuel Cells 2014;14:221–30. http://dx.doi.org/10.1002/fuce.201300276.

[22] Dekker NJJ, Rietveld G. Highly efficient conversion of ammonia in electricity by solid oxide fuel cells. J Fuel Cell Sci Technol 2006;3:499–502. http://dx.doi.org/10.1115/1.2349536.

[23] Fournier G, Cumming I, Hellgardt K. High performance direct ammonia solid oxide fuel cell. J Power Sources 2006;162:198–206. http://dx.doi.org/10.1016/j.jpowsour.2006.06.047.

[24] Fuerte A, Valenzuela RX, Escudero MJ, Daza L. Ammonia as efficient fuel for SOFC. J Power Sources 2009;192:170–4. http://dx.doi.org/10.1016/j.jpowsour.2008.11.037.

[25] Limin Z, You C, Weishen Y, Liwu LIN. Short communication a direct ammonia tubular solid oxide fuel cell. Chin J Catal 2007;28:749–51.

[26] Ma Q, Ma J, Zhou S, Yan R, Gao J, Meng G. A high-performance ammonia-fueled SOFC based on a YSZ thin-film electrolyte. J Power Sources 2007;164:86–9. http://dx.doi.org/10.1016/j.jpowsour.2006.09.093.

[27] Wojcik A, Middleton H, Damopoulos I, Van herle J. Ammonia as a fuel in solid oxide fuel cells. J Power Sources 2003;118:342–8. http://dx.doi.org/10.1016/S0378-7753(03)00083-1.

[28] Farhad S, Hamdullahpur F. Conceptual design of a novel ammonia-fuelled portable solid oxide fuel cell system. J Power Sources 2010;195:3084–90. http://dx.doi.org/10.1016/j.jpowsour.2009.11.115.

[29] Di Carlo A, Dell'Era A, Del Prete Z. 3D simulation of hydrogen production by ammonia decomposition in a catalytic membrane reactor. Int J Hydrogen Energy 2011;36:11815–24. http://dx.doi.org/10.1016/j.ijhydene.2011.06.029.

[30] Penchini D, Cinti G, Discepoli G, Sisani E, Desideri U. Characterization of a 100 W SOFC stack fed by carbon monoxide rich fuels. Int J Hydrogen Energy 2013;38:525–31. http://dx.doi.org/10.1016/j.ijhydene.2012.09.060.

[31] Barelli L, Cinti G, Desideri U, Ottaviano PA. SOFC thermal transients: modeling by application of experimental system identification techniques. Fuel Cells 2014;14:107–22. http://dx.doi.org/10.1002/fuce.201300164.

[32] Penchini D, Cinti G, Discepoli G, Desideri U. Theoretical study and performance evaluation of hydrogen production by 200 W solid oxide electrolyzer stack. Int J Hydrogen Energy 2014;39:9457–66. http://dx.doi.org/10.1016/j.ijhydene.2014.04.052.

[33] Fang Q, Blum L, Peters R, Peksen M, Batfalsky P, Stolten D. SOFC stack performance under high fuel utilization. Int J Hydrogen Energy 2015;40:1128–36. http://dx.doi.org/10.1016/j.ijhydene.2014.11.094.

[34] Deshpande PA, Madras G. Catalytic hydrogen combustion for treatment of combustible gases from fuel cell processors. Appl Catal B Environ 2010;100:481–90. http://dx.doi.org/10.1016/j.apcatb.2010.08.026.

Allegato A

Curriculum Vitae di Manuela Cecconi

1999. Dottore di Ricerca in Ingegneria Geotecnica

2000-2003. Assegnista di Ricerca, Università di Perugia

2004. Vincitrice di concorso ad un posto di Ricercatore Universitario (Settore ICAR07, Geotecnica), Università di Perugia.

2005. Presa di servizio come Ricercatore Universitario in Ingegneria Geotecnica, Università di Perugia

2008. Ricercatore Confermato in Ingegneria Geotecnica (RU), Università di Perugia

2014. Conseguimento in data 07/02/2014 dell'abilitazione nazionale alla seconda fascia di docenza (Professore Associato) nel settore 08/B1 (Geotecnica, ICAR/07).

Autrice di n. 91 pubblicazioni scientifiche (v. Elenco pubblicazioni più significative) comprendenti articoli su Rivista nazionale e internazionale, articoli pubblicati su Atti di Convegni, Workshop, Conferenze, in ambito nazionale ed internazionale, monografie, così suddivisi:

> Riviste: 22
> Abstract in Rivista: 1
> Contributo in volume (Capitolo o Saggio): 6
> Contributi in Atti di Convegno: 57
> Monografie: 3
> Traduzioni: 1
> Curatele: 1

Indicatori bibliometrici (da banca dati Scopus, aggiornata al mese di giugno 2017)
numero documenti indicizzati: 28
numero citazioni: 141
h-index: 6

Attività di Ricerca

Diversi sono i temi di ricerca affrontati dalla scrivente e documentati da pubblicazioni scientifiche. In particolare, risultano di particolare rilievo i seguenti temi:

a) Comportamento meccanico delle pozzolane del sottosuolo di Roma: prove meccaniche di laboratorio, caratteristiche di compressibilità, rigidezza, resistenza a taglio.

b) Processi di destrutturazione di terreni "cementati" nei problemi di stabilità dei versanti e dei fronti di scavo, in relazione alle caratteristiche micro-e macro strutturali dei depositi piroclastici.

c) Fenomeni di rottura dei grani e valutazione quantitativa degli effetti di "crushing" sulla resistenza al taglio. Formulazione di un modello costitutivo per terreni granulari con grani frantumabili.

d) Caratteristiche di rigidezza a deformazioni molto piccole di terreni piroclastici.

e) Comportamento meccanico e proprietà idrauliche di terreni granulari in condizioni di parziale saturazione.

f) Comportamento delle strutture di sostegno in condizioni statiche e sismiche. Sviluppo di metodi di calcolo agli spostamenti nella progettazione e nella valutazione della

vulnerabilità sismica di opere geotecniche in condizioni sismiche. Definizione degli spostamenti accettabili in funzione delle prestazioni richieste e dei livelli di deformazione critici, individuazione dei meccanismi di collasso, valutazione delle capacità dissipative dei sistemi terreno/struttura per diverse tipologie di strutture di sostegno;

g) Indagine sperimentale finalizzata alla valutazione del comportamento meccanico e idraulico di terreni e rocce tenere piroclastiche dell'Italia Centrale e Meridionale. Prove meccaniche di laboratorio (convenzionali e non) e analisi microstrutturali.

h) Stabilizzazione a calce di terreni piroclastici dell'Italia Centrale. Sperimentazione in laboratorio secondo un approccio multi-scala; idoneità dei terreni, proprietà di ritenzione, parametri di trattamento. Evoluzione chimico-fisica dei processi indotti dall'addizione della calce. Effetti della stabilizzazione sulle caratteristiche di compressibilità, resistenza al taglio. (Attività sperimentale condotta presso il Laboratorio di Geotecnica del Polo di Ingegneria ed il Laboratorio di Scienze della Terra di UNIPG, il Laboratorio di Geotecnica dell'Università di Cassino ed i Laboratori dell'Institut des Materiaux IMN di Nantes. Tale attività di ricerca ha costituito l'oggetto di un progetto di ricerca di base, per cui la sottoscritta ha conseguito un premio, Ricerca di base 2014);

i) Analisi degli effetti meccanici ed idraulici, indotti dall'inerbimento con radici profonde, sulle condizioni di equilibrio e di sicurezza di versanti, limitatamente a fenomeni di instabilità superficiale.

j) Fondazioni superficiali in condizioni statiche e sismiche.

k) Analisi non dimensionale nella valutazione delle condizioni di stabilità di versanti in roccia in condizioni sismiche.

Finanziamenti ottenuti e premi

-Vincitrice di uno dei tre premi di ricerca previsti dal Bando "Procedura Comparativa D.D. n. 20/2015" per l'Assegnazione quota dipartimentale fondo ricerca di base di Ateneo 2014, Università di Perugia. Titolo del progetto: "L'impiego di terreni piroclastici nella stabilizzazione a calce", Responsabile del progetto: Manuela Cecconi.
-Partecipazione, in qualità di Partecipante al Programma di Ricerca, al Progetto PRIN 2008 (finanziato) "Tecniche di miglioramento dei terreni basate sull'impiego di calce e cemento".
-Progetto Giovani Ricercatori 2000.

Partecipazione a Progetti di Ricerca

2014, 2015: Progetto ReLUIS 3 (ReLUIS 3- DPC 2014). "Strutture in muratura, wp1 – qualità muraria, proprietà meccaniche delle murature, indagini diagnostiche"

2011-2013. Studio e attività di consulenza sugli "Effetti delle tecniche di inerbimento con impianto di radici Prati Armati nella protezione da fenomeni di erosione".

2010-2013: Progetto ReLUIS 2 (ReLUIS 2- DPC 2009-2012). "Sviluppo di approcci agli spostamenti per la valutazione della vulnerabilità". Linea 2, Task 8.

2008-2011: Convenzione di ricerca con EUCENTRE 2008-2011 sul "Rischio sismico di dighe in terra".

2005-2008: Progetto ReLUIS 1 (RELUIS-DPC 2005-2008). Linea di ricerca n. 4 "Sviluppo di approcci agli spostamenti per il progetto e la valutazione della vulnerabilità", Unità di Ricerca n. 12, *Strutture di Sostegno*.

1999-2001, 2008. Partecipazione ai Progetti PRIN, in qualità di Partecipante al Programma di Ricerca.

Seminari, Organizzazione di Workshop/Convegni, Svolgimento di corsi ad invito (più recenti)

- Lezione ad invito "Prove in situ, Programmazione, Esecuzione, Interpretazione e Scopi" (2016) nell'ambito del Corso di Formazione organizzato dall'Alta Scuola - Le indagini geognostiche programmazione, esecuzione, interpretazione e scopi - Fermo, 27 - 28 ottobre 2016.

-Organizzatrice (membro del Comitato Organizzatore) e Curatore degli Atti del Convegno Internazionale Workshop on Volcanic Rocks and Soils, Ischia (2015).

-Corso di Formazione professionale "La Progettazione Geotecnica secondo le attuali normative". Fondazione Ordine degli Ingegneri di Perugia (2015).

-Docente del Corso "Resistenza al taglio dei terreni granulari", Università degli Studi di Messina, Progetto CERISI, Centro di Eccellenza Ricerca e Innovazione Strutture e Infrastrutture di grandi dimensioni" (2014).

-Relazione ad invito "Proprietà geotecniche di terreni stabilizzati", nell'ambito del Convegno ALIG-AGI sulla Stabilizzazione a calce dei terreni, Napoli (2012).

-Docente nell'ambito del programma di formazione permanente 2010/2011, Politecnico di Milano, "Progetto di opere di sostegno in condizioni statiche e sismiche alla luce della normativa", Milano (2011).

-Relazione ad invito: "L'inerbimento superficiale di pendii: un semplice modello di calcolo per la valutazione della sicurezza", Giornata di Studio: "Erosione e la messa in sicurezza delle discariche a pendio", Politecnico di Torino (2010).

-Docente del Corso sulle Nuove Norme Tecniche per le Costruzioni organizzato dall'Ordine degli Ingegneri della Provincia di Perugia. "Progetto di strutture di sostegno in condizioni statiche e sismiche" (2009).

-Organizzatrice della II Giornata di studio sulla Meccanica dei terreni non saturi, Università degli Studi di Perugia (2007).

Revisore per le seguenti Riviste Internazionali

Acta Geotechnica
Bulletin of Engineering Geology and the Environment
Bulletin of Earthquake Engineering
Ecological Engineering
Engineering Structures
Environmental Geotechnics
Environmental Science and Pollution Research
Géotechnique Letters
Geotechnical and Geological Engineering
Rock Mechanics and Rock Engineering
Geotechnical Testing Journal (ASTM)
Soil & Foundations.
Soil Dynamics and Earthquake Engineering.

Attività didattica istituzionale

Dal 2003 al 2014, docenza in affidamento dei seguenti insegnamenti:
-*Geotecnica per la Gestione del Territorio*
-*Scavi e Strutture di Sostegno*

-*Rischio Sismico*
-*Opere geotecniche in zona sismica*,
erogati nel Corso di Laurea in Ingegneria Gestionale (A.A. 2003-2004, Polo Scientifico e Didattico di Terni dell'Università di Perugia) e nei Corsi di Laurea Specialistica in Ingegneria Civile e Ingegneria per l'Ambiente e il Territorio, Facoltà di Ingegneria, Università di Perugia (a partire dall'anno accademico 2005-2006).

A.A. 2014-2015. Docenza in affidamento dei seguenti insegnamenti:
-*Opere geotecniche in zona sismica* (5cfu)
-*Geotecnica Applicata alle Opere di Ingegneria* (6 cfu),
erogati nel Corso di Laurea Specialistica in Ingegneria per l'Ambiente e il Territorio (Dipartimento di Ingegneria Civile ed Ambientale, Università di Perugia) e nel Corso di Laurea Specialistica in Scienze e Tecnologie Geologiche (Dipartimento di Fisica e Geologia, Università di Perugia).

A.A. 2015-2016. Docenza in affidamento del seguente insegnamento:
-*Opere geotecniche in zona sismica* (5cfu)
erogato nel Corso di Laurea Specialistica in Ingegneria per l'Ambiente e il Territorio (Dipartimento di Ingegneria Civile ed Ambientale, Università di Perugia)

A.A. 2016-2017. Docenza in affidamento dei seguenti insegnamenti:
-*Opere geotecniche in zona sismica* (5cfu)
-*Geotecnica Applicata alle Opere di Ingegneria* (6 cfu),
erogati nel Corso di Laurea Specialistica in Ingegneria per l'Ambiente e il Territorio (Dipartimento di Ingegneria Civile ed Ambientale, Università di Perugia) e nel Corso di Laurea Specialistica in Scienze e Tecnologie Geologiche (Dipartimento di Fisica e Geologia, Università di Perugia).

Master di Specializzazione (II livello)

A.A. 2000-2001, 2001-2002:
Docente di Master di specializzazione *Stabilizzazione e Conservazione dei Centri storici in territori instabili (Alta Scuola)*, Centro Studi di Orvieto. Insegnamento: *Complementi di Meccanica delle Terre*.
A.A. 2003-2004, 2005-2006, 2007-2008, 2009-2010, 2011-2012:
Docente di Master di II livello: *Miglioramento sismico, restauro e consolidamento del costruito storico e monumentale*, Università di Perugia. Insegnamento *Fondazioni* (40 ore).
A.A. 2011-2012, 2013-2014:
Docente di Master di II livello: *Miglioramento sismico, restauro e consolidamento del costruito storico monumentale*", Edizione Inter-Ateneo Università di Perugia, L'Aquila. Insegnamento *Fondazioni* (20 ore)"
A.A. 2014-2015:
Docente di Master di II livello *Miglioramento sismico, restauro e consolidamento del costruito storico e monumentale*", Università di Perugia, L'Aquila e Ferrara: Insegnamento *Fondazioni* (20 ore).
A.A. 2015-2016:
Docente di Master di II livello "Miglioramento sismico, restauro e consolidamento del costruito storico e monumentale", Università di Ferrara. Insegnamento del modulo di "Opere Geotecniche" (12 ore).

Docente di Master di I livello in: Ingegneria della Sicurezza ed analisi dei rischi in ambito industriale, Università di Perugia. Insegnamento del modulo di "Sicurezza dei fronti di scavo e delle Cave" (8ore).

Relatrice e Correlatrice di una sessantina di Tesi di Laurea (Corsi di Laurea: Ing. Civile e Ing. per l'Ambiente ed il Territorio). Correlatrice di n.4 Tesi di Dottorato.
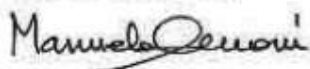
Ad oggi, la sottoscritta è stata Relatrice e Correlatrice di una sessantina di Tesi di Laurea (Corsi di Laurea: Ing. Civile, Ing. per l'Ambiente ed il Territorio, Scienze e Tecnologie Geologiche) e Correlatrice di n.4 Tesi di Dottorato. Negli ultimi dieci anni accademici, la sottoscritta ha fornito con continuità assistenza agli esami e spiegazioni agli Studenti, secondo l'orario di ricevimento previsto all'inizio di ogni A.A., nell'ambito dei Corsi di:

- Geotecnica (Corso di Laurea: Ingegneria Civile - Laurea triennale).
- Opere Geotecniche in zona sismica (Corso di Laurea Magistrale: Ingegneria per l'Ambiente e il Territorio).
- Geotecnica Applicata alle Opere di Ingegneria Corso di Laurea Magistrale in Scienze e Tecnologie Geologiche"

Perugia, giugno 2017

In fede,

Manuela Cecconi

Elenco delle pubblicazioni più significative

Riviste

Guidobaldi G., Cambi C., Cecconi M., Deneele D., Paris M., Russo G., Vitale E. Multi-scale analysis of the mechanical improvement induced by lime addition on a pyroclastic soil (2017). *Engineering Geology* 221 (2017) 193–201.

Cecconi M., Cencetti C., Melelli L., Pane V., Vecchietti A. Non-Dimensional Analysis for rock slope plane failure in seismic conditions (2017). Submitted to *Bulletin of Engineering Geology And the Environment.*

Pane, V., Bellavita, D., Cecconi, M., Vecchietti, A. Hydraulic failure of diaphragm walls: a possible methodology for safety improvement (2016) *Geotechnical and Geological Engineering* (2017). 35: 765–780.

Pane, V., Vecchietti, A., Cecconi, M. A numerical study on the seismic bearing capacity of shallow foundations (2016). *Bulletin of Earthquake Engineering,* 14 (11), pp. 2931-2958.

Melelli, L., Cencetti, C., Cecconi, M., Faralli, L., Vecchietti, A., Pane, V. The hermitage of Cerbaiolo (Tuscany, Italy): stability conditions and geomorphological characterization (2016) *Environmental Earth Sciences,* 75 (4), art. no. 322, pp. 1-14.

Cecconi, M., Pane, V., Vecchietti, A. Seismic displacement-based design of embedded retaining structures (2015) *Bulletin of Earthquake Engineering,* 13 (7), pp. 1979-2001.

Pane, V., Cecconi, M., Napoli, P. Hydraulic Heave Failure in EC7: Suggestions for Verification (2015) *Geotechnical and Geological Engineering,* 33 (3), pp. 739-750.

Cecconi M., Napoli P., Pane V. (2015). "Effects of soil vegetation on shallow slope instability". *Environmental Geote*chnics, vol. 2, issue EG3, p. 130–136.

Cecconi M., Russo G. (2013). Microstructural features of lime-stabilised pyroclastic soils. *Géotechnique Letters* (ISSN:2045-2543) p. 124 - 129 Vol. 3.

Pane V., Cecconi M., Cattoni E. (2012). Osservazioni sul progetto di paratie secondo gli Eurocodici e le Norme Tecniche per le Costruzioni (NTC08). *Progettazione Sismica* (ISSN:1973-7432) p. 37 - 47 Vol. 01/2012.

Cecconi M., Scarapazzi M., Viggiani G. (2010). On the geology and the geotechnical properties of pyroclastic flow deposits of the Colli Albani. *Bulletin of Engineering Geology and the Environment* (ISSN:1435-9529) p. 185 - 206 Vol. 69/2010.

Pane V. , Cecconi M.(2010). Progetto e dimensionamento di paratie in condizioni sismiche. *Progettazione Sismica* (ISSN:1973-7432) p. 19 - 35 Vol. 01/2010.

Cecconi M., Vecchietti S., Pane V. (2009). Il metodo DDBD per la valutazione delle spinte sismiche sulle strutture di sostegno. *Progettazione Sismica* (ISSN:1973-7432) p. 67 - 82 Vol. 02/2009

Cattoni E., Cecconi M., Pane V. (2007). Geotechnical properties of an unsaturated pyroclastic soil from Roma. *Bulletin of Engineering Geology and the Environment* (ISSN:1435-9529) p. 403 - 414 Vol. 66.

Pane V., Cecconi M. (2004). Sollecitazioni e spostamenti di paratie vincolate in testa in terreni incoerenti: uno studio parametrico. *Rivista Italiana di Geotecnica* (ISSN:0557-1405) p. 58 - 73 Vol. 1.

Cecconi M., De Simone A., Tamagnini C., Viggiani G.M. (2002). A constitutive model for granular materials with grain crushing and its application to a pyroclastic soil. *International Journal for Numerical and Analytical Methods in Geomechanics* (ISSN:0363-9061) p. 1531 - 1560 Vol. 26.

Tamagnini C., Pane V., Cecconi M. (2002). Studio parametrico del comportamento di paratie ancorate. *Rivista Italiana di Geotecnica* (ISSN:0557-1405), p. 23 - 43 Vol. 1/2002.

Cecconi M., Viggiani G. (2001). Structural features and mechanical behaviour of a pyroclastic weak rock. *International Journal for Numerical And Analytical Methods in Geomechanics* (ISSN:0363-9061) p. 1525 – 1557, Vol. 25.

Congressi, Simposi e Workshop

Guidobaldi G., Cambi C., Cecconi M., Pane V., Deneele D., Paris M., Russo G., Vitale E. (2017b) "Microstructural and mechanical investigation of the effects induced by lime treatment on a zeolitic pyroclastic soil", accepted for *2nd Symp. on Coupled Phenomena in Environmental Geotechnics (CPEG2)*, Leeds, UK 2017.

Cambi, C., Guidobaldi, G., Cecconi, M., Comodi, P., Russo, G. On the ICL test in soil stabilization (2016) 1st IMEKO TC4 *International Workshop on Metrology for Geotechnics*, Metro Geotechnics 2016, pp. 31-34.

Vitale, E., Cecconi, M., Croce, P., Deneele, D., Pane, V., Russo, G., Vecchietti, A. Influence of Pore Water Chemistry on Hydraulic Conductivity of Kaolinite Suspensions (2016) *Procedia Engineering*, 158, pp. 81-86.

Cecconi, M., Scarapazzi, M., Viggiani, G.M.B. A micro- and macro-scale investigation of the geotechnical properties of a pyroclastic flow deposit of the Colli Albani (2015) Volcanic Rocks and Soils - *Proceedings of the International Workshop on Volcanic Rocks and Soils*, 2015, pp. 95-96.

Cecconi, M., Rotonda, T., Verrucci, L., Tommasi, P., Viggiani, G. Microstructural features and strength properties of weak pyroclastic rocks from Central Italy (2015) Volcanic Rocks and Soils - *Proceedings of the International Workshop on Volcanic Rocks and Soils*, 2015, pp. 107-108.

Russo, G., Vitale, E., Cecconi, M., Pane, V., Deneele, D., Cambi, C., Guidobaldi, G. Microstructure insights in mechanical improvement of a lime-stabilised pyroclastic soil (2015) Volcanic Rocks and Soils - *Proceedings of the International Workshop on Volcanic Rocks and Soils*, 2015, pp. 153-154.

Cecconi M., Mannocchi F., Napoli P., Pane V., Todisco F., Urciuoli G., Vecchietti A . (2014). "Interventi di protezione dei versanti per il controllo dei fenomeni erosivi e la stabilizzazione superficiale", Associazione Geotecnica Italiana, *XXV Convegno Nazionale di Geotecnica*, Baveno 4-6 giugno 2014, ISBN9788897517030, Edizioni AGI, Roma, p. 441- 448.

Cecconi M., Pane V., Napoli P., C. Zarotti (2013). "Mechanical and hydraulic effects of deep roots planting on slope stability". Proc. of the Int. Symp. ISSMGE TC215 Coupled Phenomena in Environmental Geotechnics CRC Press Taylor & Francis Group, 1-3 July 2013, Torino (Italy), vol. 1, 533- 540.

Cecconi M., Capotosto A., Russo G. (2013). "Mechanical behaviour of two lime stabilised pyroclastic soils", TerDOUEST 2013, 18-19 June 18-19th , Colloque «Le traitement des sols pour un terrassement durable» Ecole des Ponts ParisTech-Marne La Vallée, France.

Cattoni E., Cecconi M., Pane V., Vecchietti S.(2012). Development of DDBD method for retaining walls subjected to seismic loads. II International Conference on Performance Based Design in Earthquake Geotechnical Engineering M. Maugeri and C. Soccodato Editors, Pàtron Editore Bologna, p. 1510- 1521, vol.2, 28-30 may 2012, Taormina (Italy).

Cecconi M., Ferretti A., Cattoni E., Russo G, Capotosto A. (2012). Collapse upon wetting of lime stabilised pyroclastic soils. E-UNSAT 2012 - 2nd European Conference on Unsaturated Soils, Unsaturated Soils: Research and Applications. C. Mancuso, C. Jommi, F. D'Onza Editors, Springer, Napoli, 20-22 giugno 2012, Vol. 1 p. 397 – 404.

Cecconi M., Ferretti A., Russo G., Capotosto A. (2011). Mechanical properties of two lime stabilized pyroclastic soils. Int. Symposium on Deformation Characteristics of Geomaterials Chung CK., Jung YH., Kim HK., Lee JS., Kim D.S Editors, 772- 778, vol.II, 1-3 September 2011, Seoul, Korea.

Cecconi M., Rotonda T., Tommasi P., Viggiani G. MB. (2011). Microstructural features and compressibility of volcanic deposits from Central Italy.. V International Symposium on Deformation Characteristics of Geomaterials Chung CK., Jung YH., Kim HK., Lee JS., Kim D.S Editors, 884- 891, vol.II, 1-3 September 2011, Seoul, Korea.

Russo G., Croce P., Cecconi M., Pane V. (2011). Proprietà fisiche e meccaniche di terreni stabilizzati a calce.. XXIV Convegno Nazionale di Geotecnica - Innovazione tecnologica nell'Ingegneria Geotecnica Edizioni AGI, Città di Castello (PG): 557- 564, vol.2, 22-24 giugno 2011, Napoli.

Pane V., Cecconi M., Cattoni E. (2011). On the design of embedded retaining structures following Eurocodes and the Italian national code. XV European Conf. on Soil Mechanics and Geotechnical Engineering - ERTC 12 Workshop - Evaluation of Geotechnical Aspects of EC8 M. Maugeri Editor, 1-12, 11 September 2011, Athens.

Cecconi M., Pane V., Marmottini F., Russo G., Croce P., Dal Vecchio S. (2010). Lime stabilisation of pyroclastic soils. Proc. of the 5th Int. Conference on Unsaturated Soils Balkema, 537- 541, vol.2, 6-8 september 2010, Barcellona.

Cecconi M.; Russo G (2008). Prediction of soil-water retention properties of a lime-stabilised compacted silt. E-Unsat, The First European Conf. on Unsaturated Soils Toll, Augarde, Gallipoli and Wheeler Eds, London: 271- 276, 2 - 4 luglio, Durham, UK.

Cecconi M; V. Pane; Vecchietti S. (2008). The DDBD method in the a-seismic design of anchored diaphragm walls. MERCEA08 Int. Conf. on Seismic Engng. Santini and Moraci Eds., AIP Conf. Proc., 695- 702, vol.1, 8-11 luglio, Reggio Calabria

Viggiani GMB., Cecconi M. (2007). Pyroclastic flow deposits from the Colli Albani. The example of the Pozzolana Nera. Second International Workshop on Characterisation and Engineering Properties of Natural Soils. Tan T.S., Phoon K.K. and Hight D.W. and Leroueil Editors, p. 2411 - 2447

Vecchietti S; Cecconi M; V. Pane (2007). Displacement-methods for the design of earth retaining structures. 4th Int. Conf. on Earthquake Geotechnical Engineering Pitilakis Editor, Springer, 1- 12, 25 - 28 giugno, Thessaloniki, Greece.

Cecconi M; Vecchietti S; V. Pane (2007). The DDBD method in the design of cantilever diaphragm walls. Int. Conf. Ottawa 2007, The Diamond Jubilee 1- 8, 21-24 October 2007, Ottawa, Ontario, Canada.

Pane V., Cecconi M., Vecchietti S. (2007). Metodo DDBD per il progetto degli spostamenti di strutture di sostegno. Anidis 2007, XII Convegno Nazionale di Ingegneria Sismica Associazione Nazionale Italiana di Ingegneria Sismica, 1- 11, 10 - 14 giugno, Pisa

Cecconi M., Pane V., Isidori F. (2006). Un'estensione della Teoria di Broms nel calcolo dei pali sollecitati da forze orizzontali. V Convegno Nazionale dei Ricercatori in Ingegneria Geotecnica: Fondazioni superficiali e profonde Hevelius Edizioni, BENEVENTO: 295- 311, vol.1, 15-16 settembre 2006, Bari.

Cecconi M., Croce P., Viggiani G. MB. (2006). Physical model of block toppling. ICPMG06, Int. Conference on Physical Modelling in Geotechnics Ng, Zhang & Wang Eds, Taylor & Francis Group, 325- 330, vol.1, 4-6 August 2006, Hong Kong.

Cecconi M. (2006). Alcuni aspetti salienti del comportamento meccanico della Pozzolana Nera di Roma. Questioni di Ingegneria Geotecnica, Scritti in onore di Arturo Pellegrino Hevelius Edizioni, Benevento: 367- 379, vol.2, settembre 2006, Napoli.

Cattoni E., Cecconi M., Pane V. (2005). An experimental study on partially saturated pyroclastic soil: the Pozzolana Nera from Roma. Second International Workshop on Unsaturated Soils, Advances in Testing, Modelling and Engineering Applications C. Mancuso & A. Tarantino Editors, Balkema Publishers, Great Britain: 29- 42, 23-25 Giugno 2004, Anacapri (Napoli, Italy).

Cecconi M., Pane V., Vecchietti S. (2005). Some remarks on physicoempirical models for the prediction of the soil water retention curve. Experus 2005, Int. Symposium on Advanced Experimental Unsaturated Soil Mechanics Tarantino, Romero and Cui Eds, Balkema Publishers, Great Britain: 337- 343, vol.1, In:International Symposium on Advanced Experimental Unsaturated Soil Mechanics. 27-29 Giugno 2005, Trento.

Cecconi M., Pane V., Cattoni E. (2005). Effects of grain size and grain crushing on the shear strength of a pyroclastic crushable soil. Geoprob2005, Int. Conference on Problematic Soils Bilsel and Nalbantoglu Eds, 397- 406, vol.1, 25-27 May 2005, Famagusta, North Cyprus.

Cecconi M., Evangelista A., Nicotera M.V., Pane V., Cattoni E., Scotto di Santolo A. (2005). Wetting paths upon shearing: experimental evidence and comparative analyses of two volcanic soils in the area of Napoli and Roma. Experus 2005, Int. Symposium on Advanced Experimental Unsaturated Soil Mechanics Tarantino, Romero and Cui Eds., Balkema Publishers, Great Britain: 141- 147, 27-29 Giugno 2005, Trento.

Cecconi M., Pane V., Aneris V. (2005). Creep behaviour of a pyroclastic soil. Geoprob2005, Int. Conference on Problematic Soils Bilsel and Nalbantoglu Eds., 423- 430, vol.1, 25-27 May 2005, Famagusta, North Cyprus.

Cattoni E., Cecconi M., Jommi C. (2005). Soil dilatancy and suction: some remarks on their mutual effects on the shear strength of granular soils. IACMAG2005, 11th Int. Conference on Prediction, analysis and design in geomechanical applications Pàtron Editore, Bologna: 19- 26, vol.2, 19-24 giugno 2005, Torino.

Pane V., Cecconi M., Tamagnini C. (2003). Time dependent settlements induced by tunnelling in stiff cohesive soils: a parametric study. Proc. XIII ECSMGE Balkema.

Cecconi M., Viggiani G., De Simone A., Tamagnini C. (2003). A coarse grained weak rock with crushable grains: the Pozzolana Nera from Roma. International Workshop on "Constitutive Modelling and Analysis of Boundary Value Problems in Geotechnical Engineering – 3X4 Hevelius Editore, Benevento: 157- 185, 22-24 Aprile 2003, Napoli.

Cecconi M., De Simone A., Tamagnini C., Viggiani G. (2002). Elasto-plastic modelling of the brittle-ductile transition in a pyroclastic weak rock. Workshop on Volcanic Rocks, Eurock 2002 Dinis da Gama, Ribeiro e Sousa Editors, Lisboa, Portugal: 45- 52, vol.1, 25-28 Novembre 2002, Funchal (Madeira, Portugall).

Cecconi M., Viggiani G. (2000). Stability of sub-vertical cuts in pyroclastic deposits. Geoeng 2000 International Conference on Geotechnical & Geological Engineering 1- 7, 19-24 November 2000, Melbourne, Australia.

Cecconi M., Viggiani G. (1998). Physical and structural properties of a pyroclastic soft rock. The Geotechnics of Hard Soils - Soft Rocks Evangelista and Picarelli Editors,Balkema/Rotterdam/Brookfield 1998, 85- 91, vol.Vol. 1, In:II Int. Symp. on Hard Soils and Soft Rocks. October 1998, Naples, Italy.

Cecconi M., Viggiani G., Rampello S. (1998). An experimental investigation of the mechanical behaviour of a pyroclastic soft rock. The Geotechnics of Hard Soils - Soft Rocks Evangelista & Picarelli Editors,Balkema, Rotterdam, Brookfield, 1998, 473- 482, vol. 1, In:II Int. Symp. on Hard Soils and Soft Rocks. October 1998, Naples, Italy.

Cecconi M. (1998). Sample preparation of a problematic pyroclastic soil. Problematic Soils, IS-Tohoku98, International Symposium on Problematic Soils Yanagisawa E., Moroto N., Mitachi T., 165- 168, vol.Vol. 1, In:IS-Tohoku98, International Symposium on Problematic Soils. October 28-30, 1998, Sendai (Japan).

Monografie e capitoli di libro

Calvi, G.M., Cecconi, M., Paolucci, R. Seismic Displacement Based Design of Structures: Relevance of Soil Structure Interaction (2014) Geotechnical, Geological and Earthquake Engineering, 28, Ch. 10, pp. 241-275.

Napoli P., Cecconi M., Pane V., Calabresi G. (2014). "Interazione terreno-vegetazione nei fenomeni superficiali di instabilità dei versanti". Università di Perugia, Perugia, pp. 1 – 95 (ISBN 9788890642173). Collana CTL- Università di Perugia.

Cattoni E., Cecconi M.. (2011). Appunti di spinta delle terre e muri di sostegno. Editore CESD s.r.l., Città di Castello (PG): ITALIA. pp. 1 – 137.

Pane V., Cecconi M.. (2010). Strutture di sostegno: dimensionamento secondo le Nuove Norme Tecniche per le Costruzioni 2008 ed esempi applicativi. Morlacchi Editore, Perugia.

Traduzioni

Cecconi M., Viggiani GMB. (2006). La spinta delle terre e le opere di sostegno. Hevelius Edizioni, Benevento: pp. 1 – 446.

In fede,

Manuel Cecconi

Allegato XX - punto n.19

Elenco titoli attestanti i requisiti del candidato Dott. Luca Landi, la numerazione è rispondente a quella della delibera

1. Attività didattica

a)Didattica ufficiale presso atenei Italiani e stranieri

Primo A.A. in cui ha tenuto il corso	Numero A.A. corso	Titolarità 1=si 0 = did. integrativa	Fraz. corso	Nome del corso	CFU totali
A.A. 1998/1999	1	0	0,5	Principi e Metodologie della Progettazione Meccanica, Diploma Universitario in Tecnico Ortopedico dell'Università degli Studi di Firenze tenuto dal prof. Andrea Corvi.	2
A.A. 1999/2000	2	1	1	Principi e Metodologie della Progettazione Meccanica, Diploma Universitario in Tecnico Ortopedico dell'Università degli Studi di Firenze	2
A.A. 2001/2002	1	0	0,2	Costruzione di macchine I (V.O.), Università degli studi di Perugia, corso in laurea di Ingegneria Meccanica tenuto dal prof. C. Braccesi	10
A.A. 2002/2003	6	1	1	Qualità nella progettazione e costruzione di macchine (N.O., 3° anno triennale) del corso in laurea di Ingegneria Meccanica dell'Università di Perugia	3
A.A. 2002/2003	1	0	0,48	Costruzione di macchine I (V.O.), mutuato anche ai corsi del N.O., Università degli studi di Perugia, corso in laurea di Ingegneria Meccanica tenuto dal prof. Claudio Braccesi	12
A.A. 2003/2004	1	0	0,25	Elementi di progettazione meccanica (triennale N.O.), Costruzione di macchine (triennale N.O.), Progettazione e costruzione di macchine I (specialistica N.O.), Università degli studi di Perugia, corsi tenuti dal prof. Claudio Braccesi	24
A.A. 2004/2005	1	1	1	Metodi numerici per la progettazione meccanica, del corso di laurea specialistica in Ingegneria Meccanica dell'Università degli Studi di Perugia (1° anno laurea specialistica).	2
A.A. 2004/2005	4	1	1	Progetto e costruzione di macchine II (N.O., 1° anno specialistica), del corso di laurea specialistica in Ingegneria Meccanica dell'Università degli Studi di Perugia ;	5
A.A. 2004/2005	4	0	0,45	Elementi di progettazione meccanica (triennale N.O.), Università degli studi di Perugia, corso tenuto dal prof. C. Braccesi	6
A.A. 2004/2005	4	0	0,45	Costruzione di macchine (triennale N.O.), Università degli studi di Perugia, corso tenuto dal prof. C. Braccesi	6
A.A. 2005/2006	1	1	1	Affidabilità strutturale e qualità nella progettazione e costruzione di macchine, modulo 2 presso la facoltà di ingegneria dell'Università degli Studi di Mar del Plata (Argentina).	4

Primo A.A. in cui ha tenuto il corso	Numero A.A. corso	Titolarità 1=sì 0 = did. integrativa	Fraz. corso	Nome del corso	CFU totali
A.A. 2005/2006	3	1	1	Abilità informatiche per la progettazione meccanica, del corso di laurea di Ingegneria Meccanica dell'Università degli Studi di Perugia (3° anno laurea di base)	2
A.A. 2008/2009	Fino ad oggi	1	1	Progetto e costruzione di macchine, modulo B (1° anno specialistica), del corso di laurea specialistica in Ingegneria Meccanica dell'Università degli Studi di Perugia ;	5
A.A. 2008/2009	4	1	0,57	Qualità' aspetti misuristici progettuali costruttivi, Modulo A, qualità nella progettazione e costruzione di macchine (3° anno triennale) laurea di Ingegneria Meccanica dell'Università degli Studi di Perugia	7 (4)
A.A. 2008/2009	5	0	0,45	Costruzione di macchine (triennale corso annuale), Università degli studi di Perugia, corso tenuto dal prof. C. Braccesi	12
A.A. 2012/2013	Fino ad oggi	1	1	Attività progettuali (mod.B)	2
A.A. 20013/2014	Fino ad oggi	1	1	Progettazione dei Sistemi Industriali (mod.B complementi di costruzioni di macchine) – Laurea Specialistica in Ingegneria Industriale-Università degli studi di Perugia, sede distaccata di Terni	8

b)Partecipazione agli esami di profitto ed alla preparazione delle prove progettuali finali per la laurea in ingegneria triennale del Dipartimento di Ingegneria. Svolgimento a cicli di esercitazioni e di attività di supporto alla didattica nello stesso SSD.

Sin dall'anno accademico 2001/2002 il candidato ha partecipato costantemente alla redazione degli scritti dell'esame di Costruzione di Macchine della laurea triennale di ing. Meccanica sede di Perugia ed ha fatto parte delle commissioni esaminatrici agli esami di profitto in tutti gli insegnamenti ricompresi nel settore scientifico-disciplinare ING/IND 14. Ha prima coadiuvato e poi avuto come titolarità il corso si attività progettuali come da allegato al punto a) durante il quale viene prevista anche la stesura e revisione delle prove finali propedeutiche alla laurea triennale di ingegneria meccanica sede di Perugia. Le ore di didattica integrativa ufficiali sono comprese nel precedente punto a).

c) attività di guida nella preparazione di tesi di laurea (come relatore o correlatore negli ultimi 10 anni);

Negli ultimi 10 anni lo scrivente è stato co-relatore o relatore di 21 tesi di laurea presso i corsi di laurea magistrale in ingegneria meccanica sede di Perugia o laurea magistrale in ingegneria industriale presso il polo di Terni.

d) attività di docenza in Master accademici in corsi SSD ING-IND/14 e eventuale attività didattica presso altri atenei (italiani o stranieri) rappresenterà un titolo di preferenza.

Nell' A.A 2015/2016 il candidato è stato docente incaricato del Modulo sicurezza delle Macchine, Master I livello Ingegneria della Sicurezza in ambito Industriale (5 CFU), erogato in quell'anno per la prima volta dal Dipartimento di Ingegneria dell' Università di Perugia.

I corsi tenuti in passato presso l'Università degli studi di Firenze e Mar Del Plata (Argentina) sono ricompresi al punto a).

2. Attività scientifica

a) una significativa produzione scientifica, continuativa negli ultimi 10 anni, attestata dalla presenza su database riconosciuti dalla ASN e da congressi nazionali rilevanti per il SSD e dalla pubblicazione di almeno un lavoro su rivista di eccellente collocazione secondo l'ultima rilevazione VQR.

Negli ultimi 10 anni (dal 2007) il candidato ha prodotto 34 lavori su riviste internazionali, nazionali e/o presentate personalmente quando relative a congressi internazionali o nazionali (di rilevanza per il SSD ING-IND 14).

11 di esse sono rintracciabili su database riconosciuti ed ulteriori 2 relative al 2016 sono in via di pubblicazione su detti database.

Nella ultima valutazione della qualità della didattica una delle due pubblicazioni presentate era su rivista di eccellente collocazione editoriale.

b)partecipazione a comitati tecnici e gruppi di ricerca nazionali ed internazionali relativi alla normazione tecnica ed allo sviluppo normativo,

- nominato membro della Commissione Tecnica Macchine Utensili UNI CT024, dal 12-2015,
- membro esperto Italiano per il comitato tecnico ISO/TC39/SC10/WG12 – "Environmental evaluation of machine tools" ed inoltre nominato Membro Gruppo di Lavoro 2 "Valutazione ambientale delle macchine utensili" della Commissione Macchine Utensili UNI CT24, dal 3 2015,
- eletto membro del consiglio di presidenza della STANIMUC, STANdard per l'Industria Manifatturiera Utilizzatori e Costruttori, è una Associazione a carattere tecnico, senza fine di lucro, che opera nell'ambito delle attività pre-normative e normative nel settore dell'utilizzazione e costruzione delle macchine utensili, dei sistemi di produzione e dei relativi componenti destinati a fabbricare, assemblare, manipolare e misurare prodotti e manufatti, dal 7 - 2013,
- membro esperto Italiano per il comitato tecnico ISO/TC39/SC10/WG3 – "Turning Machines", ed nello stesso tempoe nominato quale Membro Gruppo di Lavoro 3 "Sicurezza delle macchine utensili per asportazione" della Commissione Macchine Utensili UNI CT024,dall' 11-2011,
- membro esperto Italiano per il comitato tecnico ISO/TC39/SC10/WG4 – "Machining centres", dall'11-2011.

c) partecipazione scientifica a progetti di ricerca, ammessi al finanziamento sulla base di bandi competitivi che prevedano la revisione tra pari negli ultimi 5 anni,

Il candidato negli ultimi 5 anni è stato coordinatore scientifico delle seguenti ricerche ammesse al finanziamento sulla base di bandi competitivi:

- "Progettazione prototipale di sistemi innovativi di carico e scarico" bando UNICO POR CREO 2008 regione toscana linea di finanziamento 1.3.b - dal 30/4/2012.
- "Implementazione del processo di programmazione della produzione e delle soluzioni gestionali per mezzo dei sistemi NTS BUSINESS" bando UNICO POR CREO Regione Toscana linea di finanziamento 2.3.b - dal 30/5/2013
- "Attività di progettazione di sistemi di automazione per lavorazioni non presidiate" finanziato tramite POR FESR 2014-2020 regione Toscana, con conclusione il 30-9-2017.

d) conseguimento di premi e riconoscimenti nazionali e internazionali per attività di ricerca.

- Premi UCIMU per gli anni2010, 2012, 2013, 2014 e 2016 (associazione Italiana dei Costruttori di Macchine Utensili) per il suo supporto dato alla formazione della conoscenza delle tecnologie connesse a machine utensili, robot ed automazione.

e) partecipazione in qualità di relatore a congressi e convegni nazionali e internazionali, la partecipazione come relatore invitato anche a convegni organizzati durante attività fieristiche nazionali ed internazionali rappresenterà titolo di preferenza.

- Ha presentato personalmente i propri lavori pubblicati a congressi nazionali ed internazionali,
- Ha partecipato come relatore invitato a convegni, giornate di studio di rilevanza nazionale quali Lamiera - fiera di Bologna e Milano (2 volte, di cui 1 volta in rappresentanza del SSD ING/IND 14), Bi.Mu. Fiera di Milano (ripetutamente dal 2011 anche per il suo ruolo nel CT024 dell'UNI), presentazione del 8° rapporto nazionale sugli infortuni del lavoro, invito da parte del DIT di INAIL, dicembre 2015.